2021-01-13

Liquid-Liquid Equilibrium Studies of Solvent and Bitumen Systems

Sadeghi Yamchi, Hassan

UNIVERSITY OF CALGARY

Liquid-Liquid Equilibrium Studies of Solvent and Bitumen Systems

by

Hassan Sadeghi Yamchi

A THESIS

SUBMITTED TO THE FACULTY OF GRADUATE STUDIES

IN PARTIAL FULFILMENT OF THE REQUIREMENTS FOR THE

DEGREE OF DOCTOR OF PHILOSOPHY

GRADUATE PROGRAM IN CHEMICAL AND PETROLEUM ENGINEERING

CALGARY, ALBERTA

JANUARY, 2021

Abstract

Solvent-aided and solvent-based heavy oil recovery methods have gained interest as alternatives to the conventional steam-based thermal recovery methods. Dimethyl ether (DME), propane, butane, and their mixtures (LPG) are considered proper solvents for low temperature upgrading and solvent-based bitumen and heavy oil recovery processes. One key prerequisite for simulation and optimization of these recovery processes is the liquid-liquid thermodynamic equilibrium (LLE) data of solvent and bitumen mixtures. This study presents measurements and modeling studies of the LLE of solvent (butane, DME, and LPG) and Athabasca bitumen mixtures. Phase behavior measurements including equilibrium compositions (K-value), density, and viscosity of the light phase as well as saturation pressures of the mixtures are measured at temperatures and pressures up to 100 °C and 3.5 MPa, respectively.

To model LLE data of solvent/bitumen system, detailed characterization of the light and heavy cuts (upgraded oil and asphaltenes) are conducted using a methodology that combines the gel permeation chromatography (GPC) with the simulated distillation results (SD) to provide a molecular weight distribution. Then, two pseudocomponents (one representative of maltenes and the other representative of asphaltenes) are defined based on the characterization, and LL K-values are estimated for each component. Non-Random Two Liquid (NRTL) model is then tuned to represent the experimental compositional data and K-values.

Finally, the implementation of LL K-values for simulation of asphaltene deposition in porous media is described. A modified approach is presented based on the LL K-values and a reaction-based non-equilibrium mass transfer model. The interplay of viscous fingering and asphaltene deposition during the injection of solvent is studied and sensitivity of the simulation results on grid size is investigated.

Acknowledgements

I would like to express my deepest gratitude to my supervisor, Dr. Hassan Hassanzadeh for all the support, guidance, inspiration, and patience he showed in the completion of this study. I am truly indebted to him for his time and mentorship throughout my graduate career. I am also extremely grateful to my co-supervisor Dr. Jalal Abedi for allowing me to work in his equipped laboratories during my studies.

I am thankful to my supervisory committee members, Drs. Gordon Moore and Sudarshan Mehta, for their support during my research. I also thank Drs. Martin Jasso and Xiaoli Li to accept to be in my examination committee.

A special thanks goes to Dr. Mohsen Zirrahi who took the time, and had the patience, to discuss and share many ideas with me. Not to mention, he was the key to resolve every single experimental problem that I encountered during my work. I am also sincerely grateful to Ali Haddadnia for his continues support throughout the project. I was also fortunate to work with a talented group of people in SHARP research group who created an exciting and fun atmosphere in which to work. I wish the best to all of them.

I wish to express my appreciation for financial support from the Natural Sciences and Engineering Research Council of Canada and all member companies of the SHARP Research Consortium: Canadian Natural Resources Ltd., Cenovus Energy, CNOOC International, Cona Resources Ltd., Husky Energy, Imperial Oil Limited, Kuwait Oil Company, Osum Oil Sands, and Suncor Energy. The support of the Department of Chemical and Petroleum Engineering and the Schulich School of Engineering at the University of Calgary is acknowledged.

Finally, I would like to thank four very important people in my life. I thank my two beautiful sisters and my brother who supported me unconditionally in every step of my life. Words cannot describe

my gratitude to them and hopefully, I deserve their love. I also thank my father who has been and continues to be, hugely inspirational to me. I thank him for his love and guidance.

Dedicated to the memory of my mother

Table of Contents

Abstract ii
Acknowledgements iii
Table of Contents vi
List of Tables viii
List of Figures and Illustrations ix
List of Symbols, Abbreviations and Nomenclature xii

CHAPTER ONE: OVERVIEW 1
1.1 Motivations, Objectives, Steps, and Organization 1
1.2 Dissertation Outline 3
1.3 References 5

CHAPTER TWO: LIQUID-LIQUID EQUILIBRIUM OF BUTANE + ADDITIVES/BITUMEN 8
2.1 Preface 8
2.2 Abstract 8
2.3 Introduction 9
2.4 Experimental Apparatus 13
2.5 Results and Discussion 17
2.5.1 Effect of Propane Addition 17
2.5.2 Effect of Toluene Addition 20
2.5.3 Effect of Dimethyl Ether Addition 24
2.6 Summary and Conclusion 28
2.7 References 30

CHAPTER THREE: LIQUID-LIQUID EQUILIBRIUM OF DIMETHYL ETHER (DME)/BITUMEN MIXTURES 33
3.1 Preface 33
3.2 Abstract 33
3.3 Introduction 34
3.4 Experimental Setup 38
3.5 Methodology of Determining the Composition of Each Phase 43
3.6 Thermodynamic Modeling 50
3.7 Results and Discussion 51
3.8 Conclusions 63
3.9 References 65

CHAPTER FOUR: LIQUID-LIQUID EQUILIBRIUM OF PROPANE + BUTANE + BITUMEN SYSTEM 69
4.1 Preface 69
4.2 Abstract 69
4.3 Introduction 70
4.4 Experimental Setup and Procedures 74
4.5 Thermodynamic Modeling 82
4.6 Results and Discussion 83

4.7 Summary and Conclusions 95
4.8 References 97

CHAPTER FIVE: NUMERICAL SIMULATION OF ASPHALTENE DEPOSITION IN POROUS MEDIA INDUCED BY SOLVENT INJECTION 101
5.1 Preface 101
5.2 Abstract 101
5.3 Introduction 102
5.4 Problem Description 106
5.5 The Governing Equations 108
5.6 Fluid Model 111
5.6.1 Density of DME/Bitumen (Asphaltenes + Maltenes) Mixtures 112
5.6.2 Viscosity of DME/Bitumen (Asphaltenes + Maltenes) Mixtures 113
5.6.3 Liquid-Liquid Equilibrium K-values 115
5.7 Results and Discussion 117
5.7.1 Upscaling of Deposition Rate 125
5.8 Summary and Conclusions 130
5.9 References 132

CHAPTER SIX: CONCLUSIONS AND RECOMMENDATIONS 137
6.1 Conclusions 137
6.1.1 Effect of Additives on Liquid-Liquid Equilibrium of Butane/Bitumen 137
6.1.2 Liquid-Liquid Equilibrium of DME/Bitumen Mixtures 138
6.1.3 Liquid-Liquid Equilibrium of Propane + Butane + Bitumen Mixtures 139
6.1.4 Numerical Simulation of Asphaltene Deposition in Porous Media 139
6.2 Recommendations 140

APPENDIX A: VALIDATION OF THE EXPERIMENTAL APPARATUS 141
A.1 Validation of the PVT Setup 141
A.2 References 142

APPENDIX B: COPYRIGHT PERMISSIONS 143

List of Tables

Table 3.1: Composition (wt.%) of components at equilibrium conditions. 53

Table 3.2: Liquid-liquid K-values of all components in DME/bitumen system..... 56

Table 3.3: Density and viscosity of light phase and saturation pressure of DME/bitumen mixtures..... 58

Table 3.4: τ_{ij} used for calculation of compositions in NRTL model. 59

Table 4.1: Composition (wt.%) of components at equilibrium conditions. 84

Table 4.2: Liquid-liquid K-values of all components in LPG/bitumen system. 90

Table 4.3: Density and viscosity of the light phase for LPG/bitumen mixtures. 91

Table 4.4: τ_{ij} used for calculation of compositions in NRTL model. 92

Table 5.1: Density coefficients used in density correlation for DME/bitumen (asphaltene + maltene) system. 113

Table 5.2: Constants of viscosity correlation for DME/bitumen (asphaltene + maltene) system. 114

Table 5.3: Asphaltene liquid-liquid K-values for DME/bitumen system at T=80 °C and pressure range of 2.5-3 MPa. 116

Table A.1: Liquid-liquid equilibrium data for butane and Athabasca bitumen at 50 °C and 2MPa. 141

List of Figures and Illustrations

Figure 2.1: Experimental setup for PVT studies of solvent/bitumen systems, (1) Blue-M oven, (2) density data gathering unit, (3) viscosity data gathering unit, (4) feeding cell, (5) equilibration cell, (6) receiving cell, (7) densitometer, (8) viscometer, (9) sample cell, (10) Quizix pump, (11): pump controlling unit. 14

Figure 2.2: (a) density, (b) mass fraction of light phase and (c) saturation pressure of propane-butane/bitumen system. 18

Figure 2.3: Boiling point distribution of the Athabasca bitumen and heavy and light fractions extracted from propane-butane/bitumen. 19

Figure 2.4: Carbon number distribution of the Athabasca bitumen (a) light fractions, and (b) heavy fractions extracted from mixtures of propane-butane/bitumen. 20

Figure 2.5: (a) density, (b) mass fraction of light phase, and (c) saturation pressure of toluene-butane/bitumen system. 21

Figure 2.6: Boiling point distribution of the Athabasca bitumen and heavy and light fractions extracted from mixtures of toluene - butane/bitumen. 22

Figure 2.7: Carbon number distribution of the Athabasca bitumen (a) light fractions and (b) heavy fractions extracted from mixtures of toluene-butane/bitumen. 23

Figure 2.8: Density (a), mass fraction (b) of light phase and saturation pressure (c) of DME-butane/bitumen system. 25

Figure 2.9: Boiling point distribution of the Athabasca bitumen and heavy and light fractions extracted from of DME- butane/bitumen. 26

Figure 2.10: Carbon number distribution of the Athabasca bitumen, (a) light fractions, and (b) heavy fractions extracted from mixtures of DME-butane/bitumen. 27

Figure 3.1: Experimental setup for PVT studies of DME/bitumen mixtures, (1) Blue-M oven, (2) density data gathering unit, (3) viscosity data gathering unit, (4) feeding cell, (5) equilibration cell, (6) receiving cell, (7) densitometer, (8) viscometer, (9) sample cell, (10) Quizix pump, (11) pump controlling unit, and (12) filter. 39

Figure 3.2: Saturation pressure measurement of 60 wt.% DME/bitumen at 60 °C. 42

Figure 3.3: Pressure jump, once the heavy phase reaches the top of the cell equilibrium cell. 44

Figure 3.4: a) Demonstration of light and heavy phases at equilibrium condition, b) dividing bitumen to light and heavy cuts due to addition of 80 wt.% DME at 100 °C. 46

Figure 3.5: (a) GPC chromatogram, (b) MW distribution from SD for the bitumen sample. 48

Figure 3.6: MW distribution of the bitumen calculated using GPC - SD method. 49

Figure 3.7: Variation of composition of the components with DME wt.% in the feed for a) light phase, b) heavy phase at 40 °C. 52

Figure 3.8: Molecular weight distributions of the cuts recovered from different equilibrium conditions. 54

Figure 3.9: Ternary diagrams of DME/bitumen systems at different temperatures. ●, ○ experimental points; - - - model predictions; — model tie lines. 60

Figure 3.10: Heavy yield of DME/bitumen systems at different temperatures; ●, ■, ▲, ◆ are experimental data; — model predictions. 61

Figure 3.11: Comparison of experimental versus predicted K-values. 62

Figure 4.1: Experimental setup for PVT studies of LPG/bitumen mixtures, (1) Blue-M oven, (2) density data gathering unit, (3) viscosity data gathering unit, (4) feeding cell, (5) equilibration cell, (6) receiving cell, (7) densitometer, (8) viscometer, (9) sample cell, (10) Quizix pump, (11) pump controlling unit, (12) filter, (13) nitrogen cylinder, and (14) back-pressure regulator. 75

Figure 4.2: (a) Equilibration cell, (b) viscometer, and (c) densitometer located inside the oven for LLE measurements of LPG/bitumen system. 76

Figure 4.3: Stable density readings for the light phase created with mixing 45 wt.% LPG with bitumen at 80 °C, an indication of proper segregation of light and heavy phases. 79

Figure 4.4: Heavy cut accumulated at the bottom of the equilibration cell after LLE experiment at 40 °C and 45 wt.% LPG in the feed. 80

Figure 4.5: Measured compositions for (a) light phase, and (b) heavy phase for LLE tests at 21 °C. 85

Figure 4.6: Molecular weight distributions of the cuts recovered from different equilibrium conditions for LPG/bitumen mixtures. 86

Figure 4.7: Light cuts and the corresponding heavy cuts from LLE of LPG/bitumen mixtures at 80 °C and solvent concentration of (a) 45, (b) 55, and (c) 65 wt.% in the feed. 88

Figure 4.8: Ternary diagrams of LPG/bitumen systems at different temperatures. ○ experimental composition of the light phase; ● experimental composition of the heavy phase; - - - model predictions; — model tie lines. 93

Figure 4.9: A comparison of the ternary diagrams of LPG/bitumen and DME/bitumen systems at 80 °C. ○, ● experimental compositions of light and heavy phases for LPG/bitumen system; ○, ● experimental compositions of light and heavy phases for DME/bitumen

system; - - - model predictions. DME/bitumen data was obtained from our previous study (Sadeghi Yamchi et al., 2020)..... 94

Figure 4.10: Heavy yield of LPG/bitumen systems at different temperatures; ●, ■, ▲, ◆ are experimental data; — model predictions. 95

Figure 5.1: Schematic of induced asphaltene deposition in porous medium due to miscible displacement of bitumen with hot and pressurized dimethyl ether (DME). 108

Figure 5.2: Log viscosity (cP) of bitumen and its fractions versus temperature; ● data points, — model predictions. The experimental data are obtained from Zirrahi et al. (2017). 115

Figure 5.3: Effect of viscous fingering on the rate of the total mass of deposited asphaltene in the domain for fine grid models; Comparison between 2D ($\Delta x=\Delta y=0.5$ cm, $N_x=200$, $N_y=160$) and 1D ($\Delta x=0.5$ cm, $N_x=200$) models. 118

Figure 5.4: Mole fraction of DME as it displaces the oil for deposition rates of 0.5, 50, and 500 1/day after 60 and 150 min. 119

Figure 5.5: Concentration of the deposited asphaltene in kg/m^3 of the current pore volume for deposition rates of 0.5, 50, and 500 1/day after 2.5, 10, 24, 48 hours and 5 days. 120

Figure 5.6: Permeability reduction due to solid deposition for deposition rates of 0.5, 50, and 500 1/day at 2.5, 10, 24, 48 hours and 5 days. 123

Figure 5.7: (a) In-situ degree of upgrading versus time, (b) ultimate degree of upgrading for different deposition rates. 124

Figure 5.8: Comparisons of the total mass of deposited asphaltenes in the domain between the fine and coarse grid cases for four deposition rates of 0.5, 5, 50, 500 1/day. 127

Figure 5.9: Optimization results to match the deposited asphaltene curve of the base case with a deposition rate of 0.5 for a grid size of a) 1 cm, b) 2 cm, and c) 5 cm. 128

Figure 5.10: Upscaled deposition rates versus grid size; ▲, ♦, ●, ■ are data points, and ---- is a trendline. 129

List of Symbols, Abbreviations and Nomenclature

Abbreviations

AARD	Average absolute relative deviation
ASPH	Asphaltene
ASTM	American society for testing and materials
CSS	Cyclic steam stimulation
DME	Dimethyl ether
GC	Gas chromatography
GPC	Gel permeation chromatography
HPHT	High-pressure high-temperature
LL	Liquid-liquid
LLE	Liquid-liquid equilibrium
LPG	Liquified petroleum gas
MW-M	Molecular weight
NRTL	Non-random two liquids
N-solv	Hot solvent injection process
OF	Objective function
PR EoS	Peng-Robinson equation of state
PVT	Pressure-volume-temperature
SAGD	Steam-assisted gravity drainage
SD-SimDist	Simulated distillation
SG	Specific gravity
VAPEX	Vapor extraction

VLE	Vapor-liquid equilibrium
VLLE	Vapor-liquid-liquid equilibrium
VPO	Vapor pressure osmometer
wt.	Weight fraction

Nomenclature

a	Characteristic interfacial area
a_1-a_6	Coefficients of viscosity correlation
C	Concentration factor
C_p	Pressure coefficient in density correlation
C_{pt}	Coefficient in density correlation
C_t	Temperature coefficient in density correlation
D	Fickian diffusion coefficient
d	Diffusion length
E_a	Activation energy
G	Characteristic of interaction energy
k	Permeability
k	Deposition rate
N	Total number of components
Off	Cumulative yield
P	Pressure
r	Deposition rate
R	Universal gas constant

S	Saturation
T	Temperature
x	Mole fraction

Greek letters

α	Coefficient in NRTL model
α	Porosity exponent in permeability correlation
γ	Activity coefficient
η	Degree of upgrading
μ	Viscosity
ν	Molar volume
ρ	Density
τ	Energy interaction parameter
τ	Non-equilibrium mass transfer
ϕ	Porosity
ω	Mass fraction

Scripts

asph	Asphaltene
C	Cut
calc	Calculated
e	Order of the reaction
exp	Experimental

H	Heavy
i,j	Number of components
L	Light
L	Liquid phase
mix	Mixture
o	Oil
r	Relative

Chapter One: **Overview**

1.1 Motivations, Objectives, Steps, and Organization

Due to the recent environmental concerns associated with SAGD process and low oil prices, the oilsands industry is moving toward field-scale applications of low temperature solvent-aided recovery processes to reduce energy consumption and minimize environmental footprints. Interaction of the injected solvent with the host fluid of the reservoir can result in different thermodynamic conditions. Depending on the temperature, pressure, and solvent concentration, vapor-liquid (VL) (Zirrahi et al., 2014), liquid-liquid (LL) (Sadeghi Yamchi et al., 2020, 2018), or even vapor-liquid-liquid equilibria (VLLE) (Krejbjerg and Pedersen, 2006) can be formed in the reservoir. Therefore, thermodynamic studies of the solvent/bitumen system are critical for the design and optimization of a successful solvent-aided recovery process. Techniques for collecting VLE data of solvent and bitumen mixtures are well established and an extensive number of studies have addressed VLE in the literature (Al-Gawfi et al., 2019; Azinfar et al., 2018a, 2018b, 2017; Bin Dahbag et al., 2019; Haddadnia et al., 2018a, 2018b, 2018c; Zirahi et al., 2020; Zirrahi et al., 2017a, 2017b, 2017c, 2017d). In contrast, there is an evident gap for both experimental data and predictive models for LLE of solvent and bitumen mixtures. The existing works in the literature, are either limited to only determining the boundaries between VL and LL regions or they lack to offer a comprehensive characterization of the phases at equilibrium (Kariznovi, 2013; Mancilla-Polanco et al., 2017; Nourozieh, 2013; Perez Claro et al., 2019). Moreover, no study has addressed the LLE of a multi-component solvent or biobased solvent such as dimethyl ether (DME). The lack of LLE data has led to a gap in the application of compositional dependent LL K-values in the simulation of asphaltene deposition in the reservoir induced by solvent injection.

This study investigates the LLE of solvent and bitumen system. The solvents for this study are butane, DME, and a mixture of butane with propane (LPG). The main goals of this project are: 1) to measure liquid-liquid phase equilibrium data for solvent /bitumen mixtures, 2) to develop a thermodynamic model to predict the equilibrium compositions of the phases and, 3) to simulate the asphaltene deposition in porous media by implementing LLE K-values.

We established the following steps to accomplish the goals of this work:

1) Designing, fabricating, and validating a PVT apparatus to collect a comprehensive set of phase behavior data for solvent and bitumen systems.

2) Measuring the liquid-liquid equilibrium data such as the composition of the phases, density and viscosity of the light phase, heavy phase yield, and saturation pressures for solvent (butane, DME, and butane + propane)/bitumen mixtures at temperatures and pressures up to 100 °C, and 3.5 MPa, respectively.

3) Characterizing the light and heavy cuts recovered from the experiments using simulated distillation (SD) and gel permeation chromatography (GPC).

4) Defining pseudocomponents based on the detailed characterization and molecular weight distributions.

5) Developing a thermodynamic model based on Non-Random Two Liquid (NRTL) theory to predict the LLE K-values of the solvent and pseudocomponents in the system.

6) Simulating asphaltene deposition in porous media induced by solvent injection by the implementation of liquid-liquid K-values and a reaction-based non-equilibrium mass transfer model.

The results of this work address some of the existing gaps for LLE data of a multi-component solvent and bio-based solvent with bitumen mixtures and find applications in the optimization and engineering of the solvent composition for solvent-based process. Moreover, the devolved thermodynamic models can be implemented to properly estimate the partitioning of the components into the phases which can be used for further simulation works. In addition, we presented a modified approach for the numerical simulation of asphaltene deposition by implementing the LLE K-values obtained from the experiment. The simulation studies are required for prediction and mitigation of the problems associated with asphaltene precipitation and subsequent deposition.

1.2 Dissertation Outline

This thesis consists of six chapters. Chapter one includes the introduction, Chapters two to five are the core material of the thesis followed by conclusions with recommendations presented in Chapter six. Chapters two and three have been published in peer-reviewed journals, and Chapters four and five have been submitted for publication.

Chapter two investigates the LLE of butane/bitumen mixtures. Thermophysical properties including the composition, density, and viscosity of the light phase are measured and the cuts are characterized using simulated distillation. Moreover, the effect of additives such as DME, propane, and toluene on LLE of butane/bitumen is evaluated. This chapter has been published in Chemical Engineering Research and Design, volume 137, September 2018, pages 452-460.

Chapter three presents LLE measurements and modeling of DME/bitumen system. Equilibrium composition of DME, density, and viscosity of the light phase as well as saturation pressures of the mixtures are measured. Compositional analysis of the heavy and light cuts is determined by

coupling Simulated Distillation (SD) and Gel Permeation Chromatography (GPC). Furthermore, NRTL model is tuned to predict the equilibrium K-values. This chapter has been published in Fluid Phase Equilibria, volume 512, May 2020, 112549.

Comprehensive LLE measurements for LPG (propane + butane)/bitumen mixtures are reported in Chapter four. Equilibrium compositions of propane and butane along with the density and viscosity of the light phase are measured in each experiment. Then, the heavy yield or the amount of precipitation is determined. The molecular weight distribution of the cuts is determined using combined Simulated Distillation (SD) and Gel Permeation Chromatography (GPC). Additionally, NRTL model is tuned to predict the equilibrium compositions. This chapter has been submitted for publication.

A modified approach for simulation of induced asphaltene deposition due to solvent injection is discussed in Chapter five. This approach can be performed using CMG-STARS by implementing experimental LLE K-values and a reaction based non-equilibrium mass transfer term. This chapter has been submitted for publication.

Finally, Chapter six summarizes the findings and contributions of this work and suggests recommendations for future work.

Validation of the experimental setup is explained in Appendix A and copies of copyright permission for the published articles are provided in Appendix B.

1.3 References

Al-Gawfi, A., Zirrahi, M., Hassanzadeh, H., Abedi, J., 2019. Development of Generalized Correlations for Thermophysical Properties of Light Hydrocarbon Solvents (C1-C5)/Bitumen Systems Using Genetic Programming. ACS Omega 4, 6955–6967.

Azinfar, B., Haddadnia, A., Zirrahi, M., Hassanzadeh, H., Abedi, J., 2018a. Phase behaviour of butane/bitumen fractions: Experimental and modeling studies. Fuel 220, 47–59.

Azinfar, B., Haddadnia, A., Zirrahi, M., Hassanzadeh, H., Abedi, J., 2018b. A thermodynamic model to predict propane solubility in bitumen and heavy oil based on experimental fractionation and characterization. J. Pet. Sci. Eng. 168, 156–177.

Azinfar, B., Haddadnia, A., Zirrahi, M., Hassanzadeh, H., Abedi, J., 2017. Effect of Asphaltene on Phase Behavior and Thermophysical Properties of Solvent/Bitumen Systems. J. Chem. Eng. Data 62, 547–557.

Bin Dahbag, M., Zirrahi, M., Hassanzadeh, H., 2019. Solubility and Liquid Density of Ammonia/Athabasca Bitumen Mixtures at Temperatures up to 463 K: Measurements and Modeling. J. Chem. Eng. Data 64, 3592–3597.

Haddadnia, A., Azinfar, B., Zirrahi, M., Hassanzadeh, H., Abedi, J., 2018a. Thermophysical properties of dimethyl ether/Athabasca bitumen system. Can. J. Chem. Eng. 96, 597–604.

Haddadnia, A., Sadeghi Yamchi, H., Zirrahi, M., Hassanzadeh, H., Abedi, J., 2018b. New Solubility and Viscosity Measurements for Methane-, Ethane-, Propane-, and Butane-Athabasca Bitumen Systems at High Temperatures up to 260 °c. J. Chem. Eng. Data 63, 3566–3571.

Haddadnia, A., Zirrahi, M., Hassanzadeh, H., Abedi, J., 2018c. Thermo-physical properties of N-Pentane/Bitumen and N-Hexane/Bitumen mixture systems. Can. J. Chem. Eng. 96, 339–351.

Kariznovi, M., 2013. Phase Behaviour Study and Physical Properties Measurement for Athabasca Bitumen / Solvent Systems Applicable for Thermal and Hybrid Solvent Recovery Processes, PhD thesis, University of Calgary.

Krejbjerg, K., Pedersen, K.S., 2006. Controlling VLLE equilibrium with a Cubic EoS in heavy oil modeling, in: Canadian International Petroleum Conference. Calgary, Alberta.

Mancilla-Polanco, A., Schoeggl, F.F., Johnston, K., Richardson, W.D.L., Yarranton, H.W., Taylor, S.D., 2017. The phase behavior of heavy oil and propane mixtures, in: SPE Canada Heavy Oil Technical Conference. Calgary, Alberta.

Nourozieh, H., 2013. Phase Partitioning and Thermo-physical Properties of Athabasca Bitumen / Solvent Mixtures, PhD thesis, University of Calgary.

Perez Claro, Y.A., Schoeggl, F.F., Taylor, S.D., Yarranton, H.W., 2019. Phase Behavior of Mixtures of Bitumen and n-Butane. Energy and Fuels 33, 8530–8543.

Sadeghi Yamchi, H., Zirrahi, M., Hassanzadeh, H., Abedi, J., 2020. Measurements and NRTL modeling of liquid-liquid equilibrium of dimethyl ether/bitumen. Fluid Phase Equilib. 512, 112549.

Sadeghi Yamchi, H., Zirrahi, M., Hassanzadeh, H., Abedi, J., Fadaei, H., 2018. Effect of additives on liquid–liquid equilibrium properties of butane/bitumen systems with applications to solvent aided bitumen recovery processes. Chem. Eng. Res. Des. 137, 452–460.

Zirahi, A., Sadeghi Yamchi, H., Haddadnia, A., Zirrahi, M., Hassanzadeh, H., Abedi, J., 2020.

Ethyl acetate as a bio-based solvent to reduce energy intensity and CO2 emissions of in situ bitumen recovery. AIChE J. 66.

Zirrahi, M., Hassanzadeh, H., Abedi, J., 2017a. Experimental and modeling studies of MacKay River bitumen and water. J. Pet. Sci. Eng. 151, 305–310.

Zirrahi, M., Hassanzadeh, H., Abedi, J., 2017b. Experimental and modelling studies of MacKay River bitumen and light n-alkane binaries. Can. J. Chem. Eng. 95, 1417–1427.

Zirrahi, M., Hassanzadeh, H., Abedi, J., 2017c. Experimental and modeling studies of water, light n-alkanes and MacKay River bitumen ternary systems. Fuel 196, 1–12.

Zirrahi, M., Hassanzadeh, H., Abedi, J., 2017d. Water content of light n-alkanes: New measurements and cubic-plus-association equation of state modeling. AIChE J. 63, 1384–1389.

Zirrahi, M., Hassanzadeh, H., Abedi, J., Moshfeghian, M., 2014. Prediction of solubility of CH4, C2H6, CO2, N2 and CO in bitumen. Can. J. Chem. Eng. 92, 563–572.

Chapter Two: **Liquid-Liquid Equilibrium of Butane + Additives/Bitumen**

2.1 Preface

This chapter has been published in Chemical Engineering Research and Design entitled "Effect of Additives on Liquid–Liquid Equilibrium Properties of Butane/Bitumen Systems with Applications to Solvent Aided Bitumen Recovery Processes". This manuscript was co-authored by M. Zirrahi, H. Hassanzadeh, J. Abedi, and H. Fadaei. Since this dissertation has been prepared on paper-based format, unavoidably, there are some repetitive parts in each chapter, mainly Chapters 2, 3, and 4, such as experimental setup and characterization descriptions.

In this chapter liquid-liquid equilibrium (LLE) of butane/bitumen is studied and the effect of additives on the equilibrium properties is discussed.

2.2 Abstract

Solvent-aided bitumen recovery processes are relatively new approaches to reduce the negative environmental impacts and production costs of steam assisted gravity drainage (SAGD). Thermo-physical properties of these systems such as density, viscosity, phase partitioning and saturation pressure are of great importance in the design of solvent-aided processes. Butane is a promising solvent for solvent-aided bitumen recovery processes. Addition of light or heavier solvents to butane can provide an engineering solution to improve the efficiency of solvent-aided processes. In this study, equilibrium measurements of butane and bitumen mixture were conducted at temperatures of 40 and 60 °C and pressures well above the vapour pressure of the solvent. Then, the effect of introducing a second solvent as an additive to the butane-bitumen mixture was investigated. Propane, toluene, and dimethyl ether were added to the original mixtures of butane and bitumen in separate sets of experiments and changes in thermo-physical properties were

determined. It was determined that adding butane can lower the viscosity of the bitumen by several orders of magnitude. It was also concluded that although propane can significantly increase the saturation pressure of the mixture, it results in a higher amount of asphaltene precipitation. The effect of dimethyl ether however is favourable because not only increases the vapour pressure but also reduces the asphaltene precipitation similar to toluene.

2.3 Introduction

Steam assisted gravity drainage (SAGD) and other thermal recovery methods such as cyclic steam stimulation (CSS) have been applied to the heavy oil and bitumen reservoirs in Alberta for the past two decades. Associated heat within water steam is the most important element in thermal recovery processes which can facilitate the mobility of heavy oil as heat transfers to the reservoir. However, heat loss and inefficiency of SAGD requires consuming massive amount of energy which in consequence lead in emitting tons of greenhouse gases to the atmosphere. As the environmental issues become more stringent, implementation of new recovery processes in recovering heavy oil and bitumen is inevitable. Solvent-aided bitumen recovery methods are considered to be amongst new processes that are gaining popularity to compensate for the shortcomings of steam assisted gravity drainage (SAGD). In these methods, solvent reduces the viscosity of in-situ bitumen in conjunction with heat which results in increasing of the efficiency of bitumen production. Therefore, a solvent-aided process improves the efficiency of recovering bitumen and at the same time reduces the cost of operations and the adverse impacts of SAGD by using less water and less negative environmental impact.

Examples of co-injection of solvent and steam are abundant in the literature (Gupta and Gittins, 2006; Kar et al., 2017; Nasr et al., 1991; Redford, 1982; Redford and McKay, 1980). However,

these methods have not gained as much acceptance until recently due to inconclusive pilot projects, low oil prices and environmental motivation. Redford and McKay (1980) and Redford (1982) demonstrated experimentally that co-injection of the hydrocarbon additives and steam would considerably increase the recovery of Athabasca bitumen. Nasr et al. (1991) tested the co-injection of naphtha with steam and reported a significant increase in the final recovery compared to the injection of steam only. Gupta and Gittins (2006) presented the initial results of the solvent assisted process (SAP) pilot test on EnCana's Christina Lake project. The findings were promising and an increase of 150 ton/day in the heavy oil production was reported because of the co-injection of butane with steam. Another important result of their work was an improvement in the quality of the produced oil because of the extraction of the light components by butane. Kar et al. (2017) performed some propane-SAGD tests and showed that the displacement recovery and the quality of oil increased compared to SAGD.

One of the important aspects of the solvent assisted processes that should be addressed is the formation of the second dense phase, which is mostly known as the asphaltene rich phase. The effects of asphaltene precipitation on the ultimate recovery of ES-SAGD processes have been widely studied (Al-Murayri et al., 2016; Azinfar et al., 2017; Badamchi-Zadeh et al., 2011; Kar et al., 2015; Li et al., 2011; Pathak et al., 2011). However, the phase equilibrium of bitumen/solvent systems has not been studied in detail. Therefore, the phase behaviour of the solvents and bitumen or heavy oil systems should be examined to better understand the mechanisms associated with lighter component extractions as well as the overall performance of solvent-aided processes.

There are very limited number of studies that experimentally investigate liquid-liquid equilibrium of light n-alkanes and bitumen systems. Badamchi-Zadeh et al. (2009) studied propane and

Athabasca bitumen mixtures and examined their phase behaviour. They reported existence of the second dense phase at propane concentration above 20 wt.%. However, their study was mainly concentrated on mixtures with propane composition below 20 wt.%.

A comprehensive experimental study on light n-alkanes-bitumen systems can be found in publications by SHARP research group at University of Calgary (Azinfar et al., 2018a,b; Haddadnia et al., 2018a; Zirrahi et al., 2017a, 2017b). Zirrahi et al. (2017a,b) measured the solubility of light n-alkanes (methane, ethane, propane and butane) in MacKay River bitumen at temperatures up to 463.15 K and pressures up to 5 MPa. They also reported the density and viscosity of the bitumen rich phase and modelled their data by Peng-Robinson equation. Haddadnia et al. (2018a) measured the thermodynamic properties of Dimethyl Ether/Athabasca Bitumen including solubility, density, and viscosity at temperatures of 100, 125 and 150 °C and pressures up to 6 MPa. Azinfar et al. (2018a,b) studied the phase behaviour of butane and bitumen fractions extracted from vacuum distillation method and proposed a generalized EoS model for their experimental data.

A detailed study of the liquid-liquid equilibrium of n-butane/Athabasca bitumen was carried out by Nourozieh et al. (2014). The operational pressures for liquid-liquid separation in their study were 2MPa at 50 and 100 °C and 4 MPa at 150 °C. They reported a minimum butane concentration of 0.5 weight fraction in order to have two liquids in the system. Viscosity and density of both heavy and light phases were measured. They also reported fluctuations in the property measurements of the heavy phase. They concluded adding more butane to the system reduce the density and viscosity of the light phase. Their results showed that the overall concentration of butane and pressure have a significant effect on the composition of the phases. A similar study was

done by Nourozieh et al. (2012) on liquid-liquid equilibrium of Athabasca bitumen/propane systems at different temperatures and pressures as well as the extraction of light components out of those mixtures. Their results showed that at a constant temperature and initial mass fraction of the solvent, the extraction yield increased with pressure, however, the extraction yield was insensitive to the feed concentration at constant pressure. They reported that the second phase (L2) became heavier as the pressure and solvent to bitumen ratio were increased.

Gao et al. (2016) investigated multiphase behaviour of n-butane/bitumen/water systems. They observed liquid-liquid separation of hydrocarbons in n-butane/bitumen systems with/without water at n-butane concentrations of 97 mol% in wide ranges of temperatures and pressures. They visually inspected the boundaries and the color of each phase in equilibrium. Their findings indicated that with decreasing pressure the color of L2 became lighter suggesting a selective extraction of the bitumen component to the light phase by butane.

To design and operate a successful butane injection process many parameters such as asphaltene precipitation, vapour pressure of the system, and extraction efficiency should be studied and optimized. While higher vapour pressure is always desirable because of the higher driving force in the reservoir to assist the flow of the mobile bitumen toward production well, asphaltene precipitation is only favourable when it happens far from production well. Deposition of asphaltene in the reservoir results in an in-situ upgrading. Lighter solvents like propane result in higher vapour pressure and more asphaltene precipitation with the extraction of lighter components. Butane precipitates less asphaltene and has a lower vapour pressure compared to propane. These phenomena can be optimized using proper design of the solvent composition. Addition of light or heavy solvents to the base solvent can be a tool to control the aforementioned

properties. For example, in the early stages of butane injection, addition of heavy solvent prevents the asphaltene precipitation around the wellbore. After depletion of the bitumen in the area near wellbore, the addition of light solvent increases the amount of asphaltene precipitation and quality of the produced oil.

In this article, a detailed liquid-liquid equilibrium study of solvent and bitumen mixtures has been conducted. Butane/bitumen system was considered as a baseline and then the effect of adding propane, toluene, and dimethyl ether on phase equilibrium of base mixture is investigated. Moreover, the improvements of adding fractions of secondary solvent on PVT properties of the butane/bitumen mixtures are discussed. The rest of this paper is organized as follows: first we present the experimental apparatus utilized to conduct the experiments. Then, the results and discussions will be presented followed by summary and conclusion.

2.4 Experimental Apparatus

The schematic diagram of the apparatus is shown in Figure 2.1. It consists of an equilibration cell (5), densitometer (7), viscometer (8), and sampling cells (9), which all are installed inside a temperature controlled Blue-M oven (1) with density and viscosity data evaluation units (2,3), a receiving cell (6), feeding cells (4) and Quizix pumps (10) placed outside of the oven.

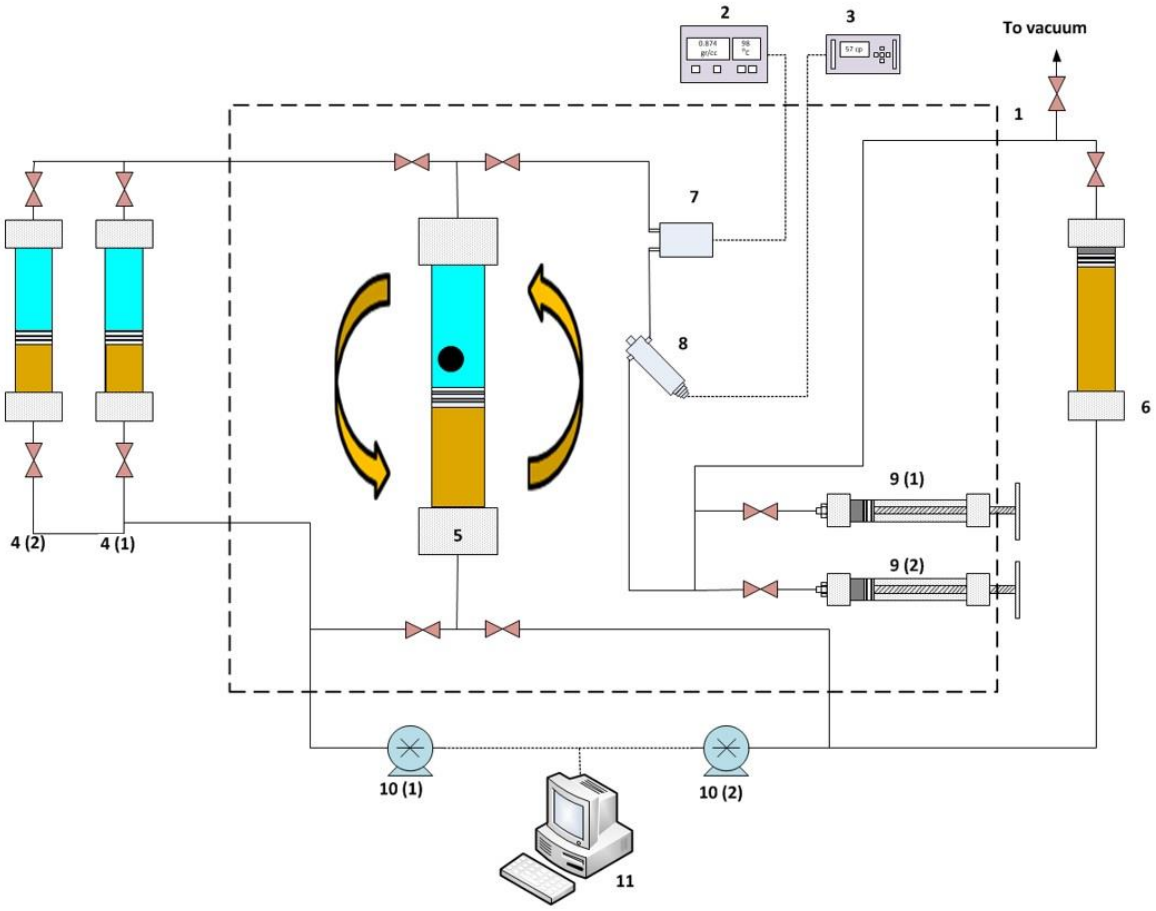

Figure 2.1: Experimental setup for PVT studies of solvent/bitumen systems, (1) Blue-M oven, (2) density data gathering unit, (3) viscosity data gathering unit, (4) feeding cell, (5) equilibration cell, (6) receiving cell, (7) densitometer, (8) viscometer, (9) sample cell, (10) Quizix pump, (11): pump controlling unit.

The two feeding cells (4) can store bitumen and solvent at room temperature and desired pressure and can be operated by Quzix pump to inject bitumen and solvents into the equilibration cell (5). Pressures of the feeding cells (4), equilibrations cell (5) and receiving cell (6) can be controlled by Quizix pumps (10). These pumps can inject or receive water with an accuracy of (±) 0.003 cm3 to

displace the piston located inside the cells and subsequently adjust the pressure. To avoid any contamination of the fluids with water pistons are sealed with Viton O-rings.

The equilibration cell (5) can rotate half a circle around an axis by means of a rocking system attached to the cell. This system and the rocking ball placed in the cell accelerate the process of mixing of bitumen and solvent. Therefore, equilibration can be achieved faster. The capacity of the cell is about 850 cc, which allows to have sufficient saturated phases for the thermo-physical property measurements such as density and viscosity. Moreover, this volume of fluids increases the reliability of the phase detection and also eases the process of acquiring samples for further compositional analysis.

Phases in equilibrium are transferred from the top of the equilibration cell through a densitometer and viscometer at constant pressure and temperature (equilibrium T and P). Injecting the fluids in a density and viscosity measuring units which are attached to the system in series, improves the detection of any small changes in the properties of the phases and overall, increases the accuracy of the detection of phases. Sampling is conducted with two small screw-cells (9). Once the readings of the viscosity and density are steady, the valves on top of the sampling cells (9) can be opened and the sample fluids can be collected by unscrewing the handle of the cell (Zirrahi et al., 2017b).

Before starting any experiment, all the cells and lines of the system were purged with butane and then it was vacuumed to remove any existing impurities. To charge the equilibration cell pre-determined volumes of bitumen and solvent were injected by means of the Quizix pump and then the mass of each substance was calculated based on its density at injection pressure and room temperature. After charging the system, the oven was turned on and set to reach the desired temperature and the pressure of the system was controlled by Quizix pump. After 2-3 days of

mixing, the equilibration cell was kept in vertical position for a day to let the formed phases segregate.

Prior to discharging the fluid, the system was pressurized with nitrogen gas up to the equilibrium pressure to prevent any pressure drop or disturbance in equilibrium. Nitrogen gas behaves as a carrier (inert) gas and has no effect on the composition of the samples. The discharged fluid on the way to the receiving cell passed through Anton Paar densitometer and Cambridge viscometer. The Anton Paar densitometer can detect densities as low as 0 - 3 g/cm^3 with an accuracy of 0.001 - 0.0001 g/cm^3. The applicable rage of temperature and pressure for density measurements are -10 to +200 °C and 0 to 10000 psi, respectively. The Cambridge viscometer is able to record viscosities in the range of 0.2 to 20000 cp with an accuracy of ±1.0% at the temperatures and pressures up to 350 °C and 20000 psi, respectively.

Collected samples were used for compositional analysis. In order to determine the amount of solvent in light phase, each sample was flashed into the gasometer (Chandler Engineering) and the volume of the gas (solvent) was measured and its mass was then calculated using the density of the gas at room temperature and pressure. In addition, Gas Chromatography (GC) was also utilized to confirm the accuracy of the results obtained from gasometer. After recovering the solvent, the extracted bitumen (light phase) was collected and heated up in a vacuum oven to obtain the light fraction from the process. Preparing the heavy fraction, however, was different than the light fraction. Since the heavy phase was highly viscous and nearly immobile at the experimental conditions toluene was added to the heavy phase after discharging the light phase from the system, this allows for an easier discharge of heavy phase without exerting extra pressure on the pumps. Thereafter, the heavy cut was extracted by evaporating the toluene and solvent from the solution.

2.5 Results and Discussion

Effects of solvent additives on liquid-liquid equilibrium of n-butane/bitumen mixtures were investigated in this study. Athabasca bitumen with MW of 520 g/g-mol and gravity of 8 °API was tested in the experiments. The SARA analysis indicated the bitumen was composed of 11.76, 57.00, 21.61, and 9.62 wt.% saturates, aromatics, resins, and asphaltenes, respectively (Kariznovi, 2013). The boiling point distribution of the bitumen sample obtained from simdist is shown in Figure 2.3. Butane, propane, dimethyl ether were purchased from Praxair Canada Co and toluene was provided by Sigma-Aldrich with a purity of 98%. First, a mixture of 60 wt.% butane and 40 wt.% bitumen was prepared and thermo-physical properties of the mixture at equilibrium were measured at 150 psi and 40 and 60 °C. Moreover, compositional analysis of the heavy and light fractions (L1 and L2) extracted from this test was conducted by means of simulated distillation.

2.5.1 Effect of Propane Addition

N-alkanes lighter than butane are more volatile and their vapour pressure is high enough to create a significant effect on the phase behaviour properties of butane and bitumen mixtures. In order to study such an effect, two different concentrations of 10 wt.% and 20 wt.% propane (weight of propane/[weight of propane + butane + bitumen]) were added to the original mixture of 60 wt.% of butane/ bitumen in separate experiments and PVT properties of the mixture were measured. This set of experiments was conducted at 60 °C and 400 psi instead of 150 psi to ensure all components are kept in the liquid phase and to avoid presence of vapour phase in the system. As presented in Figure 2.2 density and mass fraction of light phase decrease with the concentration of propane. Significant reduction in the density is because of two reasons, first, the addition of the second solvent, which is lighter than butane, and second more asphaltene precipitation occurs by

adding propane to the system, this precipitation extracts heavy compounds out of bitumen and makes the light phase even lighter. As expected, addition of propane increases the saturation pressure of the mixture drastically.

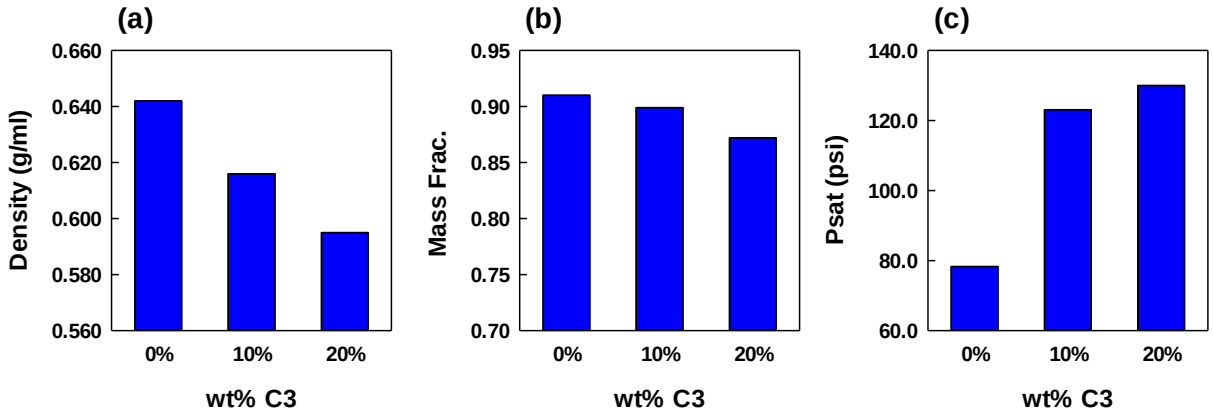

Figure 2.2: (a) density, (b) mass fraction of light phase and (c) saturation pressure of propane-butane/bitumen system.

Simdist results of the fractions extracted by adding propane to the butane and bitumen mixtures are shown in Figures 2.3 and 2.4. As the boiling point distribution of compounds in the fraction suggests, adding propane results in lighter material to be recovered. In another word, more of heavier components are precipitated out of the bitumen. This can also be inferred from the carbon number distribution. Addition of 10 wt.% or 20 wt.% of propane will increase the concentration of the lower carbon number molecules and reduce the portion of heavier molecule in the light cuts. According to the simdist results, the light cuts become lighter by adding more propane while there is no clear trend for the heavy cuts. This observation can be explained as a result of incomplete characterization of the cuts by simdist. The simulated distillation test can only characterize the carbon numbers up to C100. As it is depicted, some portion of the cuts including the heavy ends

have not been characterized and consequently, small alterations in the compositions of the cuts remain indistinguishable.

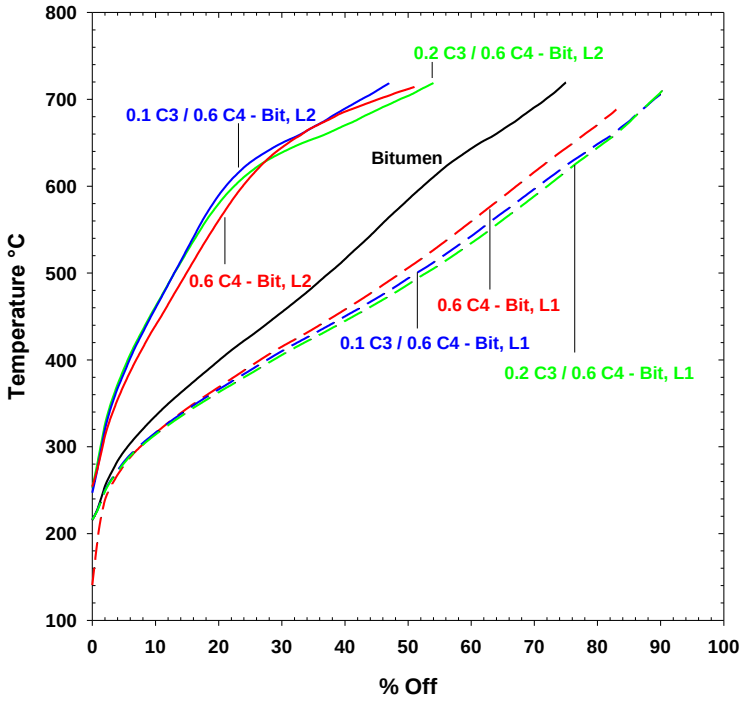

Figure 2.3: Boiling point distribution of the Athabasca bitumen and heavy and light fractions extracted from propane-butane/bitumen.

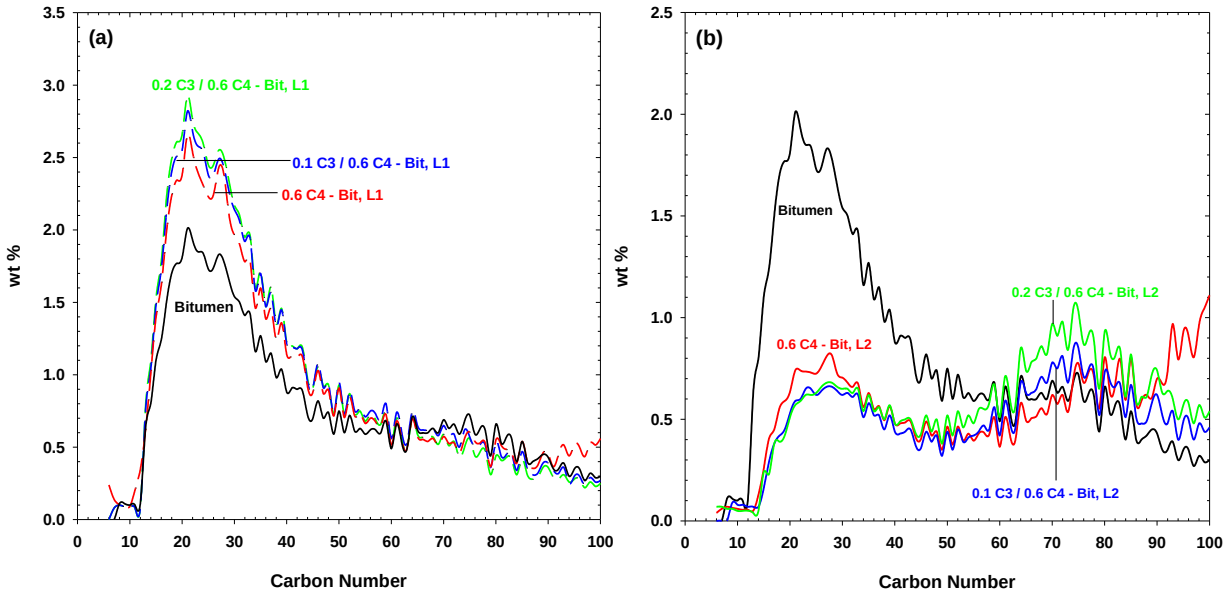

Figure 2.4: Carbon number distribution of the Athabasca bitumen (a) light fractions, and (b) heavy fractions extracted from mixtures of propane-butane/bitumen.

2.5.2 Effect of Toluene Addition

In order to study the effect of toluene addition to the original mixture of 60 wt.% of butane/bitumen, separate experiments were conducted and PVT properties of the mixture were measured. Toluene is an aromatic solvent with the capability of dissolving asphaltenes and it can reduce the problems associated with asphaltene precipitation. As it was explained in the previous section, although propane increases the vapour pressure of the original mixture substantially, it will also cause more asphaltene to be precipitated. This precipitation may be problematic and increase the overall cost of heavy oil production in the long run. Unlike propane, introducing toluene to the mixture of butane and bitumen would not affect the saturation pressure of the mixture since toluene has very low vapour pressure. However, it reduces the amount of precipitated

asphaltene significantly. These results are presented in Figures 2.5. Increase in the density of the light phase indicates that large molecules with higher molecular weight have remained soluble in the solution and asphaltene precipitation is avoided.

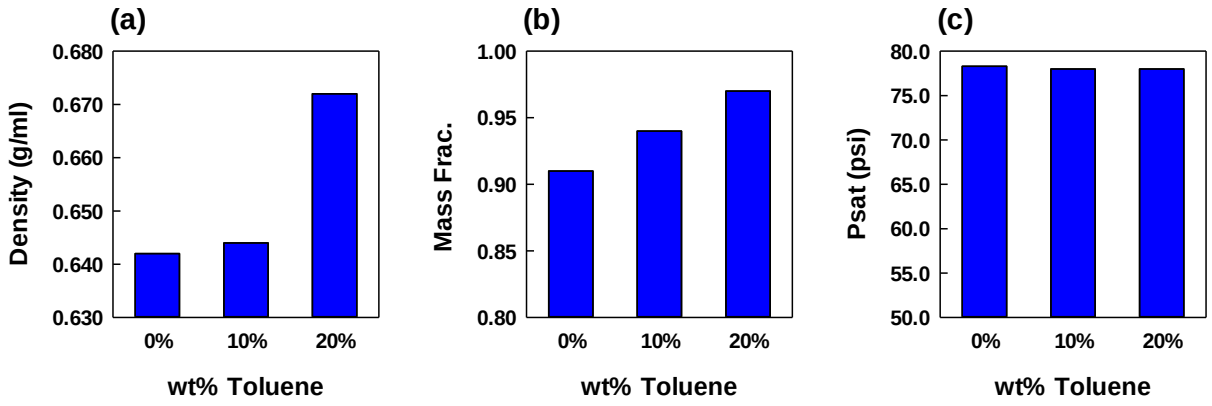

Figure 2.5: (a) density, (b) mass fraction of light phase, and (c) saturation pressure of toluene-butane/bitumen system.

Boiling point distribution of light cuts shows that as the mass fraction of toluene in the mixture increases the composition of the extracted light cut becomes heavier and approaches the composition of the original bitumen (Figure 2.6). The carbon number distribution also has the same behaviour as shown in Figure 2.7. Similar to the propane case, the differences between the heavy cuts could not be captured by simdist.

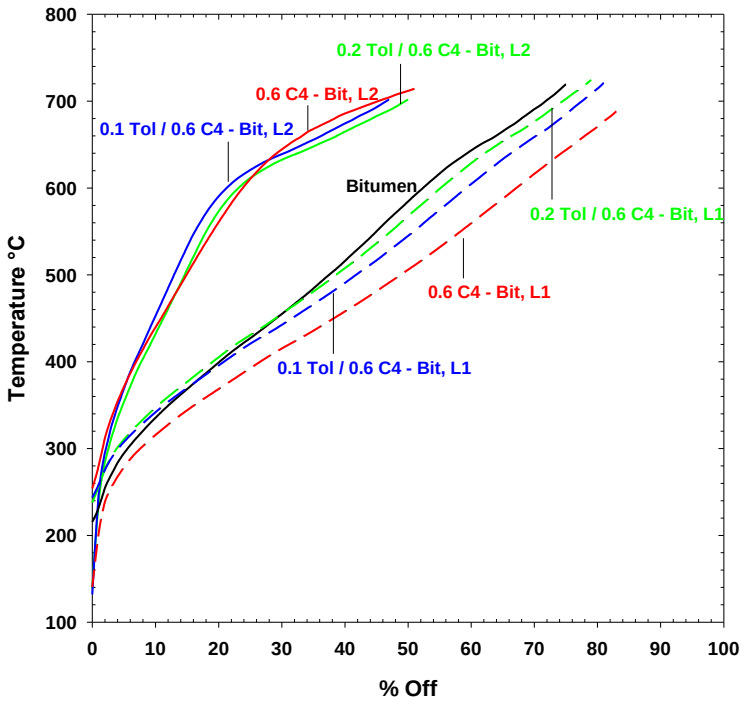

Figure 2.6: Boiling point distribution of the Athabasca bitumen and heavy and light fractions extracted from mixtures of toluene - butane/bitumen.

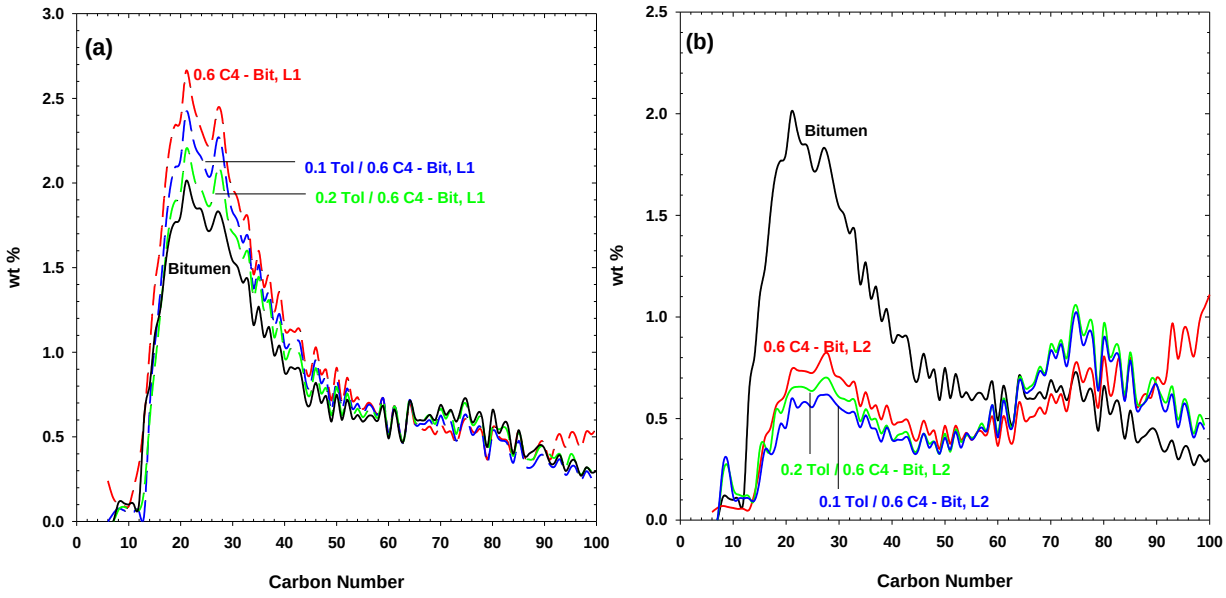

Figure 2.7: Carbon number distribution of the Athabasca bitumen (a) light fractions and (b) heavy fractions extracted from mixtures of toluene-butane/bitumen.

Toluene is an aromatic solvent that can hinder the precipitation of the heaviest and complex structures in bitumen when the equilibrium of the different components of bitumen is disturbed by adding butane. Addition of a small amount of toluene results in the elimination of asphaltene precipitation in the areas such as production well and production lines. Propane with a saturated structure can play a role similar to butane and increase the precipitation of the larger molecules when it is added to the bitumen. However, it increases the saturation pressure of the mixture (butane/propane) resulting in higher dissolution of injected fluids in bitumen and higher driving force to flow the fluids in production well. Although toluene can abundantly be obtained its use in filed scale can be costly. Moreover, as mentioned toluene addition has no effect on vapour pressure and therefore it does not increase the reservoir energy to facilitate the depletion the heavy oil.

2.5.3 Effect of Dimethyl Ether Addition

The last solvent tested was Dimethyl Ether (DME). In order to study the effect of dimethyl ether addition to the original mixture of 60 wt.% of butane/bitumen, separate experiments were conducted, and PVT properties of the mixture were measured. Dimethyl is an organic compound with a formula of CH_3OCH_3 that can be produced from natural gas and organic waste or biomass. The applications of DME is growing not just because it can be produced from many different resources of agricultural and organic waste to fossil fuels but because it is considered to be a great potential for replacement of LPG as it can be liquified and stored conveniently(Haddadnia et al., 2018b). Structurally DME is the simplest ether with polar bonds resulting in dipole interactions between the molecules. 10 wt.% and 20 wt.% of DME was added to the original mixture of butane and bitumen in two separate experiments. The tests were performed at a pressure and temperature of 300 psi and 40 °C, respectively, and thermo-physical properties of the mixtures in equilibrium were measured. The results are shown in Figure 2.8.

The density of light phase (L_1) shows a non-monotonic behaviour. At first, it increases with introducing DME to the solution (10 wt.%) and then decreases at higher mass fraction of DME (20 wt.%). In all previous cases, the light liquid phase density showed a monotonic behaviour. The non-monotonic behaviour of the liquid phase density may be attributed to the polar structure of the DME molecule. To explain this behaviour, change in the amount of asphaltene precipitation due to the addition of dimethyl ether is needed to be determined. Since dimethyl ether is a polar molecule with an oxygen atom and the angular structure of the molecule can result in molecular dipole, it is expected that a reduction of asphaltene precipitation could occur by adding this solvent. According to the results shown in Figure 2.8, the mass fraction of light phase increases with

dimethyl ether addition suggesting that asphaltene precipitation is minimal. Similar to the effect of toluene when the precipitation is low, the presence of heavy molecules in the light phase becomes dominant resulting in denser liquid phase. When the mass fraction of dimethyl ether is 10% the density of light phase is under the influence of larger molecules, which have not been precipitated yet. However, as the concentration of DME increases (20%) the presence of the solvent becomes dominant and the density of light phase decreases.

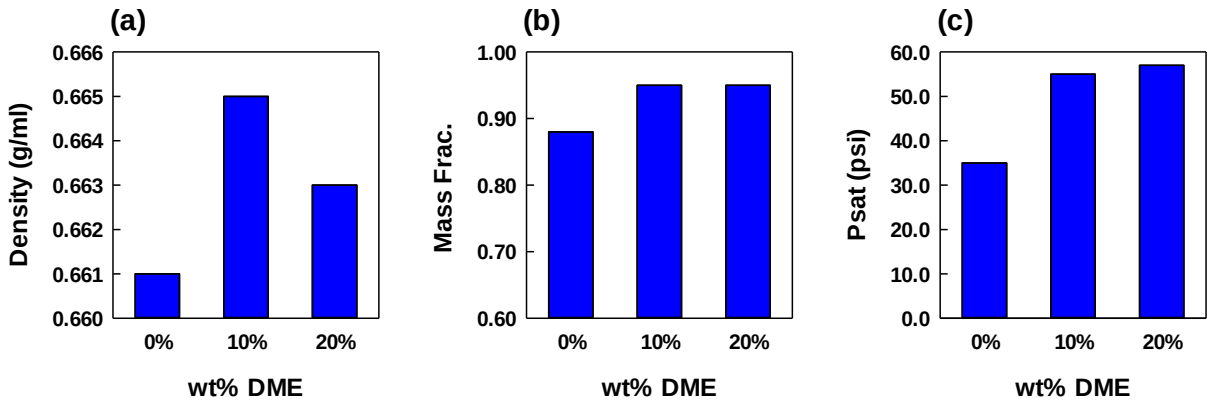

Figure 2.8: Density (a), mass fraction (b) of light phase and saturation pressure (c) of DME-butane/bitumen system.

Since vapour pressure of DME is higher than butane, there is an increase in the measured saturation pressures due to addition of DME. Examination of simdist results demonstrates that effect of DME is similar to toluene. By adding dimethyl ether, the composition of extracted light fraction becomes heavier compared to the one extracted by adding only butane to the bitumen. Both boiling point and carbon number distributions are representing the same effect (Figures 2.9 and 2.10).

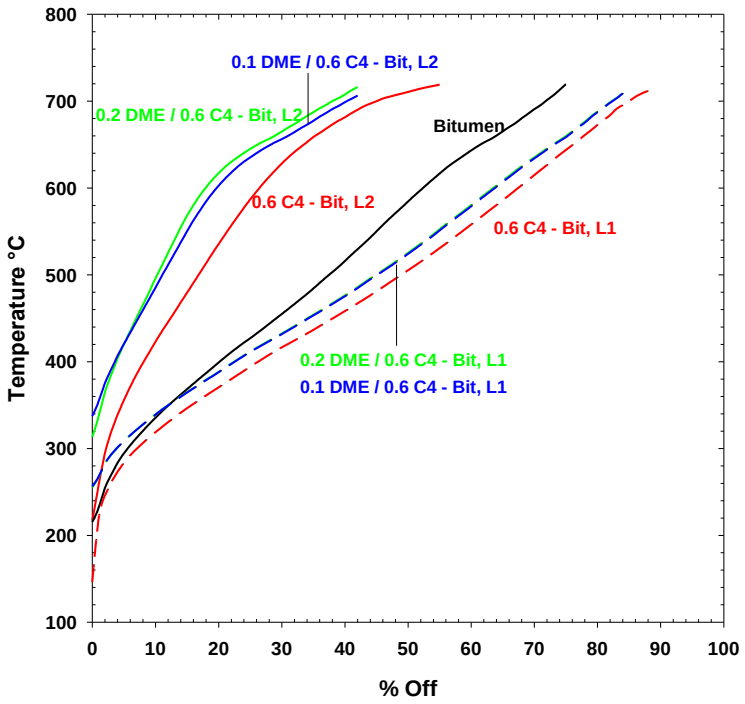

Figure 2.9: Boiling point distribution of the Athabasca bitumen and heavy and light fractions extracted from of DME- butane/bitumen.

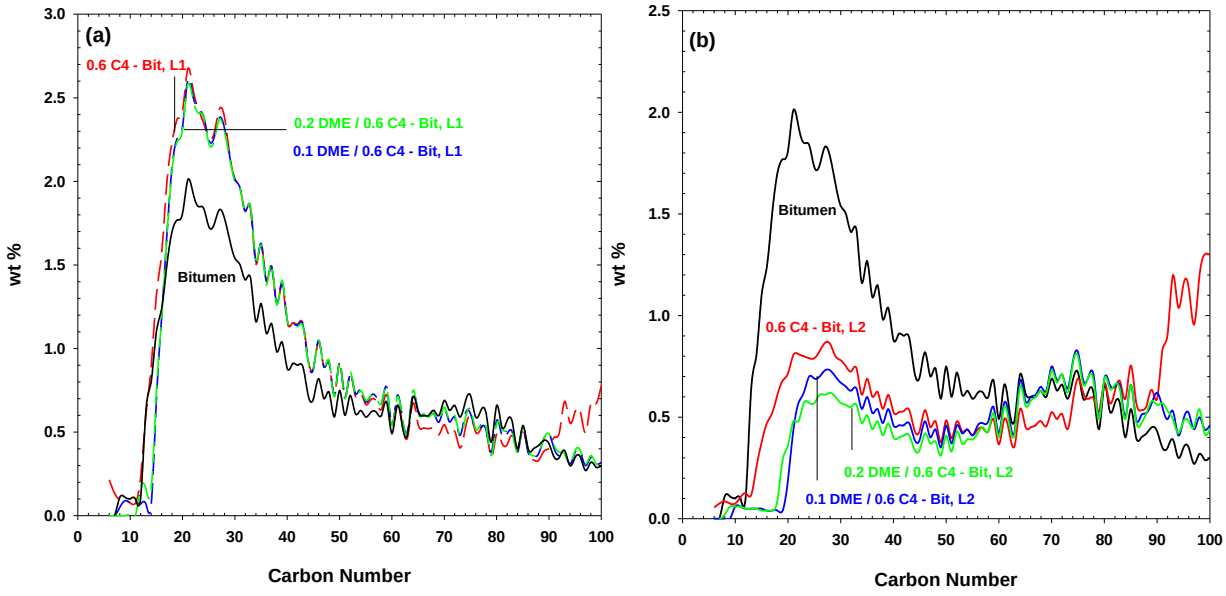

Figure 2.10: Carbon number distribution of the Athabasca bitumen, (a) light fractions, and (b) heavy fractions extracted from mixtures of DME-butane/bitumen.

The results suggest that DME has the potential to be used as an additive in solvent-aided processes because of its unique features (Haddadnia et al., 2018a). A solvent that can increase the saturation pressure and reduce asphaltene precipitation which both factors can be favourable in the production of bitumen and heavy oil. Although DME is not as effective as toluene in preventing precipitation of the heavy components of bitumen it has two great advantages over toluene. First, the use of DME in field scale can be more economical compare to toluene and second, it can facilitate the production of heavy oil by increasing the vapour pressure and consequently energy of the reservoir.

2.6 Summary and Conclusion

In solvent-aided processes, dissolution of solvent in bitumen reduces the viscosity of in-situ bitumen in conjunction with heat and increases the efficiency of bitumen production. Therefore, a solvent-aided process improves the efficiency of recovering bitumen and at the same time reduces the adverse impacts of steam assisted gravity drainage (SAGD) by using less water and less negative environmental impact. Adding n-alkane to the bitumen at a specific temperature and pressure can form two liquid phases in equilibrium. One of the formed phases is light and rich in solvent while the other one is heavy and rich in asphaltenes. Moreover, the composition of the extracted heavy and light fractions provides a measure of the quality of the produced heavy oil.

Phase equilibrium properties of solvent/bitumen systems were measured in this study. A solution of 60 wt.% butane/bitumen was considered as a base mixture and then the effect of the addition of propane, toluene and dimethyl ether as the second solvent on thermo-physical properties of the base solution was investigated.

It was found that addition of 60 wt.% butane to the bitumen would cause separation of two liquids at temperatures of 40 and 60 °C and pressure of 150 psi while the density and viscosity of the light phase in equilibrium condition were considerably low compared to the bitumen, heavy phase was hardly mobile in the same conditions.

It was demonstrated that higher propane concentration could result in higher asphaltene precipitation, whereas the effect of toluene and DME were totally opposite. While the addition of propane resulted in lighter extracted phase, toluene and DME separated heavier components into the light phase. Since the vapour pressure of propane and DME are higher than that of the butane introducing these solvents to the base mixture significantly increased the saturation pressure of the

solution. It was shown that the addition of DME as an additive, results in high saturation pressure and low asphaltene precipitation. These results suggest that DME has the potential to be used as an additive in solvent-aided recovery processes.

2.7 References

Al-Murayri, M.T., Maini, B.B., Harding, T.G., Oskouei, J., 2016. Multicomponent Solvent Co-injection with Steam in Heavy and Extra-Heavy Oil Reservoirs. Energy and Fuels 30, 2604–2616.

Azinfar, B., Haddadnia, A., Zirrahi, M., Hassanzadeh, H., Abedi, J.,2018a. A thermodynamic model to predict propane solubilityin bitumen and heavy oil based on experimental fractionationand characterization. J. Pet. Sci. Eng. 168, 156–177.

Azinfar, B., Haddadnia, A., Zirrahi, M., Hassanzadeh, H., Abedi, J., 2018b. Phase behaviour of butane/bitumen fractions: Experimental and modeling studies. Fuel 220, 47–59.

Azinfar, B., Haddadnia, A., Zirrahi, M., Hassanzadeh, H., Abedi, J., 2017. Effect of Asphaltene on Phase Behavior and Thermophysical Properties of Solvent/Bitumen Systems. J. Chem. Eng. Data 62, 547–557.

Badamchi-Zadeh, A., Kohse, B.F., Kumar, A., 2011. Modeling of Asphaltene Precipitation Due to Steam and n-alkane Co-injection in the ES-SAGD Process. Can. Unconv. Resour. Conf. 1–19.

Badamchi-Zadeh, A., Yarranton, H.W., Svrcek, W.Y., Maini, B.B., 2009. Phase behaviour and physical property measurements for VAPEX solvents: Part I. Propane and athabasca bitumen. J. Can. Pet. Technol. 48, 54–61.

Gao, J., Okuno, R., Li, H.A., 2017. An experimental study of multiphase behavior for n-butane/bitumen/water mixtures. SPE Journal 22, 783–798.

Gupta, S.C., Gittins, S.D., 2006. Christina lake solvent aided process pilot. J. Can. Pet. Technol.

45, 15–18.

Haddadnia, A., Azinfar, B., Zirrahi, M., Hassanzadeh, H., Abedi, J., 2018a. Thermophysical properties of dimethyl ether/Athabasca bitumen system. Can. J. Chem. Eng. 96, 597–604.

Haddadnia, A., Zirrahi, M., Hassanzadeh, H., Abedi, J., 2018b. Dimethylether-A Promising Solvent for ES-SAGD, in: SPE Canada Heavy Oil Technical Conference. Society of Petroleum Engineers, Calgary, Alberta, Canada.

Kar, T., Nezhad, P.B., Ng, A.Z.Y., Texas, A., Ovalles, C., Etc, C., Benson, I.P., 2017. Mobilization of Trapped Residual Oil via Secondary SAGD with Propane, in: SPE Western Regional Meeting. Society of Petroleum Engineers, Bakersfield, California, USA.

Kar, T., Yeoh, J.J., Ovalles, C., Rogel, E., Benson, I., Hascakir, B., 2015. The Impact of Asphaltene Precipitation and Clay Migration on Wettability Alteration for Steam Assisted Gravity Drainage (SAGD) and Expanding. SPE Heavy Oil Conf. - Canada.

Kariznovi, M., 2013. Phase Behaviour Study and Physical Properties Measurement for Athabasca Bitumen / Solvent Systems Applicable for Thermal and Hybrid Solvent Recovery Processes, PhD thesis, University of Calgary.

Li, W., Mamora, D.D., Li, Y., 2011. Solvent-Type and -Ratio Impacts on Solvent-Aided SAGD Process. SPE Reserv. Eval. Eng. 14, 320–331.

Nasr, T.N., Kimber, K.D., Vendrinsky, D.A., Jha, K.N., 1991. Process Enhancement in Horizontal Wells Through the Use of Vertical Drainage Channels and Hydrocarbon Additives, in: SPE Western Regional Meeting. Society of Petroleum Engineers.

Nourozieh, H., Kariznovi, M., Abedi, J., 2014. Phase behaviour study of butane / athabasca

bitumen mixtures applicable for thermal and hybrid solvent recovery processes, in: SPE Heavy Oil Conf. Canada.

Nourozieh, H., Kariznovi, M., Abedi, J., 2012. Liquid-Liquid Equilibria of Solvent/Heavy Crude Systems: In Situ Upgrading and Measurements of Physical Properties, in: SPE Western Regional Meeting. Society of Petroleum Engineers.

Pathak, V., Babadagli, T., Edmunds, N.R., 2011. Heavy oil and bitumen recovery by hot solvent injection. J. Pet. Sci. Eng. 78, 637–645.

Redford, D.A., 1982. Use of Solvents and Gases With Steam in the Recovery of Bitumen From Oil Sands. J. Can. Pet. Technol. 21, 45–53.

Redford, D.A., McKay, A.S., 1980. Hydrocarbon-Steam Processes for Recovery of Bitumen From Oil Sands. SPE/DOE Enhanced Oil Recovery Symposium.

Zirrahi, M., Hassanzadeh, H., Abedi, J., 2017a. Experimental and modelling studies of MacKay River bitumen and light n-alkane binaries. Can. J. Chem. Eng. 95, 1417–1427.

Zirrahi, M., Hassanzadeh, H., Abedi, J., 2017b. Experimental and modeling studies of MacKay River bitumen and water. J. Pet. Sci. Eng. 151, 305–310.

Chapter Three: **Liquid-Liquid Equilibrium of Dimethyl Ether (DME)/Bitumen Mixtures**

3.1 Preface

This chapter has been published in Fluid Phase Equilibria entitled "Measurements and NRTL Modeling of Liquid-Liquid Equilibrium of Dimethyl Ether/Bitumen". This manuscript was co-authored by M. Zirrahi, H. Hassanzadeh, and J. Abedi. Since this dissertation has been prepared on paper-based format, unavoidably, there are some repetitive parts in each chapter, mainly Chapters 2, 3, and 4, such as experimental setup and characterization descriptions.

In this chapter liquid-liquid equilibrium (LLE) of DME/bitumen is studied and a thermodynamic model is developed to reproduce experimental K-values.

3.2 Abstract

Solvent-aided or solvent-based heavy oil recovery methods have shown to be promising alternatives to the conventional thermal methods. Recently, dimethyl ether (DME) has been suggested as a potential candidate for solvent-aided recovery processes. Liquid-liquid equilibrium (LLE) of the DME/bitumen is essential for design and optimization of the oil recovery. While vapor-liquid equilibrium (VLE) data of DME/bitumen have been reported in the literature, LLE data and predictive models for DME/bitumen are lacking. In this work, LLE measurements of DME/bitumen mixtures were conducted. Equilibrium composition of DME, density, and viscosity of the light phase as well as saturation pressures of the mixture were measured. Compositional analysis of the heavy and light cuts was determined by coupling Simulated Distillation (SD) and Gel Permeation Chromatography (GPC). Based on the compositional analysis, bitumen was divided into two pseudocomponents and LL K-values of the components in equilibrium were calculated. Non-Random Two Liquid (NRTL) model was calibrated to represent the experimental

compositional data and K-values. AARD of the model predictions was found to be less than 6.5%. The results presented in this work provide new insight into in-situ upgrading of bitumen and enable better design and optimization of a solvent-aided oil recovery process.

3.3 Introduction

Co-injection of solvent with steam has shown promise to accelerate the extra-heavy oil or bitumen recovery and reduce the energy intensity and environmental impact of steam assisted gravity drainage (SAGD) technique (Li et al., 2011; Sabet et al., 2017). One of the major challenges in field scale application of solvent-aided recovery processes is the complex liquid-liquid equilibrium (LLE) of the solvent/bitumen mixtures, which has not been addressed in the literature. Depending on the conditions of the operations as well as the type of the solvent, solvent/bitumen mixtures can form vapor-liquid (VL), liquid-liquid (LL), or even vapor-liquid-liquid equilibria (VLLE). The formation of two liquids or asphaltene precipitation due to the injection of solvent, particularly at lower temperature applications such as Nsolv and VAPEX, has been widely reported (Badamchi-Zadeh et al., 2011; Mokrys and Butler, 1993; Zhang et al., 2019). Therefore, in addition to vapor-liquid equilibrium (VLE), liquid-liquid equilibrium (LLE) is of critical importance in evaluating the performance of solvent assisted or solvent-based processes.

Since the emergence of the concept of solvent-aided processes n-alkanes were considered as primary candidates. Therefore, phase behavior of n-alkanes and bitumen mixtures and more specifically VLE of these systems has been widely studied. The solubility of solvent in bitumen, as well as the density and viscosity changes of bitumen due to solvent dissolution have been of great interest in VLE studies. Zirrahi et al. (2017) measured solubility of light n-alkanes (C_1-C_4) in Athabasca bitumen at temperatures and pressures up to 190 °C and 5 MPa, respectively. They

modeled the experimental results with PR-EOS. Haddadnia et al. (2018a) extended their previous work and measured solubility of C_1-C_4 in MacKay River bitumen along with viscosity of the saturated liquid at temperatures of 200-260 °C and modeled the VLE of solvent and bitumen using PR-EOS. Fu et al. (1986) reported the solubility of C_1 and C_2 in Cold Lake bitumen at 150 °C. A study of propane and bitumen phase behavior was reported by Nourozieh et al. (2015). They conducted solubility, viscosity, and density measurements at temperatures up to 200 °C and pressures up to 10 MPa. Yazdani and Maini (2010) measured solubility of butane in Frog Lake heavy oil at room temperature. Dini et al. (2016) performed detailed experiments on propane and Peace River bitumen mixtures to measure phase compositions and densities in the temperature range of 303 to 393 K. Gao et al. (2018) reported phase equilibrium data, density, and viscosity of n-hexane/, n-octane/bitumen mixtures at temperatures up to 160 °C.

Recently, novel bio-based solvents have received a great deal of attention due to their potential in reducing the environmental impact of oil recovery compared to hydrocarbon-based solvents. Haddadnia et al. (2018b) performed VLE experiments on DME/bitumen mixtures including measurements of solubility of DME and demonstrated that DME can be as effective as butane in solvent-aided process. Sheng et al. (2018) conducted numerical simulations of solvent-aided recovery process and demonstrated that DME could be a promising solvent. Bin Dahbag et al. (2019) investigated the possible applications of ammonia in a thermal process by conducting phase behavior experiments of ammonia and MacKay River bitumen at temperatures and pressures up to 463 K and 4 MPa, respectively. Zirahi et al. (2019) considered ethyl acetate as an additive to be injected with steam in solvent-aided processes. Their PVT experiments revealed a considerable solubility of ethyl acetate in bitumen. It was found that ethyl acetate could also be as effective as hexane in reducing bitumen viscosity.

Co-injection of solvents with steam not only results in VLE conditions but also leads to condensation of solvent at in-situ reservoir temperatures and hence formation of LLE. Therefore, complex LLE of solvent/bitumen needs to be addressed. However, the number of articles found in this topic is scarce. Kariznovi (2013) and Nourozieh (2013) have reported the presence of liquid-liquid region in ethane/ propane/ and butane/bitumen systems. Their measurement included the composition of solvent in each phase and also the density and viscosity of the phases in equilibrium. The minimum concentration of propane and butane in the feed for liquid-liquid formation was reported to be 40 wt.% and 50 wt.%, respectively. More recently, Perez et al. (2019) investigated the phase behavior of n-butane and bitumen systems in liquid/liquid region. The composition of phases was determined based on C_5-asphaltenes and maltenes characterization scheme. The LLE data of solvent/bitumen mixtures and more specifically phase compositions are rarely found in the literature. Therefore, the number of modeling studies is also rare. Recently, Sun et al. (2019) used simulated distillation (SD) analysis of bitumen to characterize and define the pseudocomponents for modeling VLE and LLE data of a bitumen and ethane system. They concluded that splitting bitumen into four pseudocomponents can be sufficient in accurately predicting the PVT data using PR EoS.

The techniques used for collecting vapor VLE data of solvent/bitumen systems are relatively well established and fully investigated. Consequently, the number of studies on VLE of solvent/bitumen systems are numerous in the literature. On the contrary, the lack of data is evident for LLE. While detecting two liquids in a solvent and bitumen mixture might be an easy task, determining the composition of phases can be very challenging. The most important reason that makes the collection of solvent/bitumen LLE data extremely tedious is the partitioning of unknown and extra heavy constituents of bitumen into two liquid phases. Bitumen is composed of thousands of

components with molecular weights ranging from 100 up to 10000 g/mol (Azinfar et al., 2018a). Hence, determining what portion of which components exist in different phases requires a detailed characterization of both bitumen and the extracted cuts from the bitumen due to the addition of solvents. The most common methods of bitumen characterizations are vacuum distillation (Castellanos Díaz et al., 2014), simulated distillation (SD) (Azinfar et al., 2015), gel permeation chromatography (GPC) (Xu et al., 2014) and, SARA fractionation (Woods et al., 2008). Although these methods can yield information about the boiling point or molecular weight distribution of the components in the bitumen, they cannot fully characterize it. For example, vacuum distillation can distill no more than 60 wt.% of the heavy oils and bitumen sample and SD can only analyze up to 80% of bitumen which has already been deasphalted (Azinfar et al., 2018a; Sadeghi Yamchi et al., 2018). In the current study, a characterization method introduced by Azinfar et al. (2018a) will be applied to the samples for thorough measurements of molecular weight distributions.

In our previous study (Sadeghi Yamchi et al., 2018), LLE properties of butane/bitumen mixtures were experimentally investigated at lower temperatures of 40 and 60 ºC. The composition of the light phase at each equilibrium was measured and then the composition of the heavy phase was estimated with material balance. In addition, the boiling point distributions of the light and heavy cuts were determined with SD. Effect of additives such as DME, propane, and toluene was evaluated on LLE of butane/bitumen system. Interestingly, it was found that adding DME to the existing system of butane/bitumen can lower the amount of heavy component precipitation. In the current study, detailed LLE experiments of DME/bitumen systems were conducted at four different temperatures of 40, 60, 80, and 100 °C. At each temperature, three different concentrations of DME in the feed were selected such that the LLE could be achieved. Based on the detailed analysis of the cuts obtained from the combination of GPC and SD methods, two

pseudocomponents were defined for bitumen and then the composition of each pseudocomponent was determined. NRTL model was tuned to reproduce the experimental compositions for the LLE measurements of DME/bitumen systems.

3.4 Experimental Setup

To measure the phase behavior of DME and bitumen mixtures at different pressures and temperatures, the following setup with the schematic diagram presented in Figure 3.1 was utilized. The different parts of this setup, as indicated by numbers on the diagram are as follows: inside a temperature-controlled Blue-M oven (1), an equilibration or mixing cell (5), densitometer (7), viscometer (8), and a 15-micron filter (12) along with valves are located. Outside the oven, feeding cells (4), receiving cell (6), sampling cells (9), Quizix Pumps (10), density and viscosity data evaluation units (2,3), and operation unit (11) are placed.

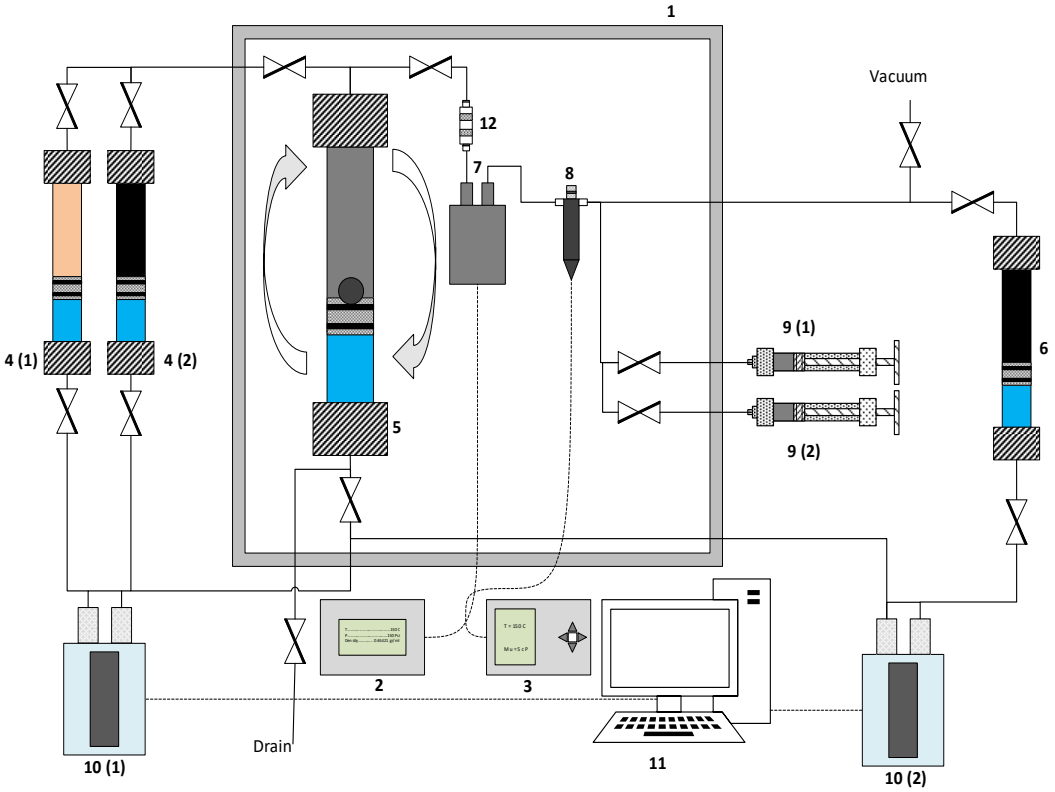

Figure 3.1: Experimental setup for PVT studies of DME/bitumen mixtures, (1) Blue-M oven, (2) density data gathering unit, (3) viscosity data gathering unit, (4) feeding cell, (5) equilibration cell, (6) receiving cell, (7) densitometer, (8) viscometer, (9) sample cell, (10) Quizix pump, (11) pump controlling unit, and (12) filter.

All the cells used in this study were equipped with a piston inside and Silicone O-rings around the piston to isolate the fluids stored in the cell from the water underneath. Water was used to adjust the pressure and displace the piston. The pressure of the cells was controlled with the Quizix pumps, which could inject or receive water with an accuracy of 0.002 cm^3 to displace the piston. One of the advantages of the cells was their internal volume of 850 ml. Higher volume of the equilibration cell enabled us to have a larger amount of the solvent and bitumen in the feed leading to the reliable phase-detection and acquisition of data.

To confirm the detection of equilibrium phases, a series of in-line densitometer and viscometer along with a 15-micron filter were used. Anton Paar densitometer in the system was able to detect the density changes in the range of 0-3 g/cm^3 with an accuracy of 0.0001 g/cm^3 and the viscometer could measure viscosity with the lowest value of 0.2 cP and highest of 20000 cP. Adding the filter to the setup provided another assurance in tracking any heavy particles that were not possibly separated from the light phase. An example of phase detection with the filter will be given in the next part.

In this study, the phase behavior of DME and bitumen was measured. The bitumen used in this study was supplied by one of the industry sponsors of SHARP research consortium. The sample was cleaned, de-watered, and filtered through a 0.5-micron filter to remove possible solid particles. The bitumen water content was measured using Karl Fischer Titration (ASTM D4928−12) to be less than ~0.1 wt.% (1000 ppm). The molecular weight of 523 g/mol was obtained for the bitumen by the vapor pressure osmometer (VPO) and the specific gravity of 1.004 (water = 1.0) was obtained by Anton Paar DMA 5000 densitometer. Detailed characterization of the bitumen using combined gel permeation chromatography (GPC) and simulated distillation (ASTM D7169) has been reported elsewhere (Azinfar et al., 2018a, 2018b). To accelerate the process of mixing, a mixture of 20 wt.% DME and bitumen was prepared and stored. To charge the equilibrium cell, a known amount of the prepared mixture of 20 wt.% DME was injected into the equilibrium cell and then the composition of the mixture was brought to the desired value by injecting more DME to the system. The mixing time of DME with an already prepared mixture was found to be much faster than the mixing of DME and bitumen. A rocking system was used to rock the equilibrium cell continuously and a stainless steel rocking ball was placed inside the equilibrium cell to agitate the mixture for proper and faster mixing.

Prior to any experiment, the equilibrium cell and its piston were rinsed and cleaned with toluene and acetone. Then, the piston was placed carefully in the cell so that there was no air trapped in the water underneath the piston. This was important because of two reasons: first, the saturation pressure measurements would not be affected by the trapped air in the system, and second, the volume of the phases could be recorded reliably for later material balance calculations. Then, the lines and fittings of the setup were also cleaned with toluene and dried with the injection of acetone and purging with nitrogen. Lastly, before charging the system, all the lines and cell was vacuumed to remove any air from the system.

To charge the system, a predetermined amount of a 20 wt.% DME/bitumen mixture was injected into the equilibrium cell. To control the injection, a back-pressure regulator was installed on top of the feeding cell to release the mixture from the feeding cell to the equilibrium cell at a controlled constant pressure. It is required to note that the mixture of 20 wt.% DME/bitumen was kept well above the saturation pressure of DME at room temperature to avoid ex-solution of DME from the mixture and any compositional changes. The volume of the injection was recorded, and the mass of each stream was calculated with the measured density at the injection pressure. Then, the required amount of DME was injected into the equilibrium cell, the temperature and pressure were set followed by 24 hours of rocking. The pressure of the equilibrium cell was kept constant by the injection of water underneath the piston in the equilibrium cell. The indication of whether the equilibrium condition has been reached or not was checked with the injection volume of the pump. If pressure was remained constant with zero injected volume, then the system was considered at equilibrium, otherwise, it was given more time to achieve equilibrium condition.

After complete mixing, the saturation pressure of the mixture was measured. To measure the saturation pressure, a stepwise expansion method was used while the cell was being vigorously rocked. In this method, 0.01 cm^3 was received from the equilibrium cell by the pump at each step and then a few minutes was given for the pressure stabilization. Since the cell was rocked intensely, this would help for the easy liberation of the gas and a faster pressure stabilization. Then, the plot of the pressure versus time (equivalent to volume) was constructed and the saturation pressure was determined as a point with the change of slope in the variation of pressure with time. An example of saturation pressure measurements is shown in Figure 3.2.

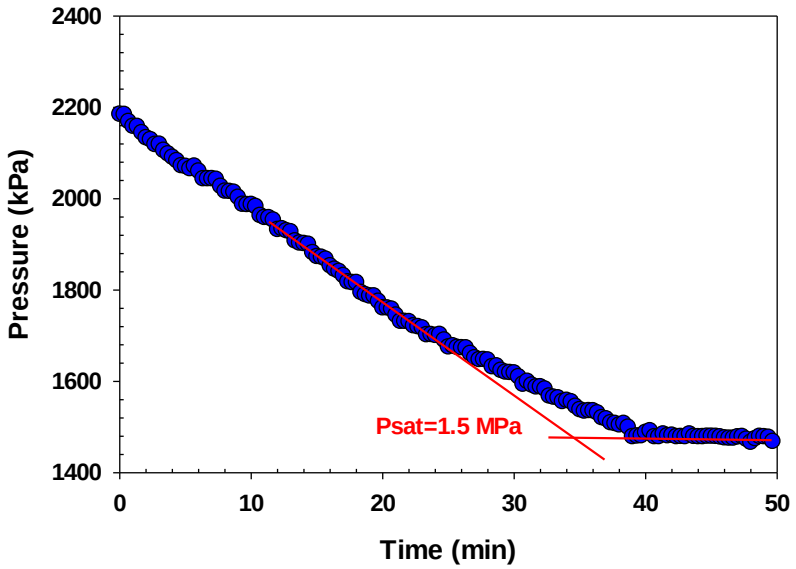

Figure 3.2: Saturation pressure measurement of 60 wt.% DME/bitumen at 60 °C.

To measure the density, viscosity, and composition of the phases at equilibrium condition, 12 hrs was given to the mixture in the equilibrium cell without any rocking while the cell was kept in a vertical position. This would give enough time for the phases to segregate. After nearly 12 hrs, the light phase was discharged from the top of the cell at constant pressure and the density and

viscosity values were measured. The combination of filter, densitometer, and viscometer indicated how uniform the light phase was or in other words it indicated whether the separation of phases was complete or more time is needed. If the injection pressure of the pump was increasing with time, it could mean that the heavy phase with large enough asphaltenic particles was accumulating behind the filter as an indication of incomplete segregation. In addition, the readings on the densitometer and viscometer were another signs of fully separated phases. On the way to the receiving cell, two samples from the light phase were collected, one for liquid gas chromatography to determine its composition and another one for gel permeation chromatography (GPC) to determine the molecular weight distribution of the cut. Here, it should be noted that the cuts are bituminous part of the phases or in other words, the collected phases were flashed at atmospheric conditions that resulted in cuts. Flashing the light phase generates the light cut. Similarly, flashing the heavy phase generates the heavy cut. While the composition of the light phase was directly measured by GC, the composition of the heavy phase, on the other hand, was calculated from material balance.

3.5 Methodology of Determining the Composition of Each Phase

As mentioned earlier, with a sample taken from the light liquid, mass fraction of DME, and bituminous part (light cut) in the light phase were directly measured by GC analysis. The total mass of the light phase was calculated based on the measured density and its corresponding volume on the pump. The volume of the light phase was taken as a point at which the heavy phase reached the top of the equilibration cell. Since the viscosity of the heavy phase was several orders of magnitude higher than that of the light phase, as it reached the top of the cell, a sudden jump in the pressure reading of the pump was observed. The corresponding discharged volume up to that point

was taken as the volume of the light phase. Figure 3.3 shows an example of the pressure jump during a test. Once the discharging process was stopped, the cell was carefully depressurized, and the cap of the cell was removed, and the content of the cell was visually inspected for the presence of heavy cut. Moreover, a sample of heavy fraction was taken for compositional analysis by the coupled GPC-SD method. Knowing the composition and total mass of the light phase, the composition of the heavy phase was, therefore, calculated from mass balance based on the initial mass of bitumen and DME in the feed.

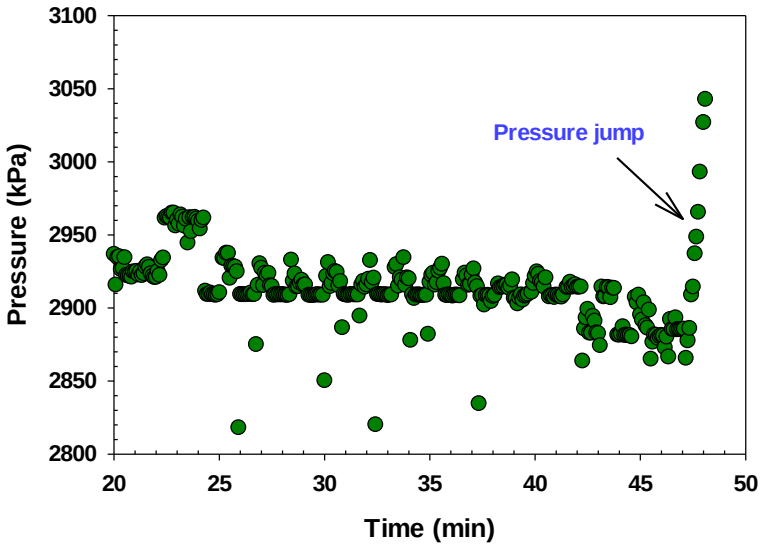

Figure 3.3: Pressure jump, once the heavy phase reaches the top of the cell equilibrium cell.

Before introducing the characterization scheme of bitumen, it is required to define some of the terminology used in this paper. ***Light phase*** is the light liquid at equilibrium condition (L_L). ***Heavy phase*** is the heavy liquid at equilibrium condition (L_H). ***Light cut*** is the bituminous part of the light phase or in other words, it is the flashed off light phase (C_L). The light phase is a mixture of DME and light cut. ***Heavy cut*** is the bituminous part of the heavy phase or in other words, it is the

flashed off heavy phase (C_H). The heavy phase is a mixture of DME and Heavy cut. ***Heavy yield*** is the fraction of the bitumen which partitions into the heavy phase. Figure 3.4 shows a demonstration of phases at equilibrium and also depicts the pictures of light and heavy cuts recovered at 80 wt.% DME in the feed and 100 °C. It also compares the cuts with the bitumen sample.

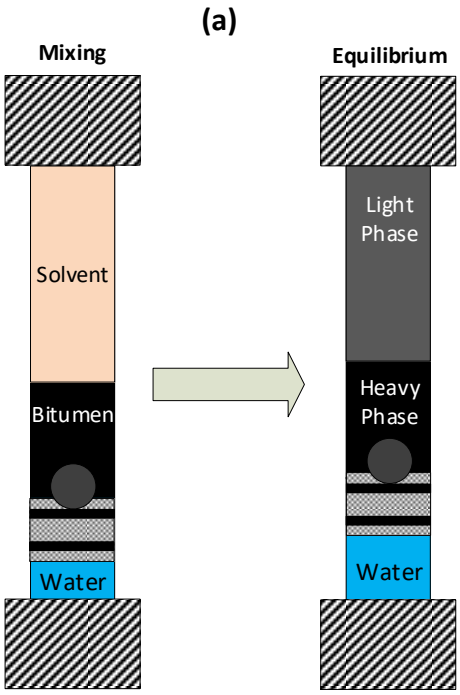

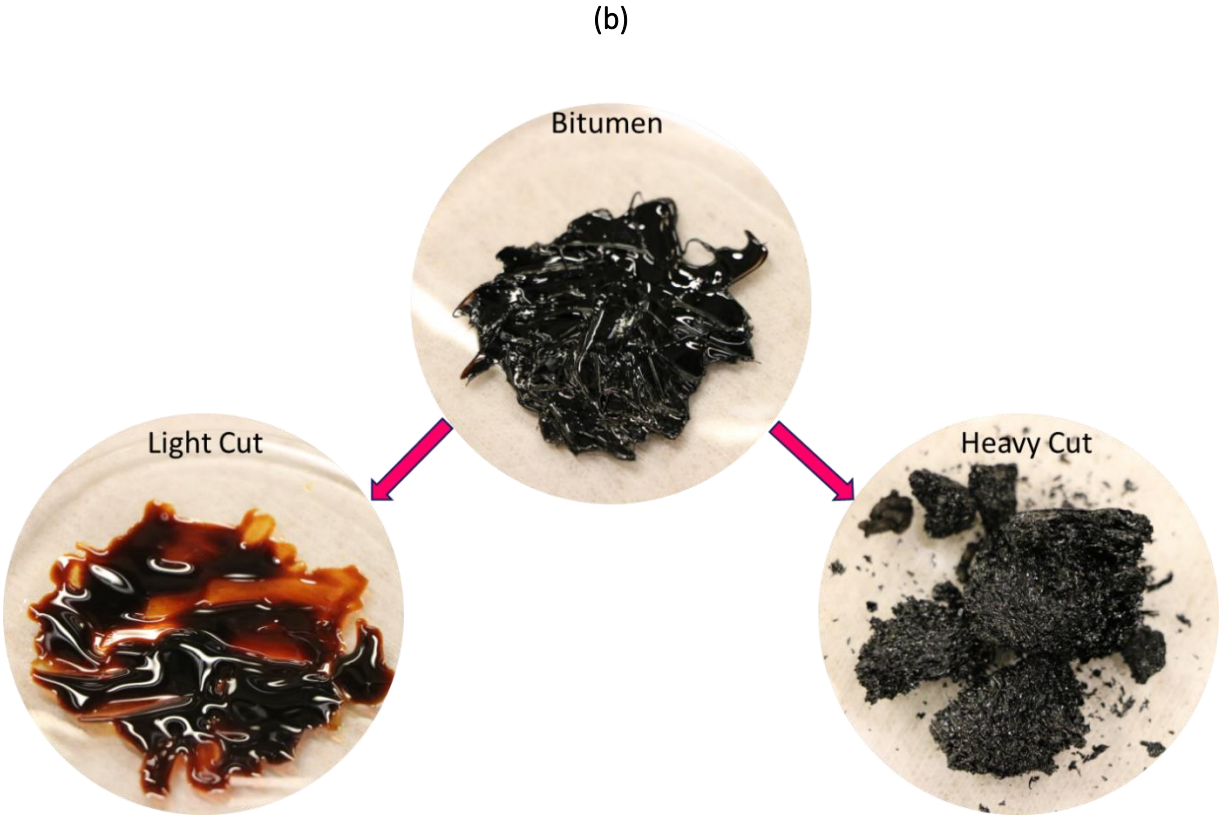

Figure 3.4: a) Demonstration of light and heavy phases at equilibrium condition, b) dividing bitumen to light and heavy cuts due to addition of 80 wt.% DME at 100 °C.

To be able to present the results in a ternary diagram, bitumen was divided into two pseudocomponents, the first one is a representative of maltenes in the bitumen, denoted by PC1 and the second pseudocomponent is the representative of asphaltenic constituents in the bitumen denoted by PC2. The two pseudocomponents scheme was not only well suited with the objective

of this paper but also resulted in a better modeling match to the experimental data. We use Whitson correlation for lumping the constituents of bitumen as given by (Whitson, 1983):

$$M_I = M_1\left(\frac{M_N}{M_1}\right)^{I/N}, \tag{3.1}$$

where $I=1,...,N$ is the number of the pseudocomponents, M_1 and M_N are the minimum and maximum molecular weight existing in the systems, respectively. I^{th} pseudocomponent includes all the components in the full characterization with MWs between M_{I-1} and M_I.

To lump the constituents of bitumen into pseudocomponents, a full characterization of bitumen is required in the first place. In this study, a characterization method presented by Azinfar et al (Azinfar et al., 2018a), which combines SD results with GPC is used. As mentioned earlier, the selection of this method over a simple SD was because SD can only characterize a bitumen cut up to 80 wt.% and it is unable to analyze the more heavy and complex components of the bitumen such the ones in asphaltenes. While combining SD with GPC can enable a full characterization since GPC can detect any component with any molecular size without any limit. Here, the characterization method is explained briefly, and it is recommended to refer to the original paper for further details.

Figure 3.5 (a) shows the GPC output chromatogram of the bitumen sample used in this study. The area under the curve for a specific time is proportional to the amount of the eluted sample from the GPC column. Therefore, by calculating the total area under the curve, the cumulative weight percentage of the eluted sample can be given as:

$$\%Off \text{ (Cumulative yield)} = 100\times\frac{\text{Area of each section}}{\text{Total area}}, \tag{3.2}$$

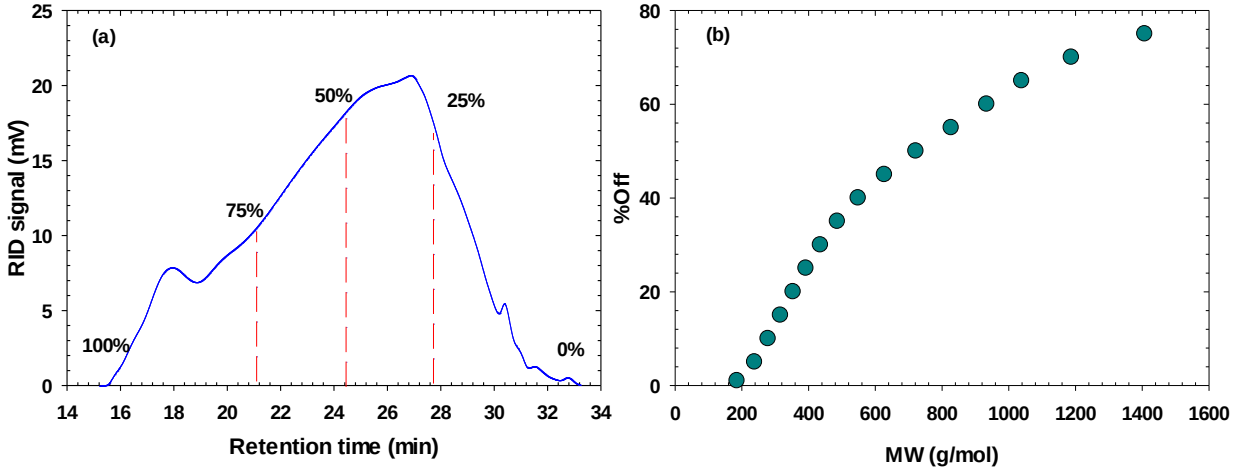

Figure 3.5: (a) GPC chromatogram, (b) MW distribution from SD for the bitumen sample.

Since the GPC separates dissolved molecules in the carrier phase based on their sizes, the heavier components are eluted first from the column and the percentage of the eluted sample increases from right to the left as shown in Figure 3.5(a). Figure 3.5 (b) shows the molecular weight distribution of the same bitumen sample as a function of *%Off* obtained from SD. Combining the results of *%Off* calculated from the GPC chromatogram and the molecular weight distribution obtained from SD, one can correlate the molecular weight of the sample from SD to the retention time of GPC. Once the relationship between the molecular weights and GPC retention time is found, the full characterization of bitumen can be determined. Figure 3.6 shows the weight percentage of every single component in the bitumen as a function of their corresponding molecular weight.

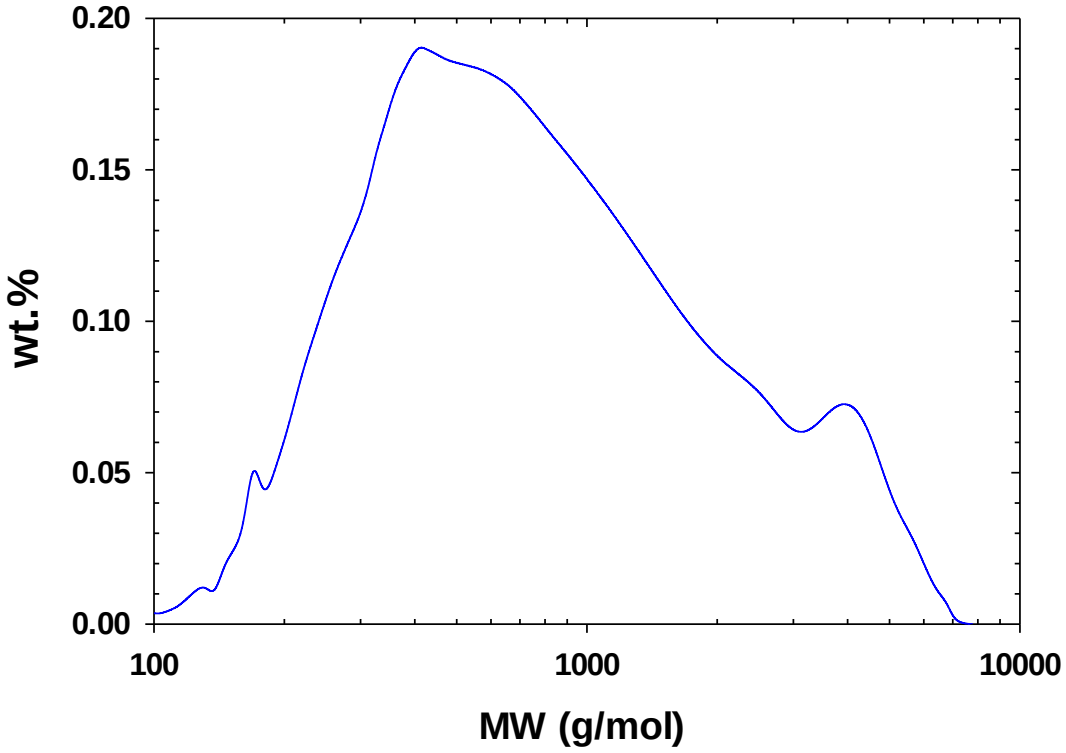

Figure 3.6: MW distribution of the bitumen calculated using GPC - SD method.

As discussed earlier, bitumen was divided into two pseudocomponents. All the components with MWs up to 605 g/mol were lumped as pseudocomponent PC1 and the rest of the constituents of the bitumen were lumped as pseudocomponent PC2 using Whitson correlation (Whitson, 1983). Based on the distribution of the components in the bitumen (Figure 3.6), PC1 was calculated to have an average molecular weight of 321 g/mol with a weight percentage of 43.62% and PC2 was calculated to have an average MW of 1227 g/mol with a weight percentage of 56.38%. It is worth noting that the average molecular weight of the bitumen sample was obtained 550 g/mol using the SD-GPC method, which is in well-agreement with the value measured by vapor pressure osmometry (VPO) as 523 g/mol.

Using the same analysis and applying it to all light and heavy cut samples extracted from the equilibrium, the composition of each pseudocomponent in each cut was calculated. In other words, the molecular weight distribution of the cuts was first determined and then all components with MW of less than 605 g/mol were grouped in PC1 and the rest were lumped as PC2 in each cut.

In order to calculate the composition of each pseudocomponent at the equilibrium condition, the following equation can be used:

$$\omega_{PC1}^{L} = (1-\omega_{DME}^{L}) \times \omega_{PC1}^{C}, \tag{3.3}$$

where ω is the weight fraction, *L* and *C* denote the liquid phase and the cut, respectively.

3.6 Thermodynamic Modeling

For a system of multicomponent, the liquid-liquid equilibrium criteria in terms of activity coefficient can be written as (Prausnitz et al., 1998):

$$x_i^{L_L} \gamma_i^{L_L} = x_i^{L_H} \gamma_i^{L_H}, \tag{3.4}$$

where *x* and γ are the mole fraction and activity coefficient of component *i*, respectively. To estimate the activity coefficient of each component, non-random two liquid (NRTL) thermodynamic model was used as given by (Renon and Pruasnitz, 1968):

$$\ln(\gamma_i) = \frac{\sum_j \tau_{ji} G_{ji} x_j}{\sum_l G_{li} x_l} + \sum_j \frac{x_j G_{ij}}{\sum_l G_{lj} x_l} \left(\tau_{ij} - \frac{\sum_r x_r \tau_{rj} G_{rj}}{\sum_l G_{lj} x_l} \right), \tag{3.5}$$

where G_{ij} is a characteristic of interaction energies between molecules of *i* and *j* given as follows (Renon and Pruasnitz, 1968):

$$G_{ij} = \exp\left(-\alpha_{ij}\tau_{ij}\right), \tag{3.6}$$

where τ_{ij} is the energy interaction parameter and α denotes the randomness of the system and is considered to be symmetric $\alpha_{ij} = \alpha_{ji}$. It has been shown that the value of α can vary from 0.20 to 0.47 and it was assumed 0.3 in this work. τ_{ij} was tuned to reproduce the experimental data.

In this study, the optimization toolbox of MATLAB (version 2018) was employed to perform regression to tune τ_{ij} of the NRTL model in flash calculations and match the experimental composition data. The objective function of the regression was defined as:

$$OF = \frac{1}{2N}\left(\sum_{i=1}^{N}\frac{\left|x_i^{L_L,calc} - x_i^{L_L,\exp}\right|}{x_i^{L_L,\exp}} + \sum_{i=1}^{N}\frac{\left|x_i^{L_H,calc} - x_i^{L_H,\exp}\right|}{x_i^{L_H,\exp}}\right), \tag{3.7}$$

where *x* is the experimental composition and *i=1,..., N* is the number of the component.

3.7 Results and Discussion

In this study, the phase behavior of DME and bitumen mixtures in the liquid-liquid region was measured. Measurements were carried out at four different temperatures ranging from 40 to 100 °C. Three different compositions of 60, 70, 80 wt.% of DME in feed were selected since the preliminary tests indicated that no liquid-liquid equilibrium formed at concentrations less than 50 wt.% of DME. The composition of the phases, which was calculated by the methodology explained in Section 3, are given in Table 3.1. The repeatability of DME composition in the light phase was found to be ± 0.7 wt.% and in the heavy phase was calculated ±4.1 wt.%. The relatively big difference between the light phase and heavy phase repeatability values originates from the fact that light phase composition was directly measured with GC as opposed to the heavy phase

composition which was calculated from material balance. As the weight fraction of DME increases in the feed, the mass fraction of DME in the light phase also increases but it decreases in heavy phase. Weight fraction of both pseudocomponents in the light phase has a decreasing trend with DME fraction in the feed. In the heavy phase, the fraction of PC1 decreases whereas the fraction of PC2 increases with adding more DME to the feed. Since DME is more compatible with PC1 (the light pseudocomponent) than PC2 (the heavy pseudocomponent), an increase in DME concentration is causing more partitioning of PC1 into the light phase and stripping more PC2 into the heavy phase. An example of this behavior at 40 °C has been illustrated in Figure 3.7.

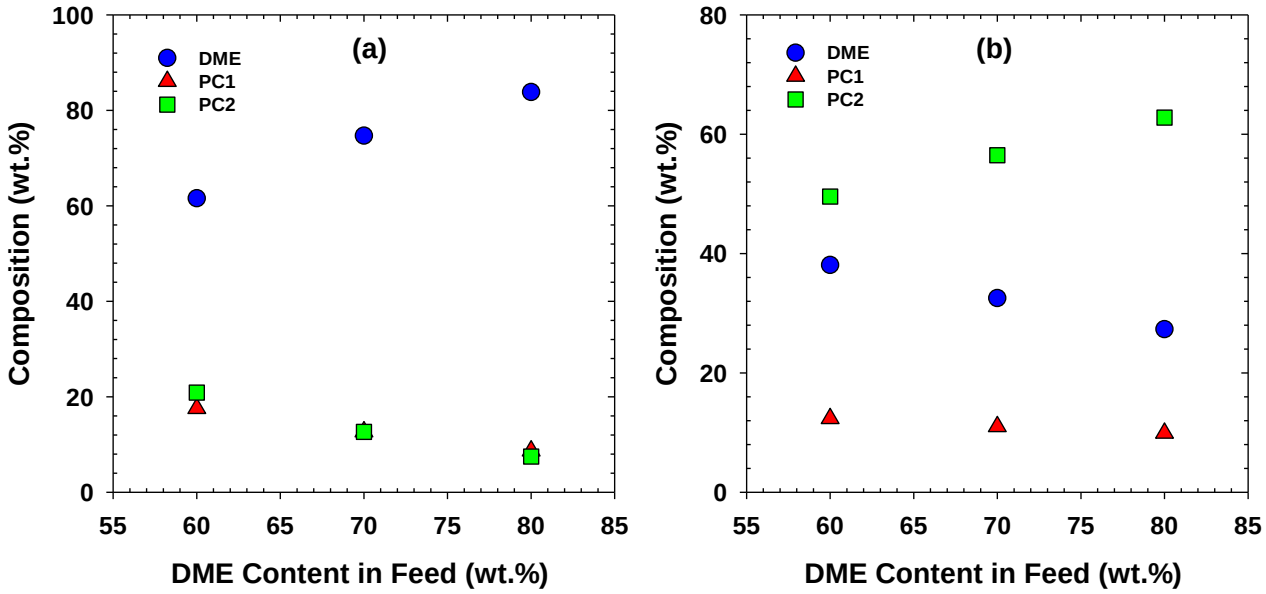

Figure 3.7: Variation of composition of the components with DME wt.% in the feed for a) light phase, b) heavy phase at 40 °C.

Given the fact that the pseudocomponents are the only constituents of the cuts recovered from the equilibrium condition, examining the detailed molecular weight distribution of the cuts can assist us in better analyzing the observed trends in the compositions as presented in the following.

Table 3.1: Composition (wt.%) of components at equilibrium conditions. [a]

T(°C)	P (MPa)	Feed			Light Phase			Heavy Phase		
		DME	PC1	PC2	DME	PC1	PC2	DME	PC1	PC2
40	2.1	60	17.45	22.55	61.59	17.55	20.86	38.08	12.36	49.56
40	2.1	70	13.09	16.91	74.69	12.67	12.64	32.51	11.01	56.49
40	2.1	80	8.72	11.28	83.85	8.68	7.47	27.30	9.91	62.79
60	2.1	60	17.45	22.55	61.78	17.28	20.94	37.94	13.26	48.80
60	2.1	60	-	-	60.80	-	-	51.31	-	-
60	2.1	70	13.09	16.91	73.72	13.51	12.77	34.97	10.53	54.50
60	2.1	70	-	-	72.89	-	-	37.75	-	-
60	2.1	80	8.72	11.28	84.67	8.04	7.29	21.33	9.38	69.29
80	2.8	60	17.45	22.55	61.97	18.24	19.79	38.23	12.29	49.48
80	2.8	70	13.09	16.91	73.07	14.46	12.47	34.95	11.78	53.27
80	2.8	80	8.72	11.28	84.35	8.88	6.77	27.25	9.87	62.88
100	4.0	60	17.45	22.55	62.20	18.62	19.18	39.54	12.84	47.62
100	4.0	70	13.09	16.91	75.16	14.15	10.69	36.55	11.97	51.48
100	4.0	70	-	-	76.28	-	-	35.19	-	-
100	4.0	80	8.72	11.28	83.78	9.82	6.40	26.45	11.43	62.12

[a]Standard uncertainties are *u(T)*= 0.228 °C, *u(P)*= 0.003 MPa, *u(composition)=0.005 wt.%*.

Expanded uncertainties are *Uc(composition)*= 0.008 wt.% (95% level of confidence).

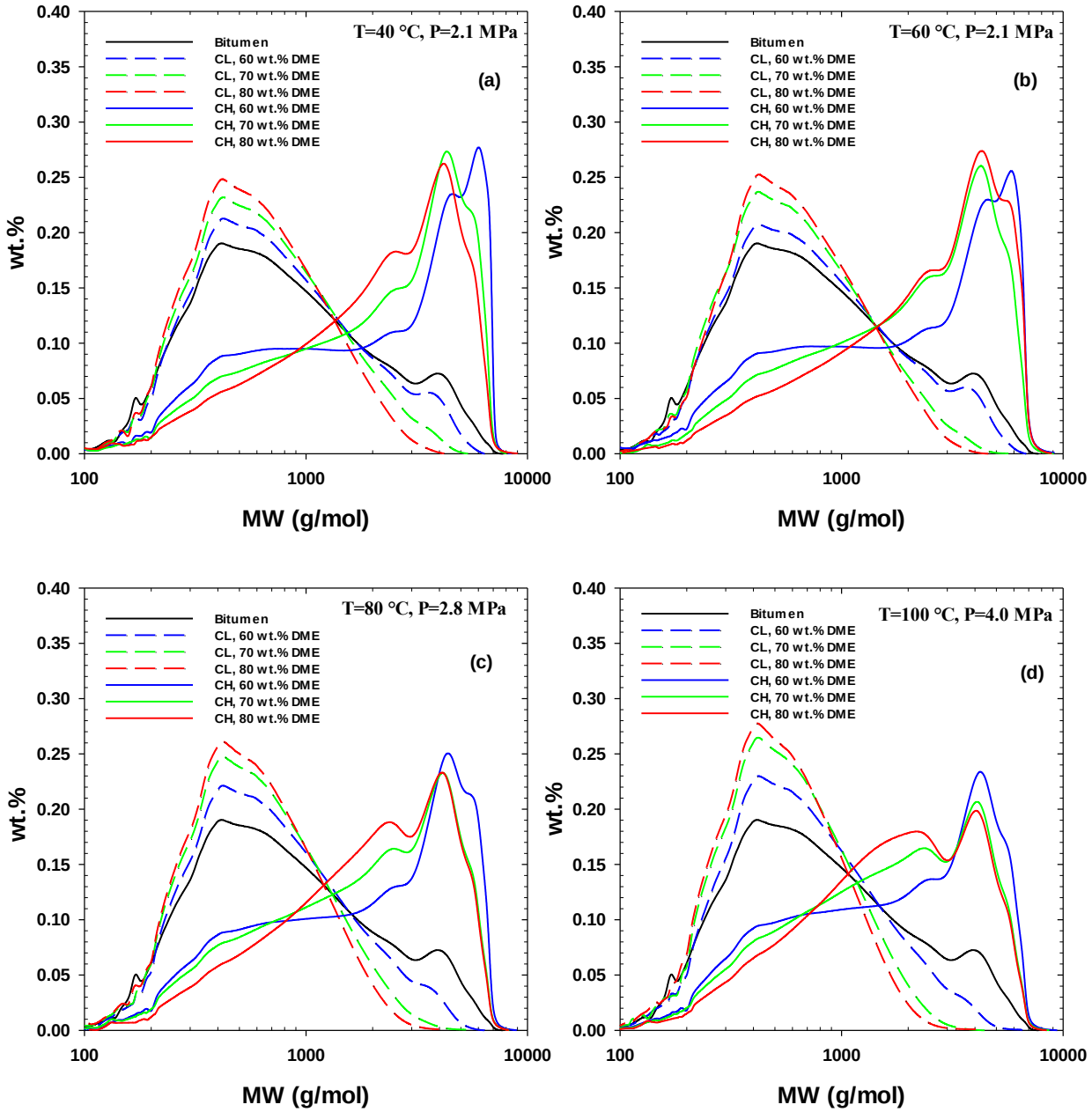

Figure 3.8: Molecular weight distributions of the cuts recovered from different equilibrium conditions.

Figure 3.8 shows the molecular weight distributions of the light and heavy cuts at different equilibrium conditions. For all tests at a constant temperature, the MW distributions of light cuts reveal that the light cut turns lighter as the mass fraction of DME in the feed increases. In other words, more light components (MW<~1000 g/mol) are extracted from the heavy cut. On the other hand, the MW distributions reveal that some heavy components (MW>~2000) transferred from the light cut to the heavy cut leading to lighter heavy cut. This behavior indicates that more of the heavier components are extracted out of the bitumen with more DME. When the concentration of DME in the feed is slightly above the onset point (i.e. 60 wt.%) only a smaller amount of precipitation occurs and consequently, the molecular weight distribution of the corresponding light cut becomes closest to the bitumen. Investigating the molecular weight distribution of heavy cuts reveals that for all temperatures, the heaviest cut is obtained when DME concentration is 60 wt.% in the feed because the heaviest components precipitate out of bitumen first. By adding more DME to the feed more precipitation happens leading to moderately lighter distributions in the heavy cuts compared to 60 wt.% heavy cut. As shown in Figure 3.8, for all temperatures, MW distribution of heavy cut at 60 wt.% DME is distinguished from that of 70 or 80 wt.% DME.

In addition to the measurement and calculation of the experimental compositions, the experimental K-values are estimated. In the calculation of the liquid-liquid K-values, the heavy phase was considered as the reference phase. In other words, the K-value of each component was calculated as the mole fraction of that component in the light phase to its mole fraction in the heavy phase. The results have been presented in Table 3.2.

Table 3.2: Liquid-liquid K-values of all components in DME/bitumen system.[a]

T(°C)	P (MPa)	wt.%$_{DME}$	K-value		
			DME	PC1	PC2
40	2.1	60	1.02	0.87	0.47
40	2.1	70	1.06	0.50	0.20
40	2.1	80	1.09	0.29	0.09
60	2.1	60	1.03	0.77	0.46
60	2.1	70	1.04	0.64	0.22
60	2.1	80	1.11	0.24	0.06
80	2.8	60	1.02	0.93	0.45
80	2.8	70	1.05	0.61	0.22
80	2.8	80	1.09	0.33	0.07
100	4.0	60	1.02	0.93	0.45
100	4.0	70	1.05	0.60	0.19
100	4.0	80	1.10	0.31	0.07

[a]Standard uncertainties are *u(T)*= 0.228 °C, *u(P)*= 0.003 MPa, *u(composition)=0.005 wt.%*.
Expanded uncertainties are *Uc(K-value)*=0.002 wt.% (95% level of confidence).

Since the mole fraction of DME in both light and heavy phases were higher than 85 mol.%, K-values of DME are close to one in all cases. K-values are the function of DME composition. While the K-value of DME increases with the DME concentration in the feed, K-values of both pseudocomponents, PC1 and PC2 decrease. From solubility point of view, increasing of K-value means reduction of solubility in the reference phase. When more DME was added to the solution, the tendency of DME to stay soluble in the heavy phase decreased. Reduction in the solubility of DME occurred as a result of an increase in the concentration of heavy component, PC2 in heavy phase.

The density and viscosity of the light phase, as well as the saturation pressure of the mixtures, are summarized in Table 3.3. Saturation pressure measurements indicated no noticeable variation with the DME composition since in the liquid-liquid region the DME has the dominant mole fraction (~90 mol%). The density of the light phase has a descending trend with DME composition. Adding more DME to the mixture not only results in an increase in the concentration of the DME in the light phase but it also leads to the extraction of more heavy components from the bitumen, consequently the density of the light phase decreases. Density measurements were repeatable within ±4.7 kg/m^3. The behavior of viscosity is also similar to that of density in terms of dependency on the solvent concentration meaning it is reduced with an increase in the DME concentration in the feed but seems scattered with temperature. The disperse behavior comes from the fact that the range of viscosities is between 0.1 and 1 cP and mostly falls below 0.5 cP, which might be in the range of experimental errors.

Table 3.3: Density and viscosity of light phase and saturation pressure of DME/bitumen mixtures.[a]

T(°C)	P (MPa)	wt.%$_{DME}$	$\rho^{L}{}_{L}$(kg/m^3)	$\mu^{L}{}_{L}$(cP)	P_{sat} (MPa)
40	2.1	60	756.5	3.7	0.9
40	2.1	70	723.6	0.4	0.9
40	2.1	80	690.6	0.4	0.9
60	2.1	60	735.0	0.7	1.5
60	2.1	60	724.6	-	-
60	2.1	70	686.9	1.0	1.5
60	2.1	70	683.0	-	-
60	2.1	80	651.4	-	1.5
80	2.8	60	696.0	0.3	2.2
80	2.8	70	647.7	0.3	2.2
80	2.8	80	620.0	0.1	2.2
100	4.0	60	663.0	0.1	3.1
100	4.0	70	612.4	0.1	3.1
100	4.0	70	606.9	-	-
100	4.0	80	570.1	0.1	3.3

[a]Standard uncertainties are *u(T)*= 0.228 °C, *u(P)*= 0.003 MPa, *u(composition)=0.005 wt.%*.

Expanded uncertainties are $Uc(\rho)$= 0.246 kg/m^3, $Uc(\mu)$= 0.034 cP, $Uc(P_{sat})$= 0.007 MPa (95% level of confidence).

Modeling of liquid-liquid equilibrium is one of the challenging tasks. The experimental compositions of the components presented previously in Table 3.1 are also predicted using NRTL thermodynamic model. Results are presented in the form of ternary diagrams for each temperature as shown in Figure 3.9. As discussed earlier, a developed flash calculation algorithm coupled with NRTL model was optimized using the optimization toolbox of MATLAB 2018. The model predictions were matched with the experimental compositions by tuning τ_{ij} in the NRTL model. The tuned values of τ_{ij} are shown in Table 3.4. As the regression was done separately for each

temperature, separate sets of τ_{ij} were obtained for each equilibrium temperature. As shown in Figure 3.9 the model was able to precisely predict the equilibrium compositions of all components in the light and heavy phases. AARD of the predictions was less than 6.5% for all cases.

Table 3.4: τ_{ij} used for calculation of compositions in NRTL model.

T(°C)	40	60	80	100
$\tau_{DME-PC1}$	40.31	51.32	48.24	41.67
$\tau_{DME-PC2}$	7.95	7.96	8.17	8.13
$\tau_{PC1-DME}$	0.66	-0.02	0.68	0.68
$\tau_{PC1-PC2}$	-0.16	0.01	-0.15	-0.15
$\tau_{PC2-DME}$	-2.30	-2.24	-2.40	-2.36
$\tau_{PC2-PC1}$	0.00	-0.01	0.00	0.00

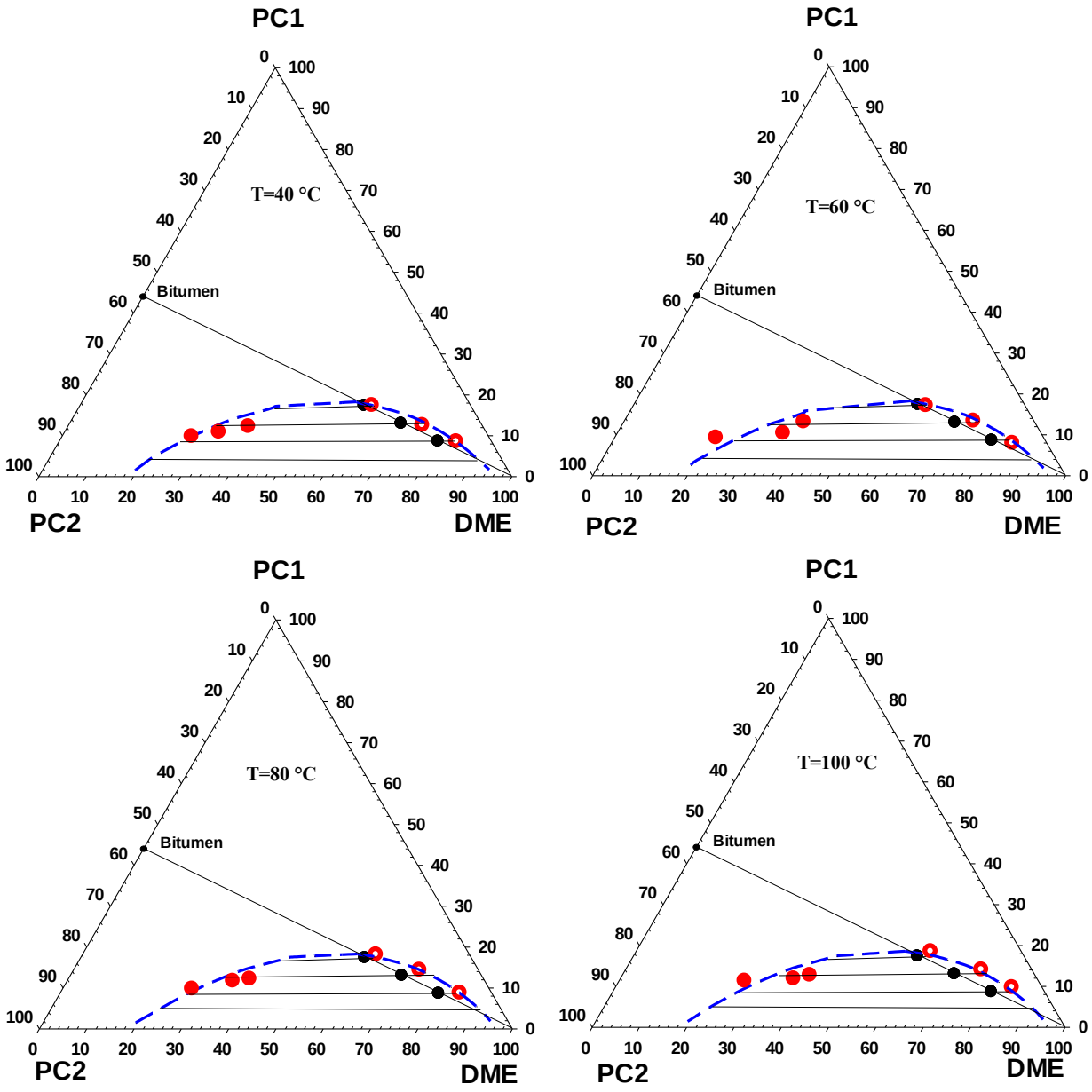

Figure 3.9: Ternary diagrams of DME/bitumen systems at different temperatures. ●, ○ experimental points; - - - model predictions; — model tie lines.

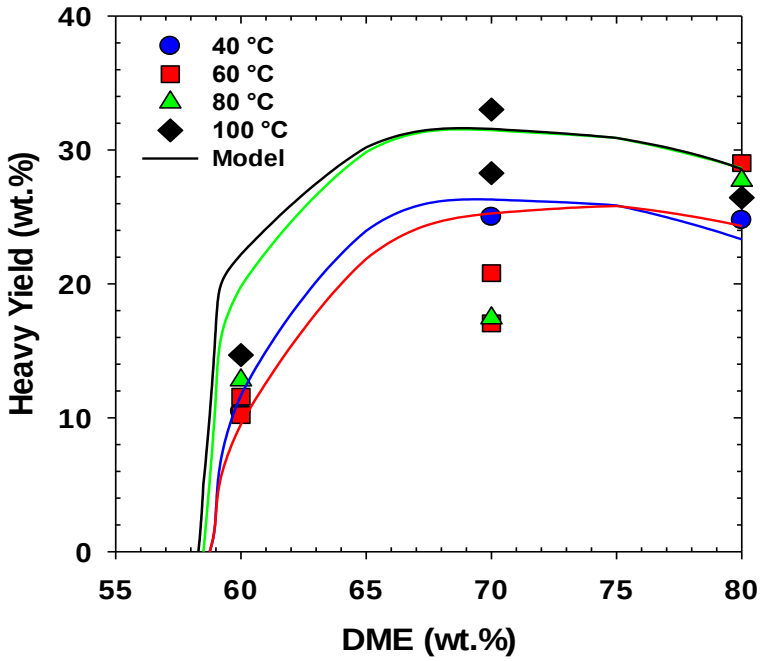

Figure 3.10: Heavy yield of DME/bitumen systems at different temperatures; ●, ■, ▲, ◆ are experimental data; — model predictions.

Heavy yield (the fraction of the bitumen which partitions into the heavy phase) or the amount of precipitation calculated with the model and a comparison with experimental measurements is shown in Figure 3.10. According to Figure 3.10, the average heavy yield in DME/bitumen systems is around 20 % with a repeatability of ±3%, which is comparable to the asphaltene precipitation with pentane. This is in agreement with our previous study where the addition of DME to a mixture of n-butane/bitumen was found to lower the heavy yield or asphaltene precipitation (Sadeghi Yamchi et al., 2018). While DME is a molecule with a similar carbon number to ethane and similar vapor pressure to propane, but the heavy yield curve is much lower than that of propane or butane and it is closer to the pentane. Even the onset point of the precipitation occurs at much higher concentration than those of propane or butane (Nourozieh, 2013). This behavior arises from the

molecular structure of DME. As discussed in the previous study (Sadeghi Yamchi et al., 2018), DME is a molecule with two methyl groups connected with an oxygen atom in between. The oxygen-carbon bonds are polar and the angular shape of the molecule results in a molecular dipole. Having polarity creates slight compatibility with resins and asphaltene molecules present in the bitumen leading to less precipitation compared to propane or butane.

Predictions of K-values are compared in Figure 3.11. The model underestimates K-values of DME and overall overestimates K-values of pseudocomponents. The predictions of the model show an AARD of approximately 20%. The estimation of K-values could be improved if we avoid using a constant MW for calculating pseudocomponents mass fractions. This is because in reality (experimental K-values) the distribution of species making the pseudocomponents varies for each equilibrium condition leading to variation in MW.

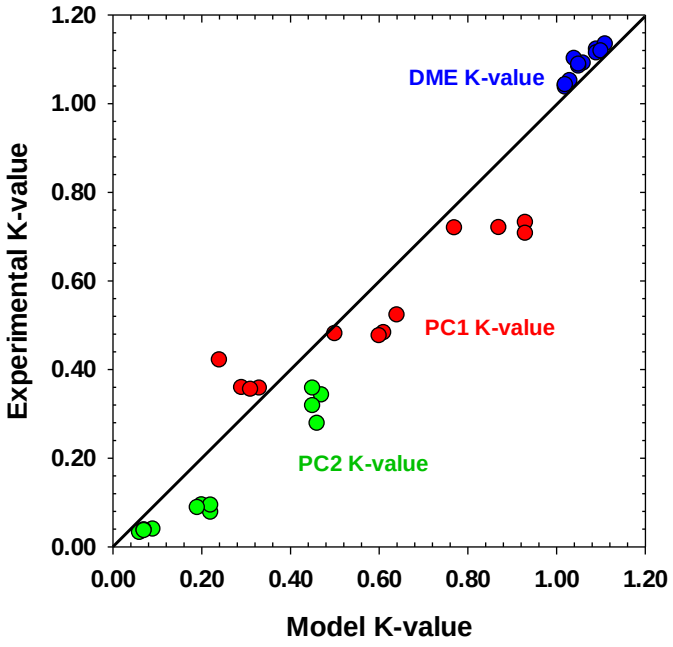

Figure 3.11: Comparison of experimental versus predicted K-values.

3.8 Conclusions

Experimental PVT measurements of DME/bitumen mixtures including density, viscosity of light phase, the composition of components in each phase (LLE K-values), saturation pressure of the mixtures and detailed analysis of the molecular weight distribution of the light and heavy cuts by simulated distillation (SD) and gel permeation chromatography (GPC) were conducted in this study. Measurements were performed at four different temperatures between 40, 60, 80, and 100 °C. Three feed concentrations of DME were selected in the LLE region at each temperature to investigate the effect of DME mass fraction as the main drive for liquid-liquid separation.

Results showed that with increasing the DME concentration in the feed at a fixed temperature, more of the components with MW<~1000 g/mol were extracted from the heavy phase and accumulated in the lighter phase. On the other hand, components with MW>~2000 g/mol were extracted from the light phase and accumulated in the heavy phase. Therefore, this resulted in lighter cuts at higher DME concentrations. Density and viscosity of the light phase also had a declining trend with DME concentration as more heavy compounds were extracted from bitumen.

The amount of precipitation with DME as the solvent is shown to be less than that of propane or butane. Since DME has a dipole molecular structure, the compatibility of heavier and polar components in the bitumen such as asphaltene is more pronounced with DME than other non-polar hydrocarbons such as propane and butane.

Based on the MW distributions obtained from SD and GPC analysis, bitumen was divided into two pseudocomponents, PC1 representative of maltenes and PC2 representative of asphaltenes. Then K-values were defined and calculated for all the components in the system. NRTL

thermodynamic model was tuned to predict experimental compositions. Estimations of the model were in good agreement with the experimental data considering the overall error of less than 6.5%.

3.9 References

Azinfar, B., Zirrahi, M., Hassanzadeh, H., Abedi, J., 2018a. Characterization of heavy crude oils and residues using combined Gel Permeation Chromatography and simulated distillation. Fuel 233, 885–893.

Azinfar, B., Haddadnia, A., Zirrahi, M., Hassanzadeh, H., Abedi, J., 2018b. A thermodynamic model to predict propane solubility in bitumen and heavy oil based on experimental fractionation and characterization. J. Pet. Sci. Eng. 168, 156–177.

Azinfar, B., Zirrahi, M., Hassanzadeh, H., Abedi, J., 2015. A method for characterization of bitumen. Fuel 153, 240–248.

Badamchi-Zadeh, A., Kohse, B.F., Kumar, A., 2011. Modeling of Asphaltene Precipitation Due to Steam and n-alkane Co-injection in the ES-SAGD Process, in: Can. Unconv. Resour. Conf.

Castellanos Díaz, O., Sánchez-Lemus, M.C., Schoeggl, F.F., Satyro, M.A., Taylor, S.D., Yarranton, H.W., 2014. Deep-vacuum fractionation of heavy oil and bitumen, part I: Apparatus and standardized procedure. Energy and Fuels 28, 2857–2865.

Bin Dahbag, M., Zirrahi, M., Hassanzadeh, H., 2019. Solubility and Liquid Density of Ammonia / Athabasca Bitumen Mixtures at Temperatures up to 463 K : Measurements and Modeling. J. Chem. Eng. Data 64, 3592–3597.

Dini, Y., Becerra, M., Shaw, J.M., 2016. Phase behavior and thermophysical properties of Peace River bitumen + propane mixtures from 303 K to 393 K. J. Chem. Eng. Data 61, 2659–2668.

Fu, C.T., Puttagunta, R., Vilcsak, G., Fu, C.-T., Puttagunla, A., Vilcsak, G., 1986. Vapour-Liquid Equilibrium Properties for Gas-Cold Lake Bitumen, in: Annual Technical Meeting.

Petroleum Society of Canada, Calgary, Alberta, Canada.

Gao, J., Okuno, R., Li, H.A., 2018. A phase-behavior study for n-Hexane/Bitumen and n-octane/bitumen mixtures. SPE J. 23, 128–144.

Haddadnia, A., Sadeghi Yamchi, H., Zirrahi, M., Hassanzadeh, H., Abedi, J., 2018a. New Solubility and Viscosity Measurements for Methane-, Ethane-, Propane-, and Butane-Athabasca Bitumen Systems at High Temperatures up to 260 °c. J. Chem. Eng. Data 63, 3566–3571.

Haddadnia, A., Azinfar, B., Zirrahi, M., Hassanzadeh, H., Abedi, J., 2018b. Thermophysical properties of dimethyl ether/Athabasca bitumen system. Can. J. Chem. Eng. 96, 597–604.

John M. Prausnitz, Rudiger N. Lichtenthaler, E.G. de A., 1998. Molecular Thermodynamics of Fluid-Phase Equilibria, Third. ed. Pearson Education.

Kariznovi, M., 2013. Phase Behaviour Study and Physical Properties Measurement for Athabasca Bitumen / Solvent Systems Applicable for Thermal and Hybrid Solvent Recovery Processes, PhD thesis, University of Calgary.

Li, W., Mamora, D.D., Li, Y., 2011. Solvent-Type and -Ratio Impacts on Solvent-Aided SAGD Process. SPE Reserv. Eval. Eng. 14, 320–331.

Mokrys, I.J., Butler, R.M., 1993. In-situ upgrading of heavy oils and bitumen by propane deasphalting: The Vapex process, in: Prod. Oper. Symp.

Nourozieh, H., 2013. Phase Partitioning and Thermo-physical Properties of Athabasca Bitumen / Solvent Mixtures, PhD thesis, University of Calgary.

Nourozieh, H., Kariznovi, M., Abedi, J., 2015. Experimental and modeling studies of phase

behavior for propane/Athabasca bitumen mixtures. Fluid Phase Equilib. 397, 37–43.

Perez Claro, Y.A., Schoeggl, F.F., Taylor, S.D., Yarranton, H.W., 2019. Phase Behavior of Mixtures of Bitumen and n -Butane . Energy & Fuels 33, 8530–8543.

Renon, H., Pruasnitz, J.M., 1968. Local compositions in thermodynamics excess functions for liquids mixtures. AIChE J. 14, 116–128.

Sabet, N., Hassanzadeh, H., Abedi, J., 2017. Selection of efficient solvent in solvent-aided thermal recovery of bitumen. Chem. Eng. Sci. 161, 198–205.

Sadeghi Yamchi, H., Zirrahi, M., Hassanzadeh, H., Abedi, J., Fadaei, H., 2018. Effect of additives on liquid–liquid equilibrium properties of butane/bitumen systems with applications to solvent aided bitumen recovery processes. Chem. Eng. Res. Des. 137, 452–460.

Sheng, K., Okuno, R., Wang, M., 2018. Dimethyl Ether as an Additive to Steam for Improved Steam-Assisted Gravity Drainage. SPE J. 23, 1201–1222.

Sun, T., Takbiri-Borujeni, A., Nourozieh, H., Gu, M., 2019. Application of Peng-Robinson equation of state for modelling the multiphase equilibrium properties in Athabasca bitumen/ethane mixtures. Fuel 252, 439–447.

Whitson, C.H., 1983. Characterizing Hydrocarbon Plus Fractions. Soc. Pet. Eng. J. 23, 683–694.

Woods, J., Kung, J., Kingston, D., Kotlyar, L., Sparks, B., McCracken, T., 2008. Canadian Crudes: A Comparative Study of SARA Fractions from a Modified HPLC Separation Technique. Oil Gas Sci. Technol. 63, 151–163.

Xu, Z., Van Den Berg, F.G.A., Sun, X., Xu, C., Zhao, S., 2014. Detailed characterization of virgin heavy oil resid and its thermally cracked resid. Energy and Fuels 28, 1664–1673.

Yazdani, A., Maini, B.B., 2010. Measurements and modelling of phase behaviour and viscosity of a heavy oil/butane system. J. Can. Pet. Technol. 49, 9–14.

Zhang, K., Zhou, X., Peng, X., Zeng, F., 2019. A comparison study between N-Solv method and cyclic hot solvent injection (CHSI) method. J. Pet. Sci. Eng. 173, 258–268.

Zirahi, A., Sadeghi Yamchi, H., Haddadnia, A., Zirrahi, M., Hassanzadeh, H., Abedi, J., 2020. Ethyl acetate as a bio-based solvent to reduce energy intensity and CO2 emissions of in situ bitumen recovery. AIChE J. 66.

Zirrahi, M., Hassanzadeh, H., Abedi, J., 2017. Experimental and modelling studies of MacKay River bitumen and light n-alkane binaries. Can. J. Chem. Eng. 95, 1417–1427.

Chapter Four: **Liquid-Liquid Equilibrium of Propane + Butane + Bitumen System**

4.1 Preface

This chapter has been submitted for publication entitled “Measurements and Modeling of Liquid-Liquid Equilibrium of Propane + Butane + Bitumen System”. This manuscript was co-authored by M. Zirrahi, H. Hassanzadeh, and J. Abedi. Since this dissertation has been prepared on paper-based format, unavoidably, there are some repetitive parts in each chapter, mainly Chapters 2, 3, and 4, such as experimental setup and characterization descriptions.

In this chapter liquid-liquid equilibrium (LLE) of LPG/bitumen is studied and a thermodynamic model is developed to reproduce experimental K-values.

4.2 Abstract

Propane, butane, and their mixtures (LPG) are considered proper solvents for low temperature upgrading and solvent-based bitumen and heavy oil recovery processes. While equilibrium data for either mixture of propane/bitumen or butane/bitumen has been reported in the literature, there is no experimental measurement or predictive model for liquid-liquid equilibrium (LLE) of propane + butane/bitumen systems. In this study, comprehensive LLE measurements for propane + butane/bitumen mixtures were conducted in a temperature range of 21 to 80 °C. Equilibrium compositions of propane and butane along with the density and viscosity of the light phase were measured in each experiment. Then, the heavy yield or the amount of precipitation was determined. Detailed characterization of light and heavy cuts was performed using combined Simulated Distillation (SD) and Gel Permeation Chromatography (GPC). The bitumen was lumped into two pseudocomponents based on the characterization and LLE K-values were estimated using Non-Random Two Liquid (NRTL) model. The tuned NRTL model predicted the experimental

compositional data with an AARD less than 8.5%. The results of this study find application in the design of the solvent-based processes with a multi-component solvent such as liquified petroleum gas (LPG) and set forth an approach for engineering and optimizing the composition of the solvent for these processes.

4.3 Introduction

Solvent-based recovery processes such as vapor extraction (VAPEX) and N-solv are bitumen recovery techniques that can be applied to shallow reservoirs with relatively thin pay zone to address inapplicability of steam-based processes and prevent significant heat losses (Butler and Mokrys, 1993). VAPEX was initially introduced by Butler and Mokrys (1991), and from the early stages of the new development, propane was introduced as one of the candidates for the VAPEX process. Higher solubilities of propane in bitumen and its lower dew point are well aligned with the criteria required for the VAPEX process. Similar to VAPEX, N-solv also fundamentally requires the injection of hot solvent with less impurities of non-condensable gases (Nennieger and Nenniger, 2005; Zhang et al., 2019). Propane and butane have been identified as suitable solvents in N-solv process (Wilson, 2015).

The application of lighter solvents such as propane and butane in bitumen recovery has been extensively evaluated. Ferguson et al. (2001) conducted a series of steam injection and steam-propane co-injection and observed improved oil rates by adding propane as an additive to the steam. Gupta et al. (2005) described Encana's pilot solvent-aided process where butane was injected after a period of a steam assisted gravity drainage (SAGD) process and showed that the rate of the production increased nearly 20% after implementing butane injection. Mohammadpoor and Torabi (2015) investigated a VAPEX process with propane and butane as the working

solvents. Their experimental and numerical studies showed propane has an advantage over butane in terms of the overall efficiency in the VAPEX process. Deng (2005) evaluated the performance of the steam-propane co-injection by performing numerical simulations and concluded that low-pressure propane injection can be economically more viable than high pressure injection. Mohebati et al. (2012) conducted a detailed numerical simulation in a 3D model and demonstrated an improved steam/oil ratio when butane was co-injected with steam compared to a SAGD process.

Low temperature solvent-based processes are two-sided. Introducing solvents to the reservoir can improve the overall efficiency of an in-situ recovery method while inducing asphaltene precipitation leading to possible impairment of the reservoir permeability which can hinder the production. There are several studies in the literature reporting asphaltene precipitation and deposition due to the injection of propane and butane (Leyva-Gomez and Babadagli, 2013; Mokrys and Butler, 1993; Pathak et al., 2012; Tian et al., 2020). While the vapor-liquid equilibrium for propane- butane-bitumen has been widely addressed in the literature (Badamchi-Zadeh et al., 2009; Frauenfeld et al., 2002; Haddadnia et al., 2018; Luo et al., 2007; Nourozieh et al., 2014; Zirrahi et al., 2017), there is a knowledge gap in the liquid-liquid equilibrium studies of either propane-bitumen or butane-bitumen mixtures due to challenges associated with the compositional measurements.

Since the viscosity and density of the heavy phase in a LLE of a solvent bitumen system are drastically different from the light phase, the boundary between phases can be easily detected using an in-line viscometer or densitometer (Nourozieh et al., 2014). On the contrary, determining the composition of the phases can be challenging. Bitumen is not a pure compound and, in fact, it is comprised of thousands of components with a molecular weight ranging from 100 up to 10,000

g/mol (Azinfar et al., 2018). As a result, quantifying proportions of the components partitioned between phases at equilibrium condition can be difficult requiring a comprehensive method to fully characterize the bitumen and its fractions. Normally, crude oils are characterized based on the boiling point distribution of their constituents. For instance, two well-established methods of characterizing conventional oils are ASTM D2887 and D1160 (2018, 2019). One similar method to obtain the boiling point distribution of the components in heavy crudes and bitumen is simulated distillation, ASTM D7169 (2018). Although simulated distillation (SD) is a convenient and time-efficient technique, it is unable to provide the full boiling point distribution for bitumen samples. Components with a boiling point greater than 720 °C remain undetected with SD. Therefore, asphaltenes and heavy residue of the bitumen which constitute the main portion of the heavy phase in a LLE cannot be characterized.

One effective analytical approach to obtain a full molecular weight distribution of a sample is Gel Permeation Chromatography (GPC) (Such et al., 1979). GPC can exclude different components based on their sizes. The mixture is dissolved in a carrier phase and then passed through a porous column saturated with a stationary liquid. Molecules with smaller sizes tend to have larger retention time in the pores of the column while components with bigger sizes bypass most of the pores and elute earlier than the smaller ones. A calibration curve is needed to correlate the elution time of a sample from the GPC column to its molecular weight. In chemical engineering applications, this calibration is generated by standards polymers such as polystyrene or polyethylene. However, the use of these polymers for oil samples can result in erroneous MW distributions. Therefore, a correction factor is required (Ferworn, 1995). For instance, Peramanu et al. (1999) measured the molecular weight distribution of Athabasca and Cold Lake bitumen and their SARA fractions using GPC calibrated by polystyrene standards. They found the correction

factor by verifying their results with vapor pressure osmometry. Huang and Radosz (1991) also implemented a similar approach to correct the measured molecular weights with GPC. Azinfar et al. (2018) generated the calibration curve for the GPC chromatogram using SD results. They were able to characterize bitumen and its fractions regardless of the complexity of the samples.

In our previous study (Sadeghi Yamchi et al., 2018), experimental measurements of LLE for butane/bitumen mixtures were carried out at temperatures of 40 and 60 °C. The composition of the heavy and light cuts collected from the experiments was analyzed using SD method. Also, the effect of additives such as dimethyl ether and propane on LLE of butane/bitumen system was investigated. It was concluded that using only SD method cannot provide the full spectrum of the MW distributions in the cuts and hence needs improvement by coupling with other analytical methods such as GPC. We used the combined SD-GPC analytical method for LLE studies of DME/bitumen system (Sadeghi Yamchi et al., 2020). In that study, we designed experiments at a wider range of temperatures from 40 to 100 °C at three different concentrations of the solvent in the feed. Combining SD and CPG enabled us to fully characterize the heavy components of bitumen, define pseudocomponents, and calculate liquid-liquid K-values for those components. Lastly, NRTL model was used to predict liquid-liquid K-values of DME/bitumen system. In the current study, LLE experiments of propane+butane (with one to one mass ratio) mixture with bitumen are conducted at temperatures from 21 to 80 °C and solvent concentrations from 45 to 65 wt.%. Based on the detailed MW distribution of the cuts obtained from the combination of GPC and SD methods, two pseudocomponents were defined for bitumen and then the composition of each pseudocomponent was determined. NRTL model was tuned to reproduce the experimental compositions, and finally, the results presented in ternary diagrams to provide a clear picture of the LL envelope for LPG/bitumen system. Since the solvent is a mixture of propane and butane it

is referred to as LPG for simplicity. The results of this study in addition to previous studies are essential for design, operation, and optimization of a successful solvent process. Application of different solvents can result in different LLE conditions in the reservoir which can directly control and impact bitumen production. For instance, the amount of asphaltene precipitation is one of those controlling factors. While the use of a solvent with potential of less precipitation might be recommended during the early stages of production to prevent damage in the vicinity of wellbore, the application of a solvent with higher asphaltene yield might be favorable to produce a better quality of oil in later stages of bitumen recovery (Gupta et al., 2005).

4.4 Experimental Setup and Procedures

The schematic of the experiential setup utilized to conduct liquid-liquid equilibrium measurements of LPG/bitumen system is depicted in Figure 4.1. In summary, the setup consists of two main sections. The first section includes the oven which accommodates the equilibration cell along with a densitometer, viscometer, and a filter. The second part includes the equipment outside of the oven such as feeding and sampling cells, pumps, and data acquisition and controlling units.

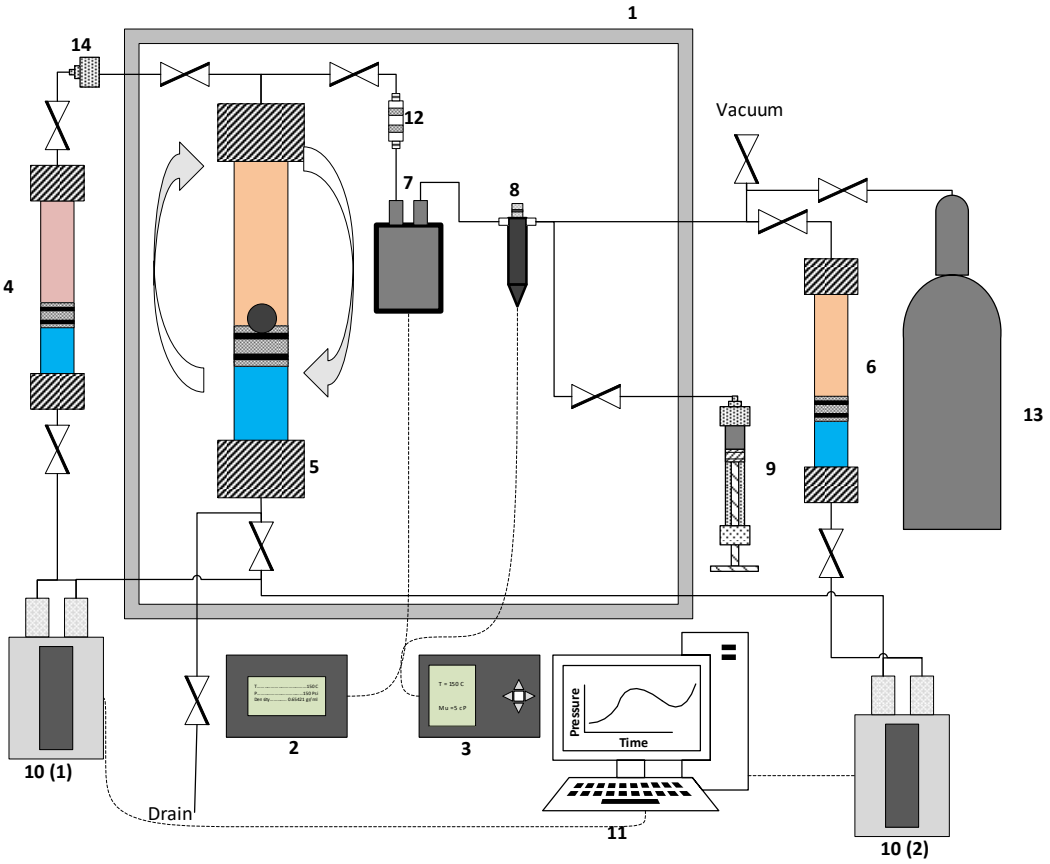

Figure 4.1: Experimental setup for PVT studies of LPG/bitumen mixtures, (1) Blue-M oven, (2) density data gathering unit, (3) viscosity data gathering unit, (4) feeding cell, (5) equilibration cell, (6) receiving cell, (7) densitometer, (8) viscometer, (9) sample cell, (10) Quizix pump, (11) pump controlling unit, (12) filter, (13) nitrogen cylinder, and (14) back-pressure regulator.

Pressures of the cells were controlled using Quizix pumps. These pumps can inject water with an accuracy of 0.002 cm^3 to displace the piston isolating the fluids inside the cell from the water underneath. The internal volume of the cells was approximately 850 cc allowing for reliable phase detection and data acquisition. The density of the phases was measured by an HPHT Anton Paar densitometer with a precision of 0.0001 g/cm^3 and the viscosity measurements were carried out with a Cambridge viscometer with an accuracy of 0.001 cP. A 15-micron filter was placed before the densitometer and viscometer to prevent the passage of any heavy particles that might have not

possibly separated from the light phase. The combination of in-line densitometer, viscometer, and filter provided an additional assurance for phase detection in the system.

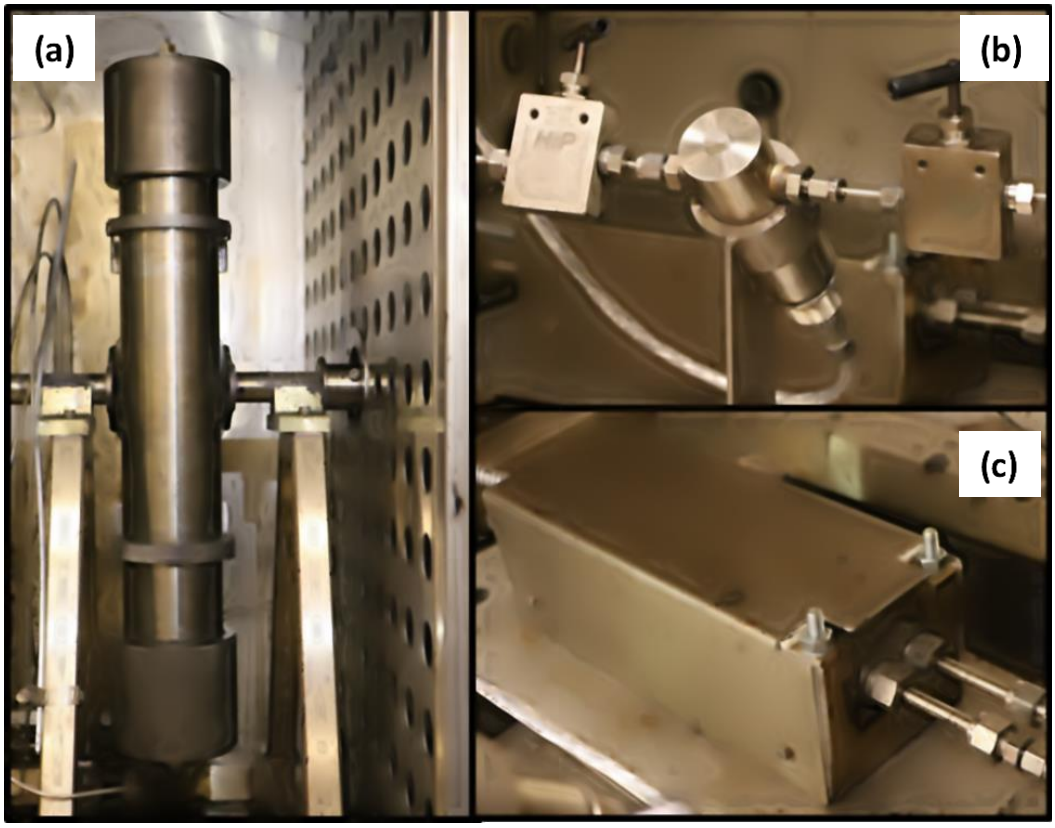

Figure 4.2: (a) Equilibration cell, (b) viscometer, and (c) densitometer located inside the oven for LLE measurements of LPG/bitumen system.

The bitumen required for liquid-liquid measurements of LPG/bitumen system in this study was supplied by one of the industry sponsors of the SHARP research consortium. The bitumen was filtered to remove possible solid particles and also dewatered to reduce its water content to less than 1000 ppm. The MW of bitumen was measured as 523 g/mol with a vapor pressure osmometer and its density at standard condition was obtained using Anton Paar DMA 5000 to have a value of 1.004 kg/m^3. The detailed characterization of bitumen can be found in our previous study (Azinfar

et al., 2018). The LPG for this study was synthesized in the lab by mixing propane and butane with a purity of 99.99% purchased from Praxair Inc.

Prior to any experiment, toluene was injected into the lines and fittings to remove any impurities from previous experiments. Then, acetone was used to wash away the toluene in the system, and lastly, air was purged into the system to dry out any remaining solvent in the lines. Once the system was cleaned, a known amount of bitumen was injected into the equilibration cell and the mass of the bitumen was recorded. Before injecting LPG into the mixing cell, the system was vacuumed for at least half an hour to remove the air and possible impurities. The LPG in the study was synthesized by mixing propane and butane with a mass ratio of 1:1. This concentration was mainly chosen since the commercial LPG is primarily formed of propane and butane. Also, a two-component mixture could lower the experimental and modeling challenges. The injection of LPG was carried out using a Quizix X6000 pump at constant pressure and room temperature. The volume of the injected LPG was recorded at the end of the process and the mass was calculated based on the density at that specific pressure and temperature. After injecting bitumen and LPG into the equilibration cell the temperature of the oven was set at 90 °C and the pump was set to operate at a constant desired pressure. The mixing time of LPG with bitumen at 90 °C was found to be much faster than the mixing of LPG and bitumen at lower experimental temperatures. A rocking system was used to rock the equilibrium cell continuously and a stainless steel rocking ball was placed inside the equilibrium cell to agitate the mixture for proper and faster mixing. After 24 hours of mixing at high temperature, the temperature of the oven was brought down to the desired experimental condition and an additional 24 hours was given to the system to reach proper equilibrium. The indication of whether the equilibrium condition was reached or not was checked with the injection volume of the pump. If pressure remained constant with zero net injected

volume, then the system was considered at equilibrium, otherwise, it was given more time to achieve equilibrium condition.

Before starting the density and viscosity measurements, the equilibration cell was kept in an up-right position for at least 12 hours to allow the light and heavy liquid phases to segregate. After 12 hours of segregation and just before discharging the fluid for density and viscosity measurements and sampling, the downstream line was pressurized with nitrogen gas to the test pressure to prevent introducing any disturbance to the equilibrium condition and avoid flashing the mixture. The fluids were discharged from the top of the cell immediately to minimize possible interaction of nitrogen with the light phase and density and viscosity of the light phase were recorded. Then, as soon as the heavy phase reached the top of the cell, the process of discharging was stopped. The readings of the densitometer and viscometer indicated how uniform was the light phase. Stable readings were an indication of proper segregation of phases and accumulation of the precipitated particles in the heavy phase at the bottom of the cell. Moreover, the placement of the filter before the densitometer and viscometer assisted for better identification of the phases and the quality of segregation. If the injection pressure of the pump was increasing with time, it could mean that the heavy phase with large enough asphaltenic particles was accumulating behind the filter as an indication of incomplete segregation. An example of density readings on densitometer at 80 °C and 45 wt.% LPG is illustrated in Figure 4.3. Initially, the densitometer records the density of the nitrogen gas, and as soon as the light phase reaches the densitometer, readings abruptly jump and stay stable until the end of the experiment.

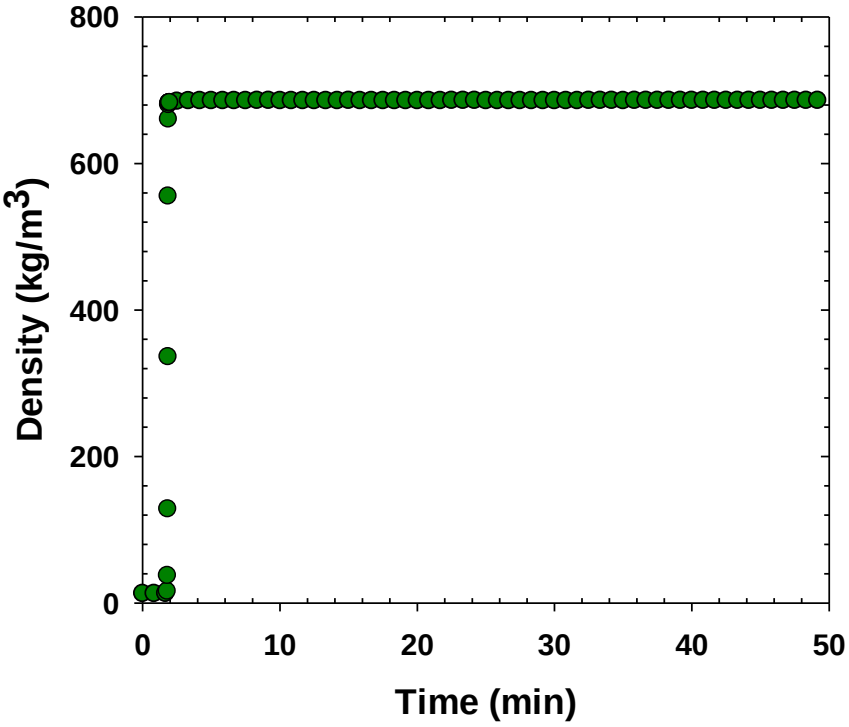

Figure 4.3: Stable density readings for the light phase created with mixing 45 wt.% LPG with bitumen at 80 °C, an indication of proper segregation of light and heavy phases.

A sample of the light phase was collected to measure the partitioning of the solvent to the light phase with gas chromatography. The composition of the solvent in the heavy phase was calculated indirectly based on material balance. Another sample from the light phase was also collected and flashed at atmospheric conditions to recover its bituminous part (light cut) for later GPC analysis. Once the light phase was discharged, the cell was depressurized and ultimately brought to the atmospheric condition to collect a sample of the heavy cut from the bottom of the cell. Figure 4.4 shows the heavy cut accumulated in the cell from a LLE test of LPG/bitumen system at 40 °C and 45 wt.% of LPG in the feed.

Figure 4.4: Heavy cut accumulated at the bottom of the equilibration cell after LLE experiment at 40 °C and 45 wt.% LPG in the feed.

The methodology of determining the composition of each phase has been discussed in detail in our previous study (Sadeghi Yamchi et al., 2020) and will be briefly explained in this article. As mentioned earlier, the composition of the solvent in the light phase was measured directly by using gas chromatography. Since the volume and density of the light phase were also directly measured during the test, the mass of the light phase was then calculated directly from the measurements. Knowing the initial mass of bitumen and LPG in the feed, the concentration of the solvent in the heavy phase was therefore calculated indirectly from mass balance equation.

The following terminology was introduced in our previous study (Sadeghi Yamchi et al., 2020) to distinguish between phases and cuts. ***Light phase*** is the light liquid at equilibrium condition (L_L). ***Heavy phase*** is the heavy liquid at equilibrium condition (L_H). ***Light cut*** is the bituminous part of

the light phase or in other words, it is the flashed off light phase (C_L). The light phase is a mixture of LPG and light cut. ***Heavy cut*** is the bituminous part of the heavy phase or in other words, it is the flashed off heavy phase (C_H). The heavy phase is a mixture of LPG and Heavy cut. ***Heavy yield*** is the fraction of the bitumen which partitions into the heavy phase.

To present the results in a ternary diagram, bitumen is divided into two pseudocomponents. However, to define the pseudocomponets, full characterization of bitumen is required. To characterize bitumen, simulated distillation was used in combination with gel permeation chromatography. The full description of the characterization method has been reported elsewhere (Azinfar et al., 2018; Sadeghi Yamchi et al., 2020). In summary, we correlated the response of the GPC chromatogram to the cumulative yield obtained from SD. Since the cumulative yield of SD is a function of MW, we were able to develop a correlation between the GPC time and the MW of the components eluted from GPC column. Once the MW distribution of bitumen was obtained, the split point of 605 g/mol was found based on Whitson theory (Whitson, 1983) to define two pseudocomponent for bitumen. Therefore, all the components with MW less than 605 g/mol were lumped as pseudocomponent PC1 with a mass fraction of 0.44, and all the components with MW larger than 605 g/mol were lumped as pseudocpmponent PC2 with a mass fraction of 0.56. The same procedure was performed on the light and heavy cuts and the mass fraction of each pseudocomponent in the cuts was obtained accordingly. To calculate the composition of each pseudocomponent at equilibrium conditions, we used the following equation:

$$\omega_{PCi}^{L} = (1-\omega_{LPG}^{L}) \times \omega_{PCi}^{C}, \tag{4.1}$$

where ω is the mass fraction, *L*, *C* and *PC* denote the liquid phase, the cut, and pseudocomponet, respectively.

4.5 Thermodynamic Modeling

For a multicomponent mixture, the liquid-liquid equilibrium criteria can be expressed as (Prausnitz et al., 1998):

$$x_i^{L_L}\gamma_i^{L_L} = x_i^{L_H}\gamma_i^{L_H}, \tag{4.2}$$

where *x* and *γ* are the mole fraction and activity coefficient of component *i*, respectively. We used non-random two liquid (NRTL) thermodynamic model to assess the activity coefficient of each component in the mixture as stated in the following equation (Renon and Pruasnitz, 1968):

$$\ln(\gamma_i) = \frac{\sum_j \tau_{ji} G_{ji} x_j}{\sum_l G_{li} x_l} + \sum_j \frac{x_j G_{ij}}{\sum_l G_{lj} x_l}\left(\tau_{ij} - \frac{\sum_r x_r \tau_{rj} G_{rj}}{\sum_l G_{lj} x_l}\right), \tag{4.3}$$

where G_{ij} is a characteristic of interaction energies between molecules of *i* and *j* given as follows (Renon and Pruasnitz, 1968):

$$G_{ij} = \exp(-\alpha_{ij}\tau_{ij}), \tag{4.4}$$

where τ_{ij} is the energy interaction parameter and α indicates the randomness of the system and is considered to be symmetric $\alpha_{ij} = \alpha_{ji}$. It has been shown that the value of α can vary from 0.20 to 0.47 and it was assumed 0.3 in this work. τ_{ij} was tuned to reproduce the experimental compositional data.

The optimization toolbox of MATLAB (version 2018) was used for the non-linear regression procedure to tune τ_{ij} of the NRTL model in flash calculations and match the experimental composition data. The following objective function was defined for non-linear regressions:

$$OF = \frac{1}{2N}\left(\sum_{i=1}^{N}\frac{\left|x_i^{L_L,calc} - x_i^{L_L,\exp}\right|}{x_i^{L_L,\exp}} + \sum_{i=1}^{N}\frac{\left|x_i^{L_H,calc} - x_i^{L_H,\exp}\right|}{x_i^{L_H,\exp}}\right), \tag{4.5}$$

where x is the mole fraction, $i=1,\ldots,N$ is the number of the component, and L_L, L_H, *calc*, *exp* denote light liquid, heavy liquid, calculated value, and experimental value, respectively.

4.6 Results and Discussion

Liquid-liquid equilibrium measurements of LPG and bitumen system were conducted in this study. As mentioned earlier, the LPG was synthesized in the lab by mixing propane and n-butane with a 1:1 mass ratio. The experiments were carried out in a temperature range between 21°C (room temperature) and 80 °C. Pressure was maintained constant at 3.4MPa for all the tests. In order to perform measurements in LLE region, three different concentrations of 45, 55, and 65 wt.% LPG in the feed was selected as preliminary observations indicated no LLE could form at solvent concentrations below 40 wt.%. The measured concentrations of the solvent and pseudocomponents are summarized in Table 4.1.

Table 4.1: Composition (wt.%) of components at equilibrium conditions. [a]

T (°C)	P (MPa)	Feed				Light Phase				Heavy Phase			
		C_3	C_4	PC_1	PC_2	C_3	C_4	PC_1	PC_2	C_3	C_4	PC_1	PC_2
21	3.4	22.50	22.50	23.99	31.01	23.71	24.12	23.91	28.26	16.86	14.79	20.85	47.50
21	3.4	27.50	27.50	19.63	25.37	32.03	32.04	19.16	16.77	12.78	12.77	18.77	55.68
21	3.4	32.50	32.50	15.27	19.73	36.75	37.85	14.59	10.81	12.84	7.72	18.52	60.92
40	3.4	22.50	22.50	23.99	31.01	24.09	23.83	23.70	28.38	14.62	15.92	19.77	49.69
40	3.4	27.50	27.50	19.63	25.37	32.59	32.43	19.03	15.95	12.97	13.43	18.88	54.72
40	3.4	32.50	32.50	15.27	19.73	37.10	38.37	14.11	10.42	13.26	7.94	18.14	60.66
40	2.1	25.00	25.00	-	-	28.13	28.98	-	-	16.72	14.46	-	-
60	3.4	22.50	22.50	23.99	31.01	23.83	23.62	24.05	28.50	15.14	16.26	18.93	49.67
60	3.4	27.50	27.50	19.63	25.37	32.40	32.17	19.22	16.21	14.52	15.13	17.60	52.75
60	3.4	32.50	32.50	15.27	19.73	38.14	37.20	14.31	10.35	9.11	12.99	18.06	59.84
80	3.4	22.50	22.50	23.99	31.01	24.42	24.06	23.78	27.74	14.54	16.07	19.03	50.36
80	3.4	27.50	27.50	19.63	25.37	32.55	33.03	19.08	15.34	13.16	11.80	19.21	55.83
80	3.4	27.50	27.50	19.63	25.37	34.15	32.63	-	-	11.50	15.15	-	-
80	3.4	32.50	32.50	15.27	19.73	36.98	38.88	14.45	9.69	14.52	6.91	18.64	59.93

[a]Standard uncertainties are $u(T)$= 0.228 °C, $u(P)$= 0.003 MPa, $u(composition)$=0.005 wt.%.

Expanded uncertainties are $Uc(composition)$= 0.008 wt.% (95% level of confidence).

To illustrate and better identify the trends, the compositions of the components in the heavy and light pashes at 21°C are plotted versus the feed concentration in Figure 4.5. The mass fraction of both components of the solvent (propane and butane) in the light phase is increasing with the increase of the solvent fraction in the feed. In contrast, the mass fraction of both pseudocomponents PC1 and PC2 are decreasing. In the heavy phase, only the concentration of PC2 is increasing. PC2 is the heaviest pseudocomponent that has the least affinity with the solvent. Therefore, as more solvent is added to the mixture, PC2 partitions more to the heavy phase and gets separated from

the light phase. Also, it was observed that the tendency of both propane and butane is nearly equal to partition to the light phase as such the ratio of propane to butane remains constant from feed to the light phase.

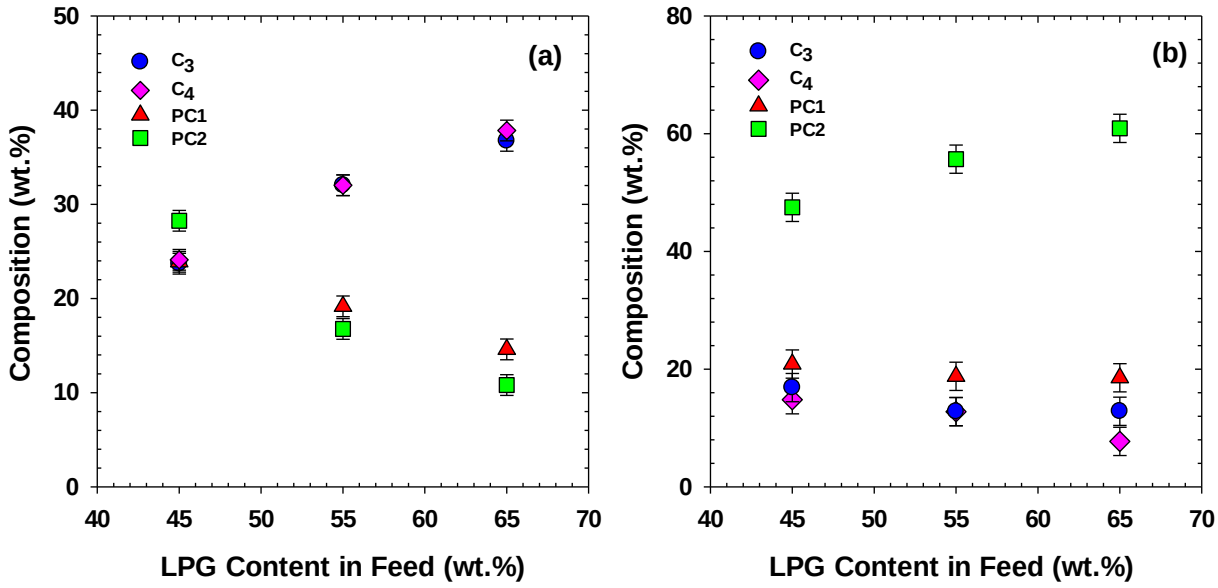

Figure 4.5: Measured compositions for (a) light phase, and (b) heavy phase for LLE tests at 21 °C.

The repeatability of the measurements for solvent concentration in the light phase and heavy phase was found to be 1.0% and 2.4%, respectively. The noticeable difference between the two values stems from the application of two different methods based on which the measurements were taken. The light phase composition was directly measured with GC and then the composition of the heavy phase was obtained from material balance calculations.

To obtain more details about the composition of the light and heavy cuts we used SD and GPC results to determine the molecular weight distributions of the cuts.

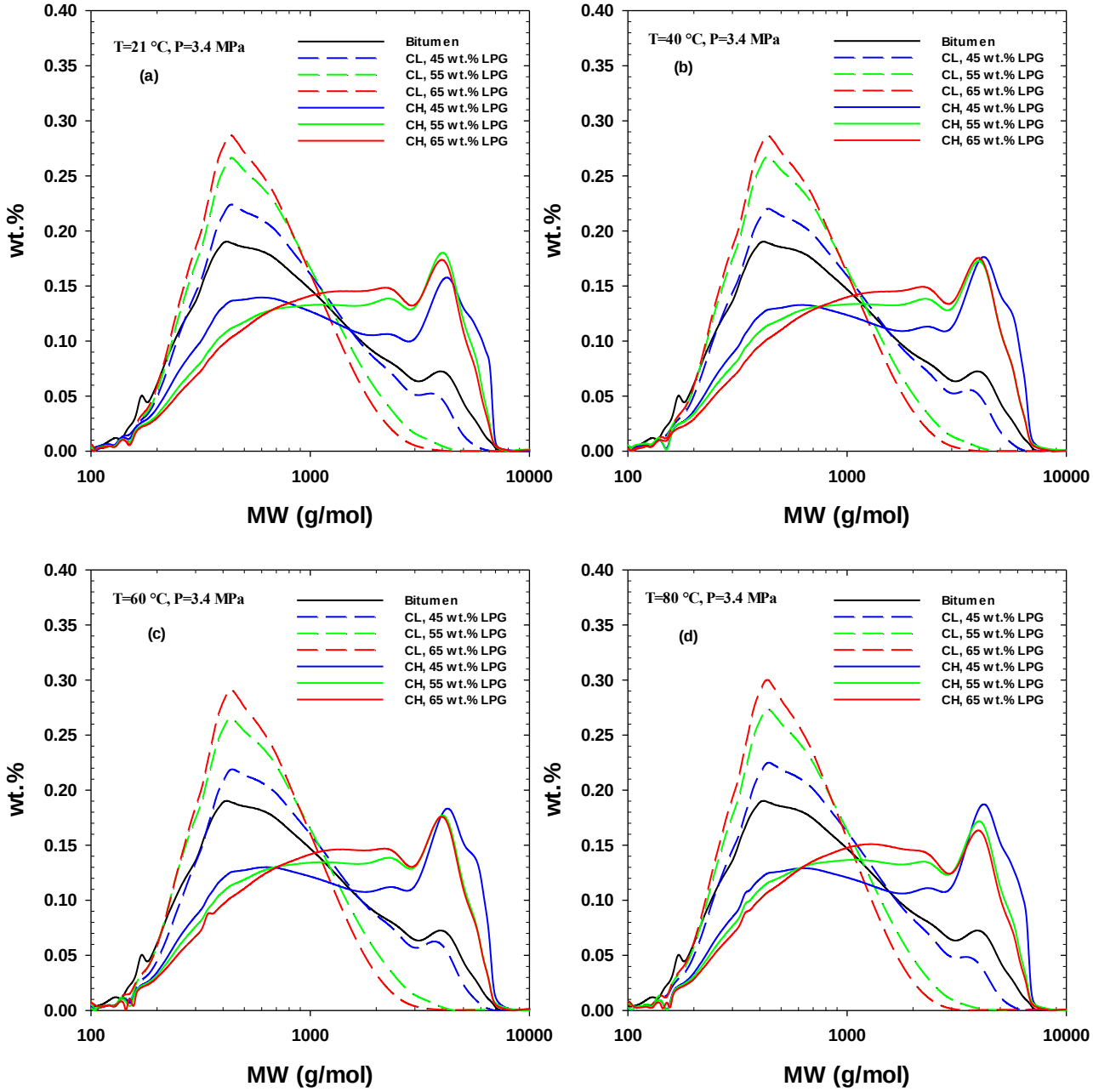

Figure 4.6: Molecular weight distributions of the cuts recovered from different equilibrium conditions for LPG/bitumen mixtures.

Figure 4.6 shows the MW distribution of the light and heavy cuts at four different experimental temperatures. As it is illustrated, at a given temperature, the fraction of components with molecular

weights ranging from 200 to 1000 g/mol is increasing in the light cuts with adding more solvent to the system. On the other hand, the concentration of molecules with MW greater than 2000 g/mol is reduced as those molecules are separated from the cut. This behavior indicates that more of the heavier components are extracted out of the bitumen with more LPG. For instance, when the feed mass fraction of the LPG is 45 wt.% and close to the onset point, only a small amount of precipitation occurs and thus the MW distribution of the corresponding light cut remains close to that of bitumen. The visual inspection of the light cuts from LLE experiments also verifies the results obtained by MW distribution analysis. Figure 4.7 shows the picture of the three light cuts obtained by mixing 45, 55, 65 wt% LPG with bitumen, respectively, at 80 °C. As depicted, the cuts are well distinguished in terms of their appearance such that their color turns black to light brown as the solvent mass fraction increases in the feed. This transition of color is an indication of extracting more heavy components of the bitumen by adding more solvent which consequently results in more upgrading.

Figure 4.7: Light cuts and the corresponding heavy cuts from LLE of LPG/bitumen mixtures at 80 °C and solvent concentration of (a) 45, (b) 55, and (c) 65 wt.% in the feed.

Inspecting the MW distribution of the heavy cuts reveals that adding more solvent to the mixture at any temperature can produce heavy cuts that are less concentrated in components with MW

greater than 5000 g/mol and more concentrated in the molecules with MW between 1000 to 5000 g/mol. When the concentration of the solvent in the feed is close to the onset point (i.e. 45 wt.%), the precipitation is less and only the heaviest components are extracted from the bitumen. By adding more of the solvent, the amount of precipitation increases with extracting more of the intermediate components of the bitumen. The same behavior was also observed previously with a non-paraffinic and volatile solvent (Sadeghi Yamchi et al., 2020).

Once the MW distribution of the cuts is measured, the mole fraction of the pseudocomponents can be calculated. Similar to the VLE, LLE K-values for the components in the system can be estimated based on their mole fraction in the phases. In this study, the K-value of each component was calculated as the ratio of the mole fraction of that component in the light phase to its mole fraction in the heavy phase. The results have been presented in Table 4.2. It should be noted that the solvent was given as a single pseudocomponent of LPG since it was found that the tendencies of both propane and butane to partition into the light phase were equal and the mass ratio of propane to butane was maintained constant from feed to the light phase. Furthermore, one pseudocomponent for the solvent facilitated the modeling process and it was aligned with the goal of this study to present the experimental data in ternary diagrams.

Table 4.2: Liquid-liquid K-values of all components in LPG/bitumen system.[a]

T(°C)	P (MPa)	wt.%$_{LPG}$	K-value		
			LPG	PC1	PC2
21	3.4	45	1.05	0.75	0.58
21	3.4	55	1.12	0.43	0.22
21	3.4	65	1.19	0.25	0.10
40	3.4	45	1.04	0.78	0.54
40	3.4	55	1.11	0.44	0.21
40	3.4	65	1.18	0.25	0.10
60	3.4	45	1.04	0.80	0.58
60	3.4	55	1.08	0.53	0.25
60	3.4	65	1.17	0.26	0.10
80	3.4	45	1.04	0.79	0.54
80	3.4	55	1.13	0.41	0.19
80	3.4	65	1.16	0.41	0.15

[a]Standard uncertainties are *u(T)*= 0.228 °C, *u(P)*= 0.003 MPa, *u(composition)=0.005 wt.%*.
Expanded uncertainties are *Uc(K-value)*=0.002 wt.% (95% level of confidence).

K-values were found to be a strong function of the solvent concentration. The K-values of LPG increase as more solvent is added to the mixture, whereas the K-values of the pseudocomponents decrease. This trend of K-values is in correspondence with the changes in the solubilities of the components in the system. As discussed earlier adding more solvent to the system can reduce the solubility of LPG in the heavy phase as a consequence of the increase in the solubility of the heaviest pseudocomponent (PC2). Since the solubility and K-value are inversely correlated, we observe an increase in the K-values of LPG and a decrease in the K-values of the pseudocomponents. The calculated K-values for solvent were found to be close to unity with small variations since the mole fractions of LPG were greater than 90 mol.% in the light phase and it was also greater than 80 mol.% in the heavy phase.

Density and viscosity of the light phase were also measured in this study. These data are given in Table 4.3. The range for the density data is between 552 to 745 kg/m^3. In all the tests, LPG accounted for more than half of the mass of the light phase, thus the measured densities were considerably impacted by the solvent concentration. Moreover, adding more solvent to the mixture led to the separation of more heavy components from the bitumen which resulted in a further reduction in densities. The same behavior was also observed for viscosities. The high solvent concentration in the light phase resulted in viscosities less than 2 cP. The repeatability of the density and viscosity measurements were found to be 4.2 kg/m^3 and 0.1 cP, respectively.

Table 4.3: Density and viscosity of the light phase for LPG/bitumen mixtures.[a]

T(°C)	P (MPa)	wt.%$_{LPG}$	$\rho^L{}_L$(kg/m^3)	$\mu^L{}_L$(cP)
21	3.4	45	745.8	1.8
21	3.4	55	668.4	0.5
21	3.4	65	629.4	0.3
40	3.4	45	732.6	1.4
40	3.4	55	651.9	0.4
40	3.4	65	610.9	0.2
40	2.1	40	766.2	3.6
40	2.1	50	683.4	0.6
60	3.4	45	714.1	1.0
60	3.4	55	630.8	0.3
60	3.4	65	582.5	0.2
80	3.4	45	685.9	0.8
80	3.4	55	601.3	0.2
80	3.4	55	607.1	0.3
80	3.4	65	552.9	0.1

[a]Standard uncertainties are *u(T)*= 0.228 °C, *u(P)*= 0.003 MPa, *u(composition)=0.005 wt.%*.

Expanded uncertainties are $Uc(\rho)$= 0.246 kg/m^3, $Uc(\mu)$= 0.034 cP, $Uc(P_{sat})$= 0.007 MPa (95% level of confidence).

One of the objectives of this study was to model the experimental compositions. NRTL thermodynamic model, the theoretical basis of which was discussed in Section 3, was used to predict LLE compositions. Flash calculations coupled with NRTL model were optimized using the optimization toolbox of MATLAB and the τ_{ij} values of the model were tuned to reproduce the compositions of each component in the LLE. The optimization was performed separately for each temperature where the tuned τ_{ij} values are reported in Table 4.4.

Table 4.4: τ_{ij} used for calculation of compositions in NRTL model.

T(°C)	21	40	60	80
$\tau_{\text{LPG-PC1}}$	20.91	19.58	22.09	31.76
$\tau_{\text{LPG-PC2}}$	8.40	8.90	8.22	7.53
$\tau_{\text{PC1-LPG}}$	3.86	3.91	3.26	3.23
$\tau_{\text{PC1-PC2}}$	0.02	0.30	-0.06	0.01
$\tau_{\text{PC2-LPG}}$	-1.26	-1.34	-1.33	-1.64
$\tau_{\text{PC2-PC1}}$	-0.02	0.06	-0.03	-0.05

The results of the modeling are presented in Figure 4.8. As shown, the model was able to predict the experimental compositions with an AARD of 8.5%. Ternary results presented in this study are comparable with our previous study where DME was the precipitating solvent (Sadeghi Yamchi et al., 2020). Liquid-liquid envelopes for LPG and bitumen system are wider than that of DME/bitumen system as a confirmation of the early onset point for LPG as well as more precipitation (see Figure 4.9).

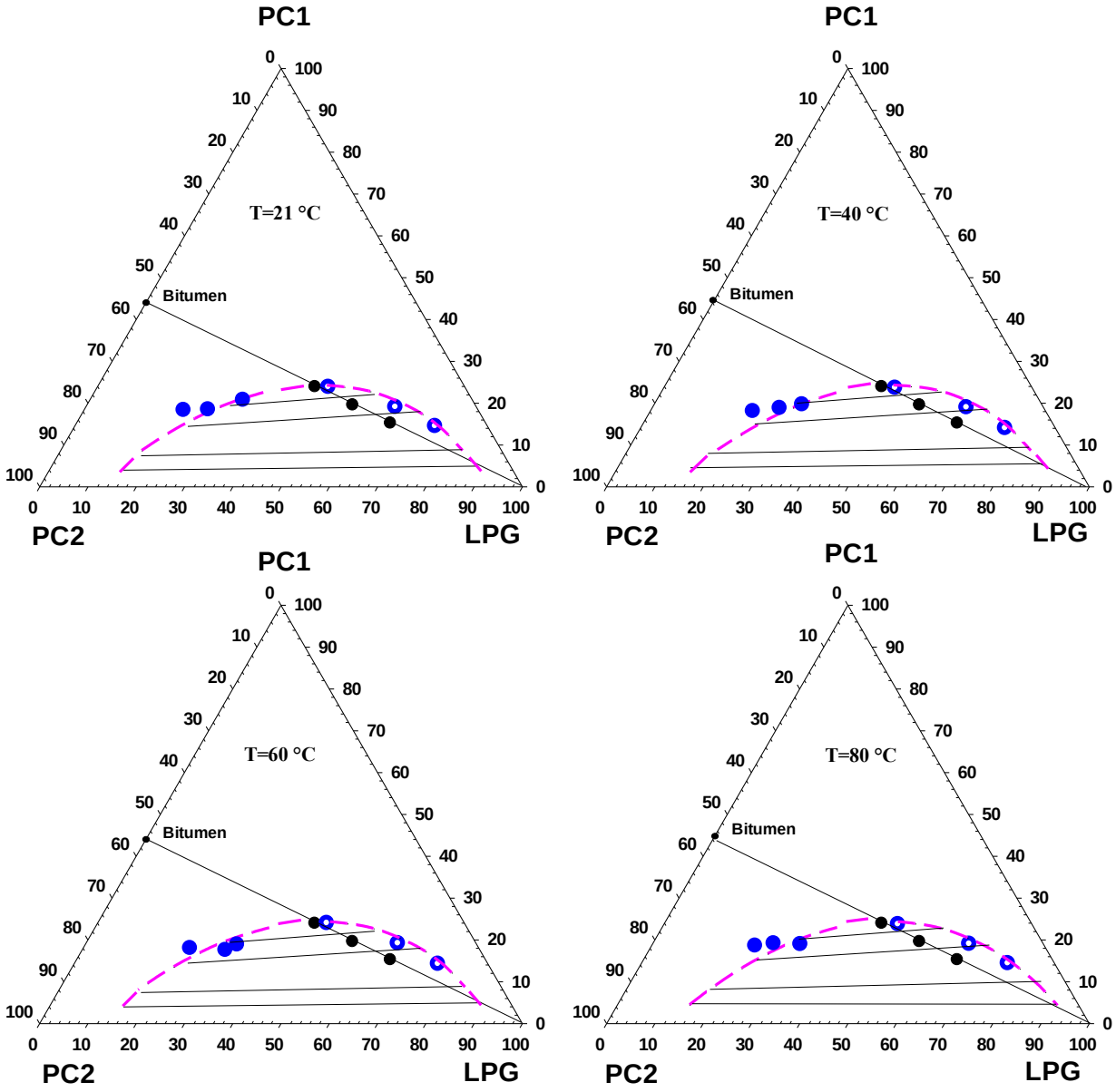

Figure 4.8: Ternary diagrams of LPG/bitumen systems at different temperatures. ○ experimental composition of the light phase; ● experimental composition of the heavy phase; - - - model predictions; — model tie lines.

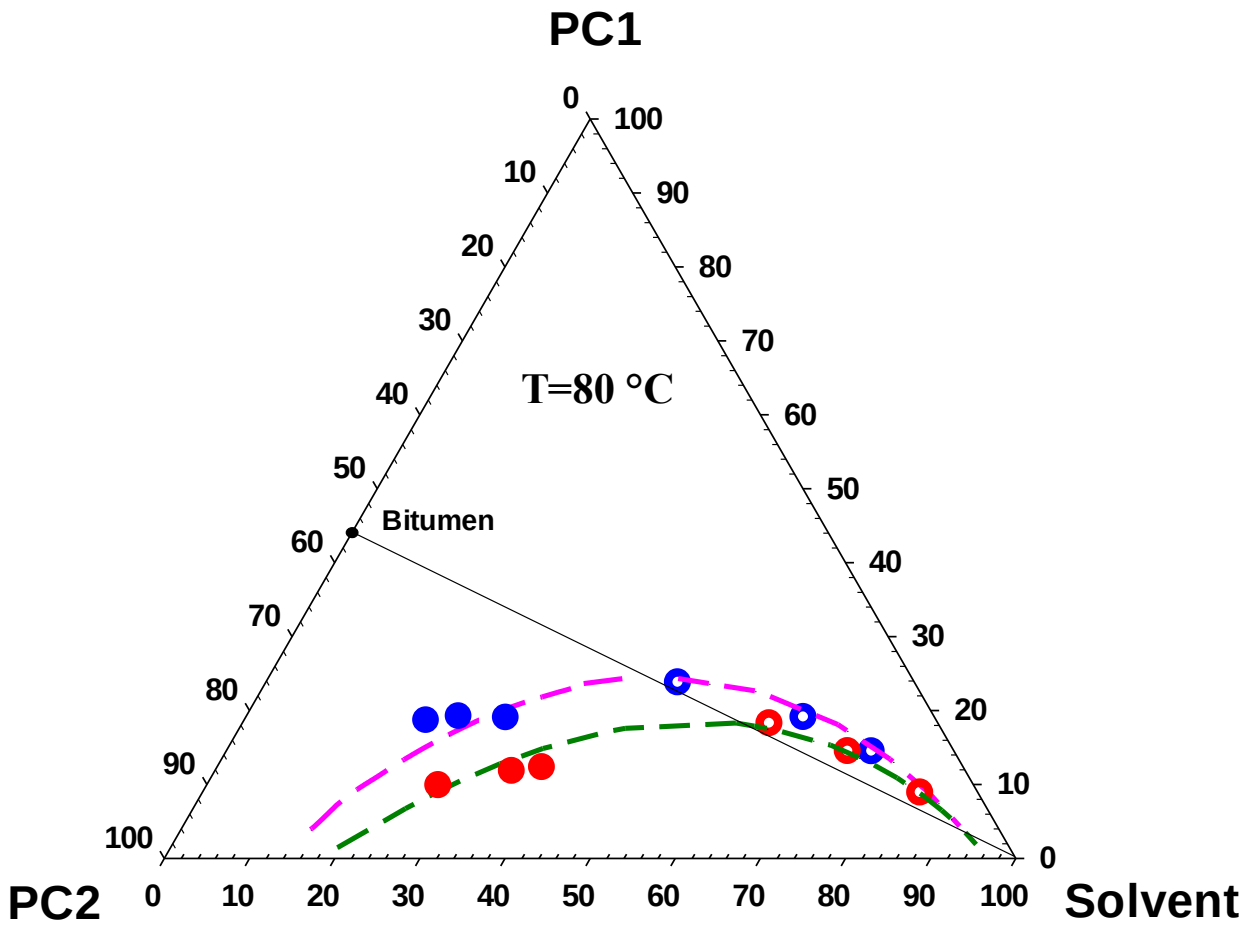

Figure 4.9: A comparison of the ternary diagrams of LPG/bitumen and DME/bitumen systems at 80 °C. ○, ● experimental compositions of light and heavy phases for LPG/bitumen system; ○, ● experimental compositions of light and heavy phases for DME/bitumen system; - - - model predictions. DME/bitumen data was obtained from our previous study (Sadeghi Yamchi et al., 2020).

Heavy yield or the fraction of bitumen which precipitates due to mixing with LPG is presented in Figure 4.10. According to the yield curve, the onset point of precipitation for LPG/bitumen system is between 40 and 45 wt.% of the solvent compared to about ~58 wt. % for dimethyl ether (DME). Mixing LPG with bitumen can precipitate nearly 25 wt.% of heavy components of the bitumen above the onset point. The precipitation can reach 40 to 45wt.% at higher concentrations of LPG.

This is in agreement with previous studies of asphaltene precipitation with n-alkanes indicating that n-alkanes with lower carbon numbers can result in higher amounts of precipitation. For instance, normal pentane (n-C_5) can precipitate nearly 20% asphaltenes from Athabasca bitumen whereas normal heptane (n-C_7) only precipitates 13% (Sadeghi Yamchi, 2014). This trend is verified with LPG experiments in this study showing that mixing bitumen with lighter n-alkanes than n-C_5 can result in even more precipitation.

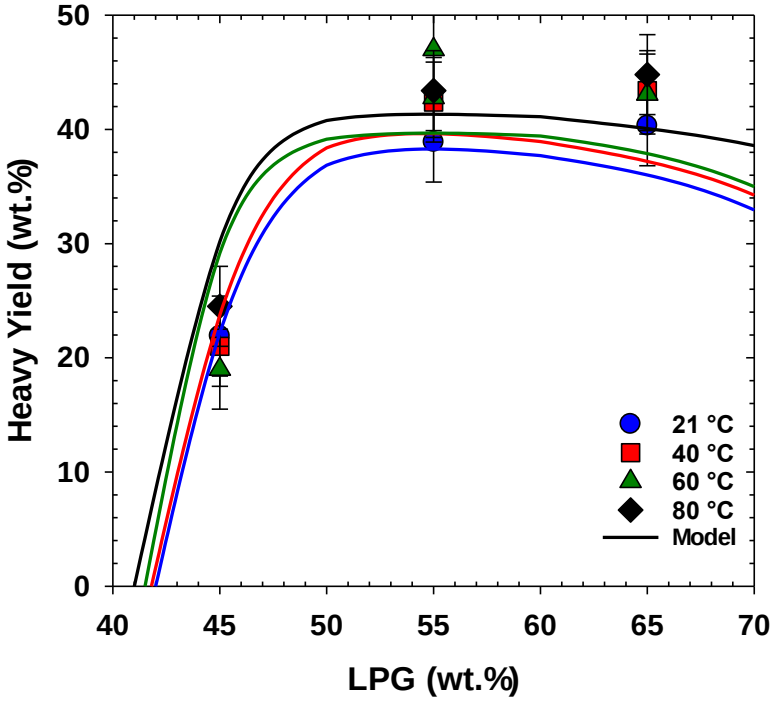

Figure 4.10: Heavy yield of LPG/bitumen systems at different temperatures; ●, ■, ▲, ◆ are experimental data; — model predictions.

4.7 Summary and Conclusions

In this study, liquid-liquid equilibrium measurements of LPG (propane+butane)/bitumen system were conducted at temperatures from 21 to 80 °C and solvent concentrations of 45, 55, 65 wt.%.

The composition of each phase along with the density and viscosity of the light phase was measured at each equilibrium condition. Moreover, a detailed characterization of the light and heavy cuts was determined using SD-GPC method.

Results showed that by increasing the solvent concentration in the feed the solubility of the solvent increased in the light phase, whereas its solubility decreased in the heavy phase because of the extraction of more heavy components from bitumen. The results also revealed that propane and butane tend to partition equally into the light phase.

Detailed characterization of the cuts indicated that increasing the solvent concentrations leads to more extraction of components with MW less than ~1000 g/mol from the heavy phase and results in more separation of the components with MW larger than ~2000 from the light phase.

It was shown that mixing LPG with bitumen could result in precipitation as high as 45% leading to high quality oil. These results are in correspondence with asphaltene precipitations using n-pentane and n-heptane indicating that lower carbon number in the n-alkane leads to more asphaltene precipitation.

Finally, bitumen was divided into two pseudocomponents based on the MW distributions obtained from SD-GPC analysis. Then, the experimental LL K-values were estimated for the components in the system and NRTL thermodynamic model was tuned to predict experimental compositions. The model was able to reproduce the experimental data with an AAD of 8.5%.

4.8 References

ASTM D1160 - 18 Standard Test Method for Distillation of Petroleum Products at Reduced Pressure, 2018. ASTM International, West Conshohocken.

ASTM D2887-19ae1, Standard Test Method for Boiling Range Distribution of Petroleum Fractions by Gas Chromatography, 2019. ASTM International, West Conshohocken.

ASTM D7196 - 18 Standard Test Method for Raveling Test of Cold-Mixed Emulsified Asphalt Samples, 2018. ASTM International, West Conshohocken.

Azinfar, B., Zirrahi, M., Hassanzadeh, H., Abedi, J., 2018. Characterization of heavy crude oils and residues using combined Gel Permeation Chromatography and simulated distillation. Fuel 233, 885–893.

Badamchi-Zadeh, A., Yarranton, H.W., Svrcek, W.Y., Maini, B.B., 2009. Phase behaviour and physical property measurements for VAPEX solvents: Part I. Propane and Athabasca bitumen. J. Can. Pet. Technol. 48, 54–61.

Butler, R.M., Mokrys, I.J., 1993. Recovery of Heavy Oils Using Vapourized Hydrocarbon Solvents: Further Development of the Vapex Process. J. Can. Pet. Technol. 32.

Butler, R.M., Mokrys, I.J., 1991. A New Process (VAPEX) For Recovering Heavy Oils Using Hot Water And Hydrocarbon Vapour. J. Can. Pet. Technol. 30.

Deng, X., 2005. Recovery performance and economics of steam/ propane hybrid process, in: SPE International Thermal Operations and Heavy Oil Symposium. Society of Petroleum Engineers, Calgary, Alberta, Canada.

Ferguson, M.A., Mamora, D.D., Goite, J.G., 2001. Steam-Propane Injection for Production

Enhancement of Heavy Morichal Oil, in: SPE International Thermal Operations and Heavy Oil Symposium Proceedings. Porlamar, Margarita Island, Venezuela.

Ferworn, K.A., 1995. Thermodynamic and kinetic modelling of asphaltene precipitation from heavy oils and bitumens, PhD thesis, University of Calgary.

Frauenfeld, T.W.J., Kissel, G.A., Shibing Zhou, W., 2002. PVT and Viscosity Measurements for Lloydminster-Aberfeldy and Cold Lake Blended Oil Systems, in: Canadian International Petroleum Conference. Calgary, Alberta, Canada.

Gupta, S., Gittins, S., Picherack, P., 2005. Field implementation of solvent aided process. J. Can. Pet. Technol. 14, 8–13.

Haddadnia, A., Sadeghi Yamchi, H., Zirrahi, M., Hassanzadeh, H., Abedi, J., 2018. New Solubility and Viscosity Measurements for Methane-, Ethane-, Propane-, and Butane-Athabasca Bitumen Systems at High Temperatures up to 260 °c. J. Chem. Eng. Data 63, 3566–3571.

Huang, S.H., Radosz, M., 1991. Phase behavior of reservoir fluids IV: Molecular weight distributions for thermodynamic modeling. Fluid Phase Equilib. 66, 23–40.

John M. Prausnitz, Rudiger N. Lichtenthaler, E.G. de Azevedo., 1998. Molecular Thermodynamics of Fluid-Phase Equilibria, Third. ed. Pearson Education.

Leyva-Gomez, H., Babadagli, T., 2013. Numerical simulation of heavy-oil/bitumen recovery by solvent injection at elevated temperatures. J. Pet. Sci. Eng. 110, 199–209.

Luo, P., Yang, C., Gu, Y., 2007. Enhanced solvent dissolution into in-situ upgraded heavy oil under different pressures. Fluid Phase Equilib. 252, 143–151.

Mohammadpoor, M., Torabi, F., 2015. Comprehensive experimental study and numerical

simulation of vapour extraction (VAPEX) process in heavy oil systems. Can. J. Chem. Eng. 93, 1929–1940.

Mohebati, M.H., Maini, B.B., Harding, T.G., 2012. Numerical-simulation investigation of the effect of heavy-oil viscosity on the performance of hydrocarbon additives in SAGD, in: SPE Reservoir Evaluation and Engineering.

Mokrys, I.J., Butler, R.M., 1993. In-situ upgrading of heavy oils and bitumen by propane deasphalting: The Vapex process. Prod. Oper. Symp. 409–424.

Nennieger, J., Nenniger, E., 2005. Method and apparatus for stimulating heavy oil production. U.S. Patent No. 6,883,607.

Nourozieh, H., Kariznovi, M., Abedi, J., 2014. Phase behaviour study of butane / Athabasca bitumen mixtures applicable for thermal and hybrid solvent recovery processes, in: SPE Heavy Oil Conf. Canada.

Pathak, V., Babadagli, T., Edmunds, N., 2012. Mechanics of heavy-oil and bitumen recovery by hot solvent injection. SPE Reserv. Eval. Eng. 15, 182–194.

Peramanu, S., Pruden, B.B., Rahimi, P., 1999. Molecular weight and specific gravity distributions for Athabasca and Cold Lake bitumens and their saturate, aromatic, resin, and asphaltene fractions. Ind. Eng. Chem. Res. 38, 3121–3130.

Renon, H., Pruasnitz, J.M., 1968. Local compositions in thermodynamics excess functions for liquids mixtures. AIChE J. 14, 116–128.

Sadeghi Yamchi, H., 2014. Effect of Refining on Asphaltene Property Distributions, Master's thesis, University of Calgary.

Sadeghi Yamchi, H., Zirrahi, M., Hassanzadeh, H., Abedi, J., 2020. Measurements and NRTL modeling of liquid-liquid equilibrium of dimethyl ether/bitumen. Fluid Phase Equilib. 512, 112549.

Sadeghi Yamchi, H., Zirrahi, M., Hassanzadeh, H., Abedi, J., Fadaei, H., 2018. Effect of additives on liquid–liquid equilibrium properties of butane/bitumen systems with applications to solvent aided bitumen recovery processes. Chem. Eng. Res. Des. 137, 452–460.

Such, C., Brule, B., Baluja-Santos, C., 1979. Characterization of a road asphalt by chromatographic techniques (GPC and HPLC). J. Liq. Chromatogr. 2, 437–453.

Tian, Y., Ju, B., Lü, G., Liu, N., Dong, Y., Ma, S., 2020. The comprehensive model for solvent assisted steam flooding in thin heavy oil reservoirs considering asphaltene deposition. J. Pet. Sci. Eng. 185, 106676.

Whitson, C.H., 1983. Characterizing Hydrocarbon Plus Fractions. Soc. Pet. Eng. J. 23, 683–694.

Wilson, K., 2015. nsolv - Non-Confidential Final Report - CCEMC Project ID: H110031 H110031.

Zhang, K., Zhou, X., Peng, X., Zeng, F., 2019. A comparison study between N-Solv method and cyclic hot solvent injection (CHSI) method. J. Pet. Sci. Eng. 173, 258–268.

Zirrahi, M., Hassanzadeh, H., Abedi, J., 2017. Experimental and modelling studies of MacKay River bitumen and light n-alkane binaries. Can. J. Chem. Eng. 95, 1417–1427.

Chapter Five: **Numerical Simulation of Asphaltene Deposition in Porous Media Induced by Solvent Injection**

5.1 Preface

This chapter has been submitted for publication in a peer-reviewed journal entitled “Numerical Simulation of Asphaltene Deposition in Porous Media Induced by Solvent Injection”. This manuscript was co-authored by M. Zirrahi, H. Hassanzadeh, and J. Abedi.

In this chapter a modified approach to reservoir simulation of asphaltene deposition is introduced by implementing LL K-values and non-equilibrium mass transfer model.

5.2 Abstract

We present numerical simulation of asphaltene deposition induced by solvent injection by the implementation of liquid-liquid equilibrium (LLE) data along with a reaction-based non-equilibrium mass transfer model. The interplay of viscous fingering and asphaltene deposition during the injection of dimethyl ether (DME) was studied. Our results reveal that one-dimensional approach fails to predict the real physics and underestimates the deposition. It is shown that DME injection leads to upgrading of the produced oil. The results indicate that the dynamics of the viscous fingering is independent of the deposition rate and governed by the viscosity ratio. Our findings also suggest that grid dependency of deposition poses a computational challenge. To address this issue, we developed scaling relations to upscale the fine-scale deposition rate to the coarse-grid numerical simulations. This study finds application in solvent-based recovery processes and paves the way for integrating LLE data in numerical simulation of asphaltene deposition.

5.3 Introduction

Asphaltenes are the heaviest and the most polar components in the oil which are formed of several aromatic rings with attached heteroatoms such as sulfur, nitrogen, and oxygen. They are defined as molecules that are soluble in an aromatic solvent such as toluene and insoluble in paraffinic solvents such as pentane and heptane (Mansoori, 1997). Asphaltenes can potentially precipitate and deposit in oil reservoirs, production tubing, and surface facilities due to changes in the pressure, temperature, and oil composition (Civan, 2015; Porter, 1989). Deposition of asphaltenes can lead to significant economic consequences. Therefore, understanding the underlying mechanisms involved in the asphaltene precipitation and our ability to model and predict this phenomenon is of great importance.

The deposition of asphaltene can occur at any stages of petroleum production (Leontaritis and Mansoori, 1988; Wang and Anthony, 2003). It has been proven that pressure drop to the bubble point can play a profound role in the asphaltene precipitation and further deposition in the primary oil recovery (De La Cruz et al., 2009). However, in the case of injection of gasses such as carbon dioxide, nitrogen, and methane compositional alteration of the oil in place is the main reason for asphaltene destabilization at the later stages of oil recovery (Srivasfava et al., 1999; Zanganeh et al., 2018).

The asphaltene content of heavy oil extracted from the oilsands can be as high as 20 wt.% depending on the solvent. For instance, if a heavy solvent such as normal heptane is mixed with Athabasca bitumen, nearly 13% of the heavy components precipitate as asphaltenes (Sadeghi Yamchi, 2014) while 20% asphaltene precipitation can occur using a lighter solvent such as pentane (Akbarzadeh et al., 2005). Only in Alberta, Canada nearly 165 billion barrels of oil

reserves are accumulated in the oil sands (CAPP, 2020). Traditionally, steam-assisted gravity drainage (SAGD) is the technique to exploit oil sand reservoirs (Gotawala and Gates, 2011). However, the emission of tons of carbon dioxide due to burning natural gas in the process of generating steam has questioned the long-term environmental sustainability of SAGD. However, due to the recent environmental constraints and low oil prices, the industry is moving toward field-scale applications of solvent-aided recovery processes to reduce energy consumption, reduce greenhouse gas emissions, and lower water treatment/usage. Application of solvents as diluents for diluting bitumen and reducing its viscosity has been established as an alternative for heavy oil or bitumen recovery (Panda et al., 2017; Sabet et al., 2017). The recent development involves the injection of hydrocarbon and non-hydrocarbon solvents, which could potentially lead to asphaltene precipitation and deposition. The deposition of asphaltenes is a multifaceted phenomenon from a heavy oil recovery perspective since it can lead to desirable in-situ upgrading of the heavy oil while reducing the permeability, which is undesirable (Monteagudo et al., 2003, 2002). Therefore, the need for a better understanding of the interplay of complex phase equilibrium and transport mechanisms at reservoir conditions is highly necessary to address the existing knowledge gaps for the efficient implementation of field scale solvent processes.

Solvents can either be co-injected into the reservoir with steam such as in Solvent-aided Steam assisted gravity drainage (SA-SAGD) or can be injected purely such as in VAPEX or NSOLV (Mokrys and Butler, 1993; Zhang et al., 2019; Zirahi et al., 2019). In both cases, the presence of solvent as an additional component into the system can add complications to both interactions of the components with each other and dominant mechanisms involved in bitumen recovery. To fully comprehend the effect of solvent on such interactions, detailed studies are required.

Addition of solvent to the reservoir can result in different thermodynamic states which can span from a simple vapor-liquid equilibrium (VLE) to more complex systems such as liquid-liquid equilibrium (LLE), or vapor-liquid-liquid equilibrium (VLLE). Vapor-liquid equilibrium of bitumen/solvent systems has been extensively studied in the literature and is beyond the scope of this work. Therefore, the reader is referred to the references mentioned in this regard for more details (Bin Dahbag et al., 2019; Dini et al., 2016; Haddadnia et al., 2018a, 2018b; Yazdani and Maini, 2010; Zirrahi et al., 2017). As opposed to VLE, comprehensive LLE studies of solvent bitumen systems that cover a wide range of temperature and pressure are scarce. Moreover, most of the studies of bitumen-solvent LLE are only limited to the determination of the phase boundaries between vapor-liquid and liquid-liquid phases and do not investigate the composition of phases in equilibrium. Cartlidge et al. (1996) used x-ray imaging to detect the LLV and SLV boundaries of Athabasca bitumen and n-dodecane mixtures pressurized by hydrogen and constructed the corresponding phase diagrams at temperatures and pressures up 450 °C and 7 MPa. Gao and Li (2017) experimentally studied the phase behavior of n-butane and bitumen mixtures with and without the presence of water. They visually inspected the mixtures to identify the phase boundaries and found that beyond 0.97 mole fraction of butane in the mixture a second liquid with a lighter color with respect to the first liquid can be detected. In a study, Johnston et al. (2017) measured the thermophysical properties of bitumen mixtures diluted with pentane at temperatures and pressures up to 280 °C and 14 MPa. They measured asphaltene yields as well as the saturation pressure of the mixtures and generated the phase diagrams. Liquid-liquid equilibrium measurements of ethane- propane- butane/bitumen systems have been reported by Kariznovi (2013) and Nourozieh (2013). The boundaries of single liquid and liquid-liquid regions were reported to happen at 40 wt.% for propane and 50 wt.% for butane. Sadeghi Yamchi et al. (2018)

studied the effect of additives such as propane, dimethyl ether (DME), and toluene on the LLE of butane/bitumen mixtures and suggested the addition of DME could lower asphaltene precipitation and increase the saturation pressure of the mixture.

Since the presence of LLE for solvent and bitumen systems has been proven thermodynamically, the precipitation or deposition of asphaltenes in porous media then becomes an inevitable phenomenon in a solvent-aided bitumen recovery. Qi et al. (2018) quantified the asphaltene deposition in pore-scale due to the injection of natural gas condensate and naphtha into a microfluid model saturated with bitumen. It was concluded that natural gas condensate can lead to more asphaltene deposition since it contained more of lighter components such as butane and pentane compared to naphtha. Keshmiri et al. (2019) performed a similar experiment with pentane and experimentally studied the asphaltene deposition. Their results highlighted the need for exploring the dynamic aspects of asphaltene precipitation rather than its pure thermodynamic equilibrium.

Despite the many experimental studies on phase equilibrium of asphaltenes and dynamics of its precipitation/deposition, this interplay of phase equilibrium and precipitation/deposition has not been numerically addressed in detail. Recently, Sabet et al. (2020a) studied asphaltene deposition in a two-dimensional porous media due to the miscible displacement of bitumen with pentane. Most of the other developed models assume one-dimensional flow considering only the primary pressure drop as the main cause of asphaltene precipitation relying on inadequate experimental data (Monteagudo et al., 2002; Wang et al., 1999). However, solvent injection to reservoirs involves severe viscous fingering and alteration of the mixture composition that leads to destabilization of asphaltenes and subsequent deposition, which cannot be captured using one-

dimensional models. Moreover, the described phenomenon occurs at a scale that is much smaller than a computationally viable simulation grid block and thus cannot be captured by using conventional reservoir simulation approaches. Therefore, upscaling of fine scale physics to larger scales remains a challenge in translating experimental observation to coarse scale reservoir models. This work is an attempt to model the problem of induced asphaltene deposition due to miscible displacement of bitumen with a solvent by the implementation of liquid-liquid K-values. The choice of the solvent was based on our previous experimental and modeling studies of liquid-liquid equilibrium of dimethyl ether (DME)/bitumen system (Sadeghi Yamchi et al., 2020). While the approach introduced is applied to DME/bitumen system, it can be applied to any solvent/bitumen mixture once the liquid-liquid phase equilibrium data are available. And finally, the grid dependency of the asphaltene deposition is studied. Detailed numerical simulations are used to upscale the fine scale deposition rate to the coarse scale and characterize the effect of numerical grid size on deposition rate.

5.4 Problem Description

Figure 5.1 depicts the schematics of the problem. The simulated domain is a two-dimensional (1×0.8) m^2 homogenous porous medium with a porosity of 0.3 and a permeability of 4×10^{-12} m^2 as are common in oilsands reservoirs. The domain is initially saturated with bitumen. The bitumen is characterized by two pseudocomponents of maltenes and asphaltenes. Detailed characterization of the bitumen has been reported previously (Sadeghi Yamchi et al., 2020). The mass fraction of asphaltenes and maltenes are 0.29 and 0.71, respectively. DME as the displacing solvent is injected from the left boundary in the liquid form at a constant rate of 4×10^{-6} m^3/s while constraining the injection pressure limit of 2700 kPa at 80 °C and the resident oil is produced from the right

boundary at a minimum pressure of 2200 kPa. Since this problem is in the isothermal condition the initial temperature of the domain was also set to be 80 °C. The significant viscosity difference of the solvent and the bitumen at the conditions of the simulation can cause severe channeling of the injected fluid in the bitumen commonly known as viscous fingering. The fingering phenomenon can increase the surface area between the solvent and bitumen as opposed to a piston-like displacement observed in one-dimensional models. As the solvent and bitumen are brought into contact, bitumen is mixed with the solvent to a point that asphaltene comes out of the solution as precipitated particles. These asphaltene particles then will be carried with the fluids and if enough time is given to these particles, they start to deposit onto the surface of the rock as solid material. The deposition of asphaltene leads to the change of the porosity which can then result in permeability reduction. At the same time, the deposition of asphaltenes leads to in-situ partial upgrading of bitumen. Porosity and permeability reduction correlations will be discussed in the next section.

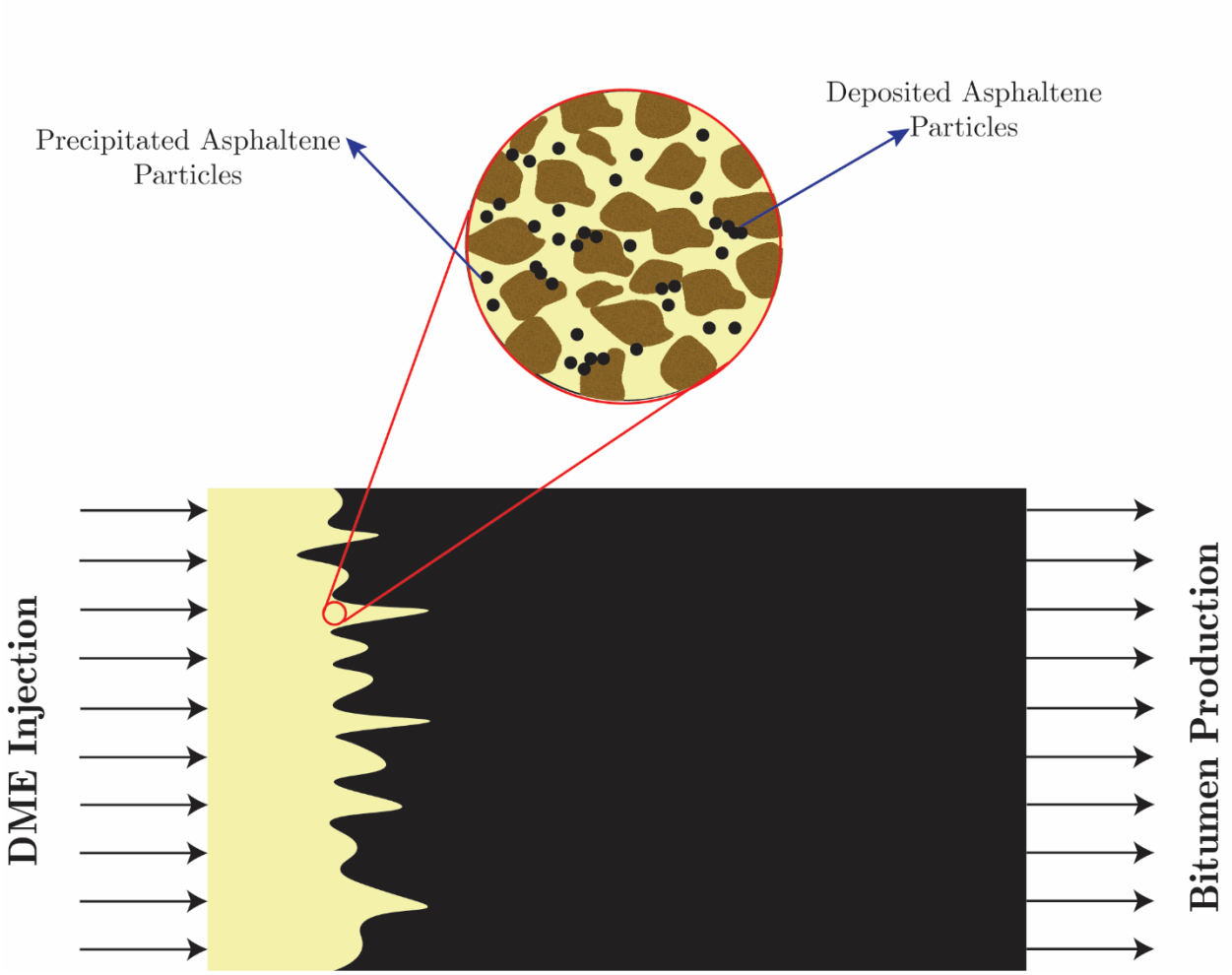

Figure 5.1: Schematic of induced asphaltene deposition in porous medium due to miscible displacement of bitumen with hot and pressurized dimethyl ether (DME).

5.5 The Governing Equations

The governing mass conservation and flow equations are given by:

$$\frac{\partial}{\partial t}\left(\phi\rho x_i\right)+\nabla.\left(\rho v x_i\right)=\tau_i, \tag{5.1}$$

$$v=-\left(\frac{kk_r}{\mu}\right)\Delta p, \tag{5.2}$$

where ϕ is porosity, ρ is the phase molar density, x_i is the mole fraction of component i, v is the velocity, k_r is the relative permeability μ is viscosity, P is pressure, and, τ is non-equilibrium interphase mass transfer term. It should be noted that the nonequilibrium term is only applied for the asphaltene components in the system since asphaltenes are the only species that precipitate and deposit onto the rock surface.

Nghiem and Sammon (1997) developed a mathematical formulation of interphase transfer function when two phases are in thermodynamic equilibrium at the interface and a diffusion-based drive moves the bulk composition toward an equilibrium. We use this conceptual non-equilibrium model developed by Nghiem and Sammon to simulate asphaltene precipitation in porous media by implementing the experimental liquid-liquid equilibrium data (CMG-STARS user guide, 2018). In order to model asphaltene deposition and capture the kinetics of the process, CMG-STARS, an industry standard reservoir simulator, allows for the definition of different states for asphaltene species. The first state is the precipitated asphaltenes in the form of liquid phase which can be obtained instantaneously with liquid-liquid K-values. The second state is the deposited asphaltene in the solid phase. Therefore, with the definition of two different components for asphaltenes (ASPH) the kinetics of the deposition can be modeled through the use of a reaction-based term as flows:

$$ASPH_{liquid} \xrightarrow{R} ASPH_{solid}, \tag{5.3}$$

where R is the reaction rate for the deposition of asphaltenes and is it is used to model non-equilibrium interphase mass transfer. Nghiem and Sammon (1997) showed that if two phases were in equilibrium at the interface, then the equilibrium mole fraction of each component could be

calculated by flashing the global composition on each grid block. Moreover, the formulation of the non-equilibrium term was given as the first order Fickian expansion as follows (Al-Gawfi et al., 2019a; Niessner and Hassanizadeh, 2009):

$$\tau_{ik} = \pm \frac{\rho_k D^{ik}}{d^{ik}} a_{\mathrm{lg}} (x_{ik} - x_{ik}^{*}), \tag{5.4}$$

where ρ_k is the density of phase *k*, D^{ik} is Fickian diffusion coefficient, a_{lg} is the characteristic interfacial area which separates two phases in contact, and d^{ik} is the diffusion length for component *i*. x_{ik}^{*} is the composition of component *i* at equilibrium or in other words is the solubility limit of component *i* and x_{ik} is the micro-scale mole fraction of component *i* in phase *k*.

The general form of reaction which can be defined as follows (CMG-STARS user guide, 2018):

$$r = r_r . \exp\left(-\frac{E_a}{RT} \right) . C_i^e , \tag{5.5}$$

where $C_i = \phi s_k \rho_k x_i$, r_r is the frequency factor, E_a is the activation energy for the reaction, R is the universal gas constant, T is the temperature, and C_i is the concentration of the component in the reaction, *s* is the saturation and the exponent *e* is the order of the reaction. The concentration is directly proportional to the mole fraction of the component as well as the density of the phase in which the reaction occurs. In the case of our problem, the nonequilibrium term is a measure of deviation from the equilibrium condition. Therefore, instead of using the absolute mole fraction the deviation of the mole fraction from the equilibrium condition is used, which is given by (CMG-STARS user guide, 2018; Nghiem and Sammon, 1997):

$$C_i = \phi s_k \rho_k (x_i - x_i^*) . \quad (5.6)$$

Assuming zero activation energy and an order of one, the specified reaction can be given by (CMG-STARS user guide, 2018; Nghiem and Sammon, 1997):

$$r = r_r . \rho (x_i - x_i^*) . \quad (5.7)$$

It is worth noting that the frequency factor r_r in Equation 7 is the lumped form of $D^{ik} a_{\lg} / d^{ik}$ defined in Equation 4 and has the dimension of [1/time].

One of the impacts of solid deposition in porous media is the reduction of available porosity. The alteration of porosity can consequently limit the path of flow for the fluids which results in permeability reduction. Therefore, we used the Carman-Kozeny correlation for permeability changes as follows:

$$\frac{k}{k_0} = \left(\frac{\phi}{\phi_0} \right)^{\alpha} \left(\frac{1-\phi_0}{1-\phi} \right)^2 , \quad (5.8)$$

where exponent α is an empirical constant. In the absence of experimental data, we use α =10 in our numerical simulations to represent severe damage as reported in a similar case (Mousavi et al., 2020).

5.6 Fluid Model

Asphaltenes precipitated by DME are the heaviest components in the bitumen. According to our previous study, the maximum amount of precipitates as of DME-asphaltenes constitutes 29 wt.% of Athabasca bitumen (Sadeghi Yamchi et al., 2020). Analyzing the molecular weight distribution obtained from GPC of the heavy cuts (DME-asphaltenes) revealed that an average MW of 1100

g/mol for the asphaltenes (Sadeghi Yamchi et al., 2020). The MW of maltenes was then estimated to be 431 through a material balance and an experimentally measured bitumen MW of 523.

5.6.1 Density of DME/Bitumen (Asphaltenes + Maltenes) Mixtures

The numerical simulator uses the following equation to calculate the molar volume of each component as a function of temperature and pressure:

$$\nu_i = \nu_i^o \exp\left[c_{t1_i}\Delta T + c_{t2_i}\frac{(T+273.15)^2 - (T_{ref}+273.15)^2}{2} - c_{p_i}\Delta P - c_{pt_i}\Delta P\Delta T \right], \quad (5.9)$$

where $\Delta T = T - T_{ref}$, $\Delta P = P - P_{ref}$, ν_i^o is the partial molar volume (inverse of the molar density) of component *i* at the reference temperature and pressure of 15.556 °C and 101.325 kPa, respectively. The molar volume of the mixture can then be calculated with a linear mixing rule with the assumption of no volume change upon the mixing:

$$\nu_o = \sum \nu_i x_i \,. \quad (5.10)$$

Using the experimental data of the mixture density one can perform non-linear regression on the data and estimate the constants of the molar volume equation. The experimental data used for this purpose was obtained from Haddadnia et al. (2018a) study. The density of asphaltenes was set to be 1200 kg/m^3 based on the previous measurements (Sadeghi Yamchi, 2014) and the partial molar volume of the maltenes with the pseudo partial molar volume of DME along with the rest of the constants in the equation were estimated through non-linear regression analysis to fit the experimental data. Table 5.1 presents the values for all the coefficients from Equation 9. The predictions of the model with the presented coefficients were found to be precise with an AARD of 0.3%.

Table 5.1: Density coefficients used in density correlation for DME/bitumen (asphaltene + maltene) system.

Component	Maltene	Asphaltene	DME
v_i^o (m^3/kmol)	4.587×10^{-4}	9.167×10^{-4}	7.231×10^{-5}
c_{t1} (1/K)	-8.608×10^{-4}	1.698×10^{-2}	-6.859×10^{-4}
c_{t2} ($1/K^2$)	-5.041×10^{-6}	-3.027×10^{-5}	4.615×10^{-6}
c_p (1/kPa)	1.403×10^{-9}	3.787×10^{-8}	1.389×10^{-5}
c_{pt} (1/kPa.K)	7.664×10^{-8}	-2.576×10^{-8}	-1.443×10^{-7}

5.6.2 Viscosity of DME/Bitumen (Asphaltenes + Maltenes) Mixtures

Similar to density, there is no through experimental measurements of maltene and asphaltene viscosity in the literature. However, the viscosity of Athabasca bitumen and the mixture of bitumen and DME is available through a wide range of temperatures and pressures (Haddadnia et al., 2018a). To model the viscosity of the bitumen and DME mixture, the following correlation is used to calculate the viscosity of asphaltenes, maltenes, and pseudo viscosity of DME in the oleic phase at different temperatures and pressures (Al-Gawfi et al., 2019b):

$$\ln(\mu_i) = a_1 \exp(a_2 + a_3 T^2 + a_4 T + a_5 P + a_6 P^2)\,, \tag{5.11}$$

where μ is in cP, T, and P are in K and kPa, respectively. Then the linear log mixing rule was employed to predict the mixture's viscosity as follows:

$$\ln(\mu_{mix}) = \sum x_i \ln(\mu_i)\,. \tag{5.12}$$

To find the constants of the equation for the components in the mixture, a similar approach to density modeling was adopted. Numerical regression was performed to match the experimental viscosity data. The estimated values of the coefficients have been brought in Table 5.2. AARD of the viscosity modeling was 12%.

Table 5.2: Constants of viscosity correlation for DME/bitumen (asphaltene + maltene) system.

Component	**Maltene**	**Asphaltene**	**DME**
a_1	8.22×10^{-16}	1.54×10^{-15}	-1.99×10^{-15}
a_2	40.90	41.52	42.16
a_3	4.29×10^{-09}	9.00×10^{-6}	3.03×10^{-5}
a_4	-1.44×10^{-02}	-1.46×10^{-2}	-1.93×10^{-2}
a_5	-7.69×10^{-08}	5.46×10^{-6}	-8.25×10^{-4}
a_6	-9.10×10^{-12}	1.59×10^{-10}	2.14×10^{-10}

As shown in Figure 5.2, the model can precisely predict the bitumen viscosity based on two pseudocomponents of asphaltenes and maltenes. Moreover, model estimations for viscosities of asphaltenes and maltenes are in correspondence with the theoretical definitions of the pseudocomponents indicating a higher viscosity for the heavy fractions of bitumen as asphaltenes and lower viscosity for maltenes.

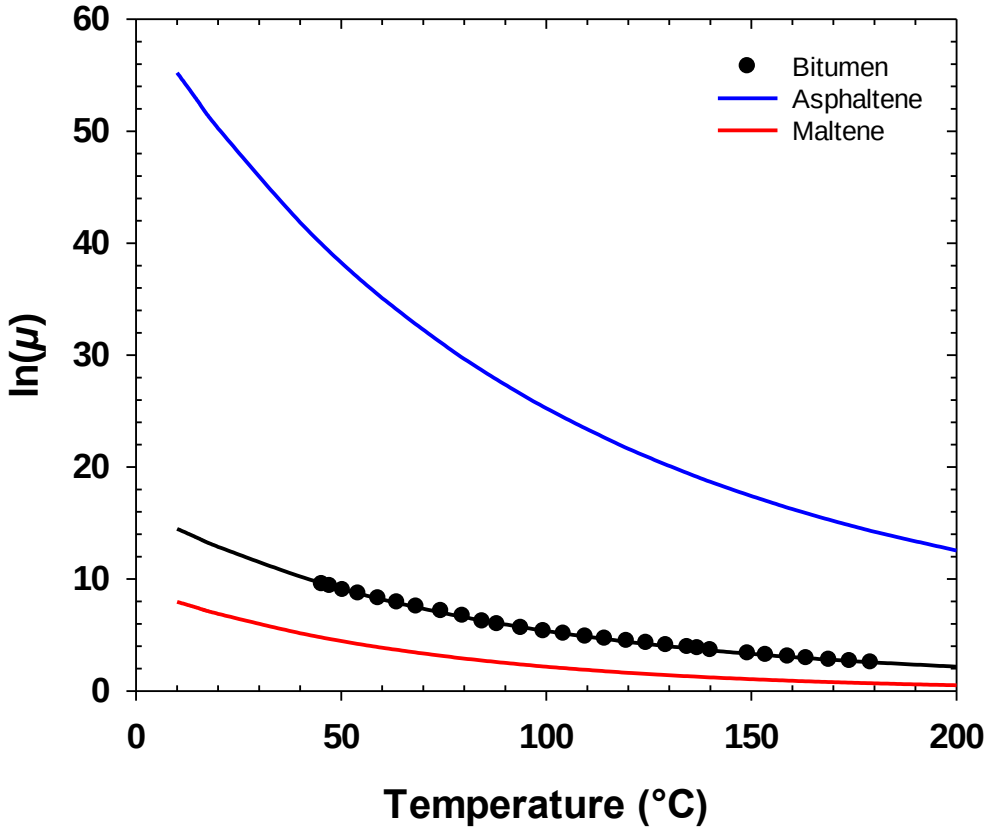

Figure 5.2: Log viscosity (cP) of bitumen and its fractions versus temperature; ● data points, — model predictions. The experimental data are obtained from Zirrahi et al. (2017).

5.6.3 Liquid-Liquid Equilibrium K-values

As discussed earlier, to simulate the asphaltene deposition in the porous media, liquid-liquid K-values of asphaltenes are required. The liquid-liquid K-value of asphaltene is defined as the mole fraction of the asphaltene in the precipitated material over its mole fraction in the oil phase. Therefore, it is required to have the thermodynamic yield curve to calculate the liquid-liquid K-values. The experimental yield curve data of DME/bitumen system has been measured and discussed in detail in our previous study (Sadeghi Yamchi et al., 2020).

To generate liquid-liquid K-values from yield data, it was assumed that only the asphaltene pseudocomponent is precipitated. This assumption was made to avoid any complications in the simulation. In reality, however, as discussed in our previous study, the precipitated material can be a mixture of asphaltene and maltenes. Considering one pseudocomponent in the precipitate, the asphaltene K-values can be calculated as the inverse of asphaltene mole fraction in bitumen:

$$K_{asph} = 1 / x_{asph} \ . \tag{5.13}$$

Since the yield curve is only a function of solvent concentration, liquid-liquid K-values of asphaltenes also inherently become dependent on the solvent concentration. Besides, K-values were assumed independent of pressure based on our experimental observation (Sadeghi Yamchi et al., 2020). The liquid-liquid K-values are shown in Table 5.3:

Table 5.3: Asphaltene liquid-liquid K-values for DME/bitumen system at T=80 °C and pressure range of 2.5-3 MPa.

x_{DME}	**Liquid-liquid K-values**
0.9400	0
0.9446	222
0.9578	1066
0.9715	9733

According to the yield curve, the asphaltene precipitation onset point for DME/bitumen systems is less than 60 wt.% of solvent (i.e., 0.94 mole fraction of DME). Hence, the liquid-liquid K-values for asphaltenes below this concentration are equal to zero. Also, at pressures, less than 2 MPa at

80 °C the mixture of DME/bitumen falls in the vapor-liquid equilibrium region and therefore resulting in zero liquid-liquid K-values.

5.7 Results and Discussion

In this section, the results of the numerical simulation of the asphaltene induced deposition during miscible displacement of bitumen with DME are discussed. As mentioned earlier, asphaltene deposition is modeled through a reaction term where the amount of the deposition is proportional to the local composition and the reaction frequency factor, which indicates the rate of deposition. However, this reaction advances only when the local mixture composition of the solvent exceeds a certain value, which is known as the asphaltene precipitation onset point.

Another controlling factor in asphaltene deposition in porous media is the viscous fingering of the solvent in bitumen. Since the viscosity ratio between the solvent and bitumen is very high, the less viscous injected solvent tends to channel through very high viscous bitumen and finally produce at the outlet boundary. One of the impacts of viscous fingering is an increase in the contact area between the solvent and bitumen. Such an increase in the contact area can lead to more mixing of the solvent with bitumen and consequently increase the amount of asphaltene precipitation and subsequently the deposition. Figure 5.3 shows the formation of viscous fingering for a fine grid model with a total grid number of 32000 ($\Delta x=\Delta y=0.5$ cm, $N_x=200$, $N_y=160$) and the corresponding mass of deposited asphaltene. One dimensional experimental and numerical models are often used to study asphaltene deposition in porous media. To demonstrate that a one-dimensional model fails to predict the correct amount of the deposited asphaltene, the results of 1D simulation is also presented. Figure 5.3 shows the same results for a one-dimensional model with the same gird size of $\Delta x=0.5$ cm. The results clearly show that a 1D model underestimates the deposited amount of

asphaltene. This is mainly due to the fact that a 1D piston-like displacement cannot simulate the channeling effect (viscous fingering) leading to less mixing and consequently predicts a lower amount of the deposited asphaltenes.

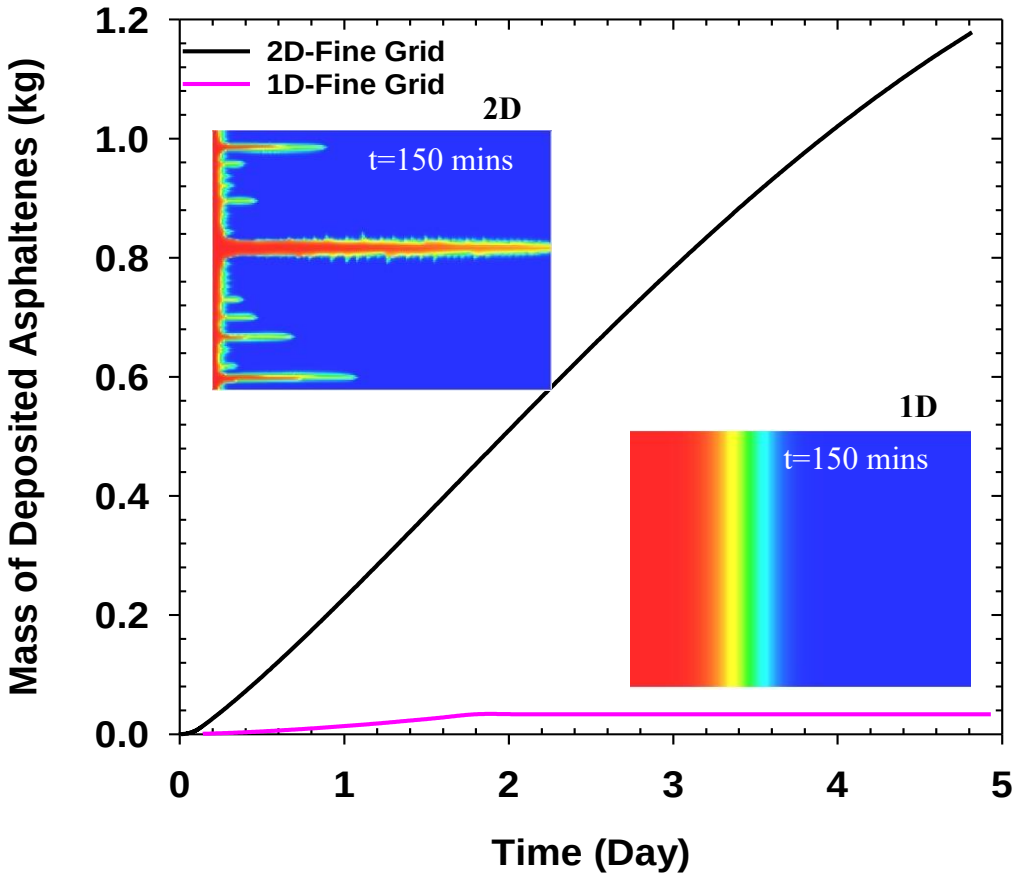

Figure 5.3: Effect of viscous fingering on the rate of the total mass of deposited asphaltene in the domain for fine grid models; Comparison between 2D ($\Delta x=\Delta y=0.5$ cm, $N_x=200$, $N_y=160$) and 1D ($\Delta x=0.5$ cm, $N_x=200$) models.

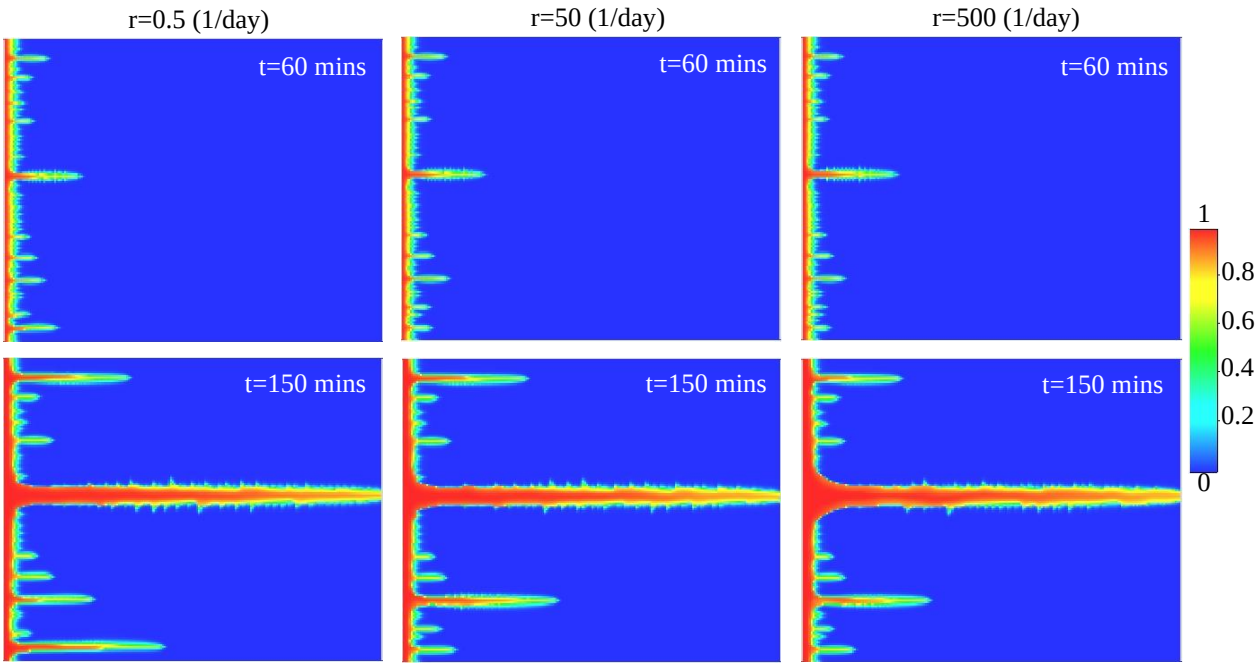

Figure 5.4: Mole fraction of DME as it displaces the oil for deposition rates of 0.5, 50, and 500 1/day after 60 and 150 min.

Figure 5.4 shows the mole fraction of DME as it displaces the oil for deposition rates of 0.5, 50, and 500 1/day after 60 and 150 min. As illustrated in Figure 5.4 for all cases viscous fingering starts to develop at the beginning of the displacement process (~1 hour). These fingers or in other words solvent channels expand with time and after two and a half hours reach the production outlet. Despite the different values for the deposition rate, the dynamics of viscous fingering are nearly identical for all cases. Although the deposition rate can significantly alter the permeability of the domain, it has minimal effect on the shape or numbers of the fingers. This behavior can be attributed to the fact that the interface of the solvent is dynamic and moves with time and it occurs in areas where the solvent concentration is far from the asphaltene precipitation onset point (x_{DME}=0.94). Therefore, the areas with asphaltene deposition fall behind the interface where already have been flooded with a significant amount of the solvent. A similar observation has been

previously observed for miscible displacement of oil by a paraffinic solvent (Sabet et al., 2020a, 2020b).

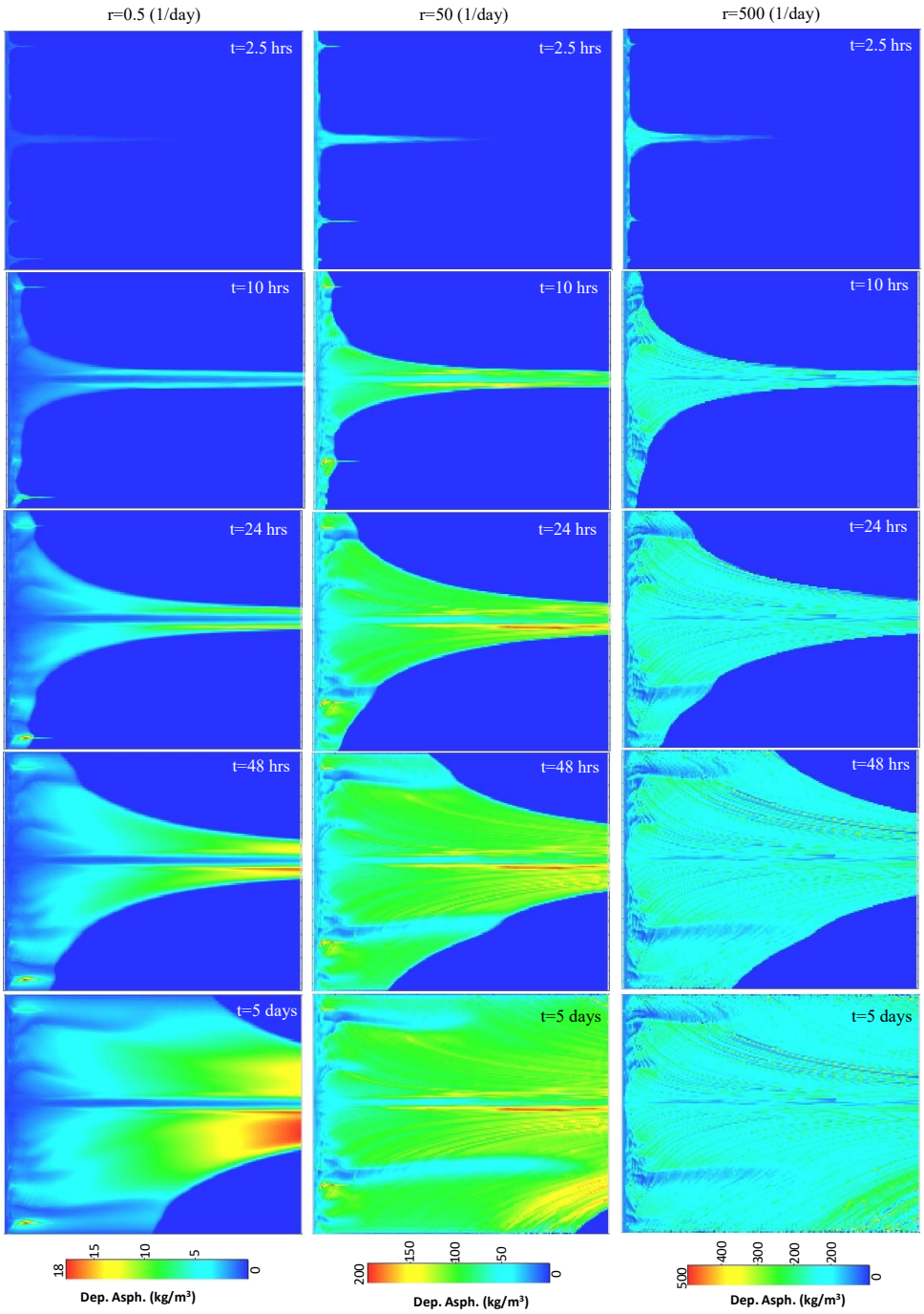

Figure 5.5: Concentration of the deposited asphaltene in kg/m^3 of the current pore volume for deposition rates of 0.5, 50, and 500 1/day after 2.5, 10, 24, 48 hours and 5 days.

The asphaltene deposition profiles are shown in Figure 5.5 for three deposition rates of 0.5, 50, and 500 1/day. The results are shown at different times between the breakthrough time (2.5 hours) and the end of the simulation (5 days). Comparing the results at the breakthrough time suggests that the initial areas with deposited asphaltenes are aligned with the fingers of the solvent in bitumen for all cases. However, different deposition rates yield different ultimate amounts of deposition. The minimum solid deposition occurs in the solvent channels where neither contact time nor contact area between the solvent and bitumen is favorable for asphaltene deposition. Conversely, areas adjacent to the solvent channels are provided with sufficient mixing time and area for excessive asphaltene deposition.

Another observation is the controlling role of the deposition rate on the distribution of solids in the domain at the end of the simulation. As shown in Figure 5.5, while the high concentration area of the deposited asphaltenes is close to the production outlet for a low deposition rate of 0.5 1/day, the solid profile becomes more uniform in the domain for higher deposition rates of 50 and 500 1/day. When the deposition rate is low (slower reaction rate), the precipitated asphaltenes are carried with the flow of the fluids towards the production outlet without being deposited. Hence, the precipitated asphaltenes are either produced or deposited near the production outlet. In contrast, when the deposition rate is high the precipitated asphaltenes deposited quickly and are not carried by flow resulting in a more uniform deposition profile.

Permeability profiles depicted in Figure 5.6 reveal identical patterns to the corresponding solid deposition profiles. Solid deposition reduces the available porosity for the fluids and therefore reduces the permeability as permeability and porosity are correlated through the Carman-Kozeny equation.

Our findings show that at higher deposition rates of 50 and 500 1/day, solid deposition can reduce the permeability by 75%. It should be noted that the extent of the permeability reduction is directly impacted by the porosity exponent in the Carman-Kozeny equation and this exponent needs to be empirically estimated through detailed experiments.

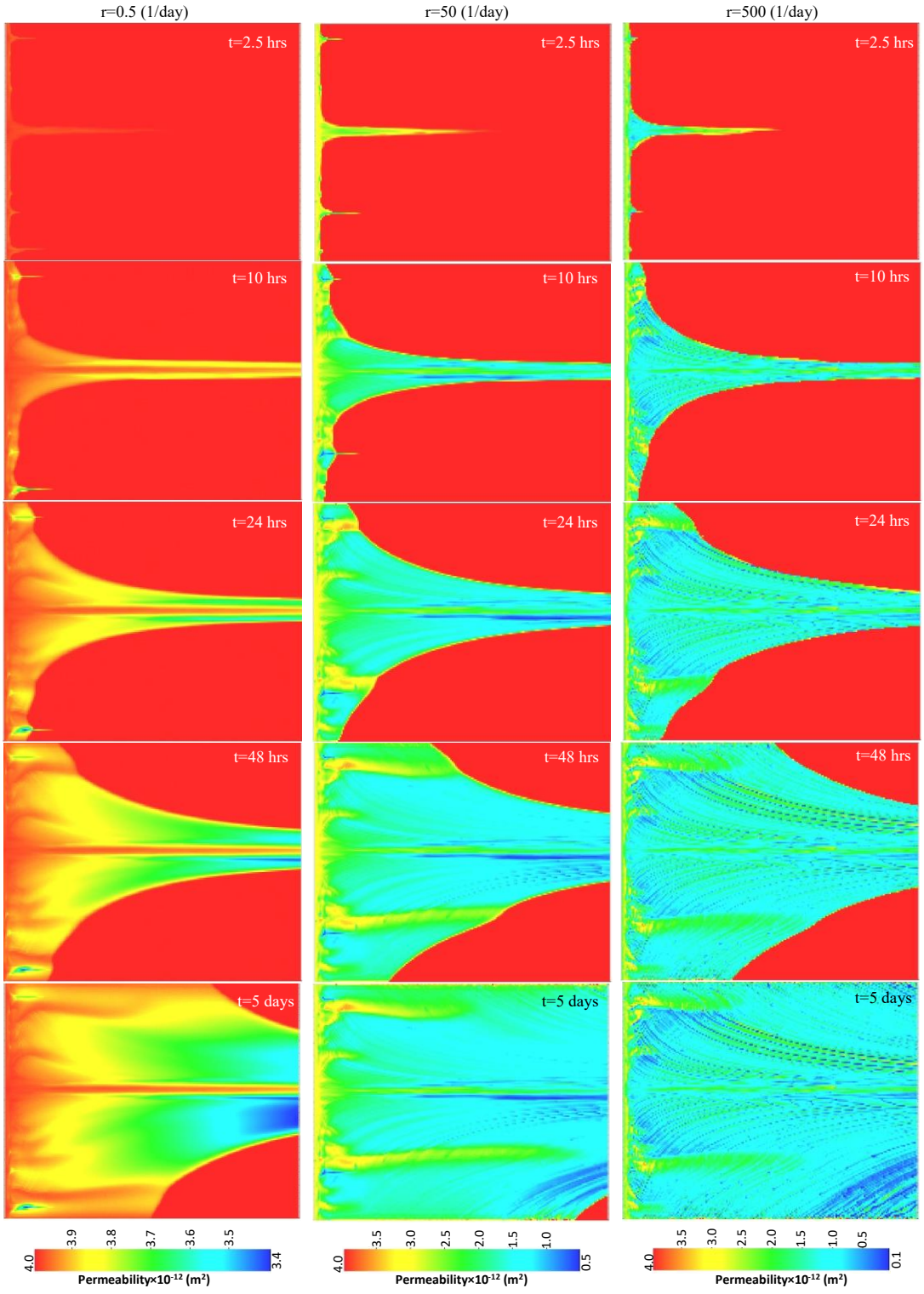

Figure 5.6: Permeability reduction due to solid deposition for deposition rates of 0.5, 50, and 500 1/day at 2.5, 10, 24, 48 hours and 5 days.

One of the direct results of the deposition of asphaltene is increasing the quality of the produced oil. Bitumen with less asphaltene has a higher API degree and is less viscous. The term "in-situ upgrading" is used as an indication of asphaltene precipitation and deposition in the reservoir due to solvent injection. The degree of upgrading can be correlated by the ratio of asphaltene content of the produced oil to the initial asphaltene content of the bitumen in place as:

$$\eta = 1 - \frac{ASPH(t)}{ASPH_i}, \tag{5.14}$$

where $ASPH(t)$ and $ASPH_i$ are the asphaltene content of the produced oil and the initial asphaltene content of bitumen, respectively.

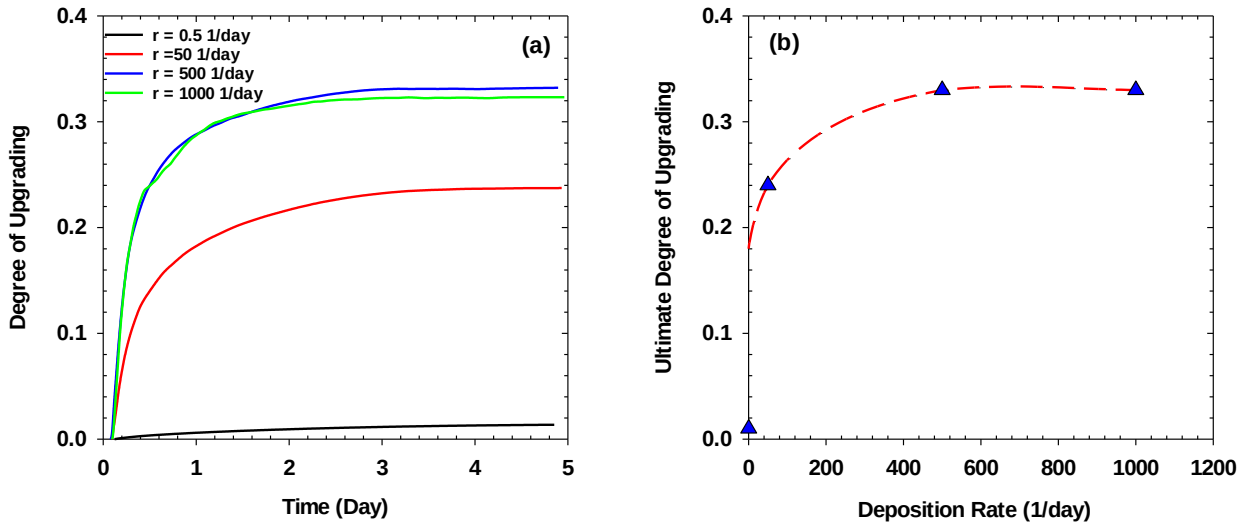

Figure 5.7: (a) In-situ degree of upgrading versus time, (b) ultimate degree of upgrading for different deposition rates.

The results of upgrading for four deposition rates of 0.5, 50, 500, 1000 day^{-1} are depicted in Figure 5.7. The analysis shows that before the solvent breakthrough, the produced oil has the same asphaltene content as the original oil. This is expected since the oil which is produced prior to the

solvent breakthrough is controlled by the pressure drop across the model. On the contrary, when the solvent reaches the production outlet, the oil is mainly produced through the leaching of a viscous oil by the injected solvent and dissolution processes. The dilution of oil by the solvent increases the degree of upgrading sharply with time and then reaches a plateau at the final stages of the process. It was also found that increasing deposition rate higher than 500 1/day has no effect on the ultimate degree of upgrading where the maximum deposition occurs in the domain, which is in agreement with the numerical simulation of asphaltene deposition reported by Sabet et al. (2020a, 2020b).

5.7.1 Upscaling of Deposition Rate

The results presented in the previous section were for a fine grid case (base case) with a grid size of 0.5 cm. A choice of small grid size in the order of 0.5 cm allows us to capture the dynamics of viscous fingering and asphaltene deposition. However, it is computationally demanding making numerical simulation of the process in larger scales impractical. Therefore, it would be practically important to upscale the deposition rate such that it gives the same amount of deposition while allows using a larger grid size. In this study, the focus is on the deposition rate which can be used to control the amount of solid deposits in the domain. All other operating parameters such as the rate of injection and injection and production pressures were maintained constant in all simulation runs.

To evaluate the impact of grid size, first, a simulation test was conducted for a fine grid base case at a given value for the deposition rate of asphaltenes. Then other cases with coarser grid blocks were simulated with the same deposition rate as of the base case to quantify the deviations of the results in terms of the amount of asphaltene deposited as the grid size increased. This procedure

was performed at four deposition rates of 0.5, 5, 50, 500 1/day, and three coarse grid sizes of 1, 2, and 5 cm. Afterward, another set of coarser grid simulations were conducted to find a deposition rate that can match the amount of asphaltene deposition obtained in fine grid simulation.

As expected, it was observed that increasing the size of the grid block could potentially change the fingering pattern and therefore impact the overall mass of the solid deposited in the domain influencing the consistency of the results. Since it was crucial to maintain the same fingering pattern regardless of the grid size, in all the coarse grid cases the middle layer in the domain was assigned a permeability value of $1.002k_i$ to obtain a similar fingering pattern to the base case as depicted in Figure 5.4.

Figure 5.8 depicts the mass of the deposited asphaltenes with time for the first set of simulations. Each graph in Figure 5.8 illustrates the results for a specific deposition rate used in the base case. It compares the amount of asphaltene deposition of the fine grid case with coarser grid cases using the same value for deposition rates. The results reveal that using the same deposition rate for the coarse case can overpredict the total volume of the deposited asphaltene in the domain. However, this difference becomes narrower when the deposition rate of the base case is very high. For instance, the total mass of deposition in the fine grid and coarse grid cases are similar when the base case deposition rate is 500 1/day. At very high levels of deposition rates, the simulation approaches the ultimate or in other words maximum amount of deposition and therefore the impact of deposition rate becomes more dominant in the process compared to the grid size.

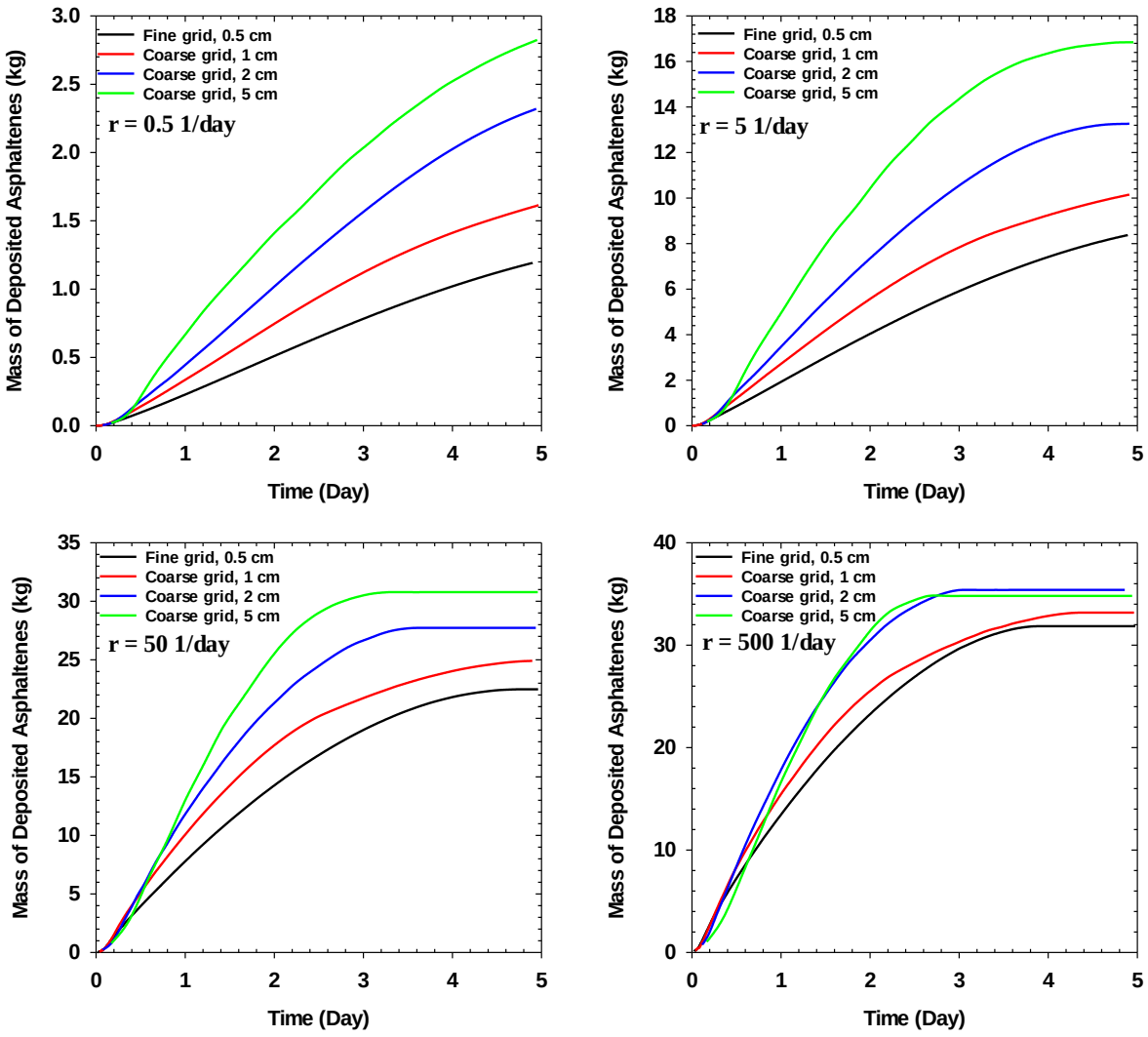

Figure 5.8: Comparisons of the total mass of deposited asphaltenes in the domain between the fine and coarse grid cases for four deposition rates of 0.5, 5, 50, 500 1/day.

In another set of runs, deposition rates of coarse grid cases were optimized to match the amount of deposited asphaltenes of the respective fine grid case. The results of this optimization for the fine grid case with a deposition rate of 0.5 are presented in Figure 5.9. To match the deposition

curve of the base case (fine grid), it was required to use deposition rates of 0.35, 0.25, and 0.2 in the coarse gird cases with block sizes of 1, 2, and 5 cm, respectively.

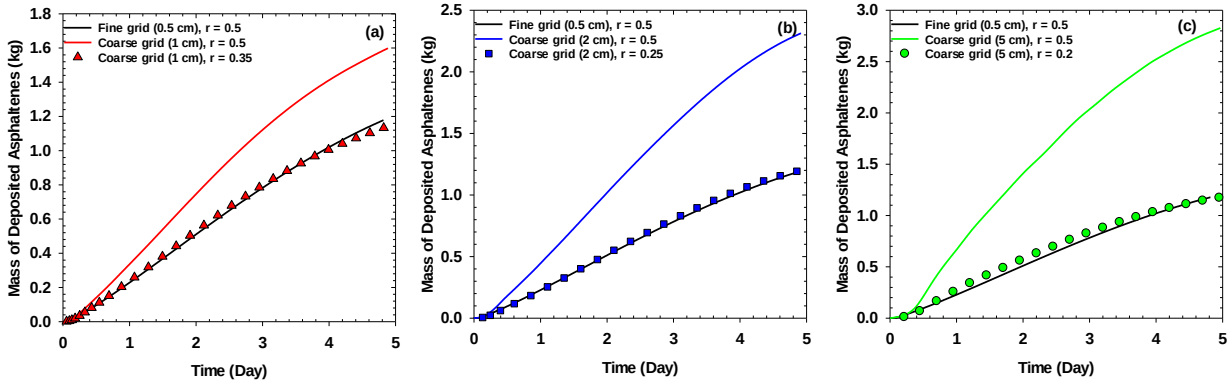

Figure 5.9: Optimization results to match the deposited asphaltene curve of the base case with a deposition rate of 0.5 for a grid size of a) 1 cm, b) 2 cm, and c) 5 cm.

The same simulations were repeated for different base case deposition rates of 5, 50, and 500, and the deposition rate in the coarse grid simulations was optimized to match the asphaltene deposition curve of the base case. Figure 5.10 shows the upscaled rates versus grid sizes for different base deposition rates.

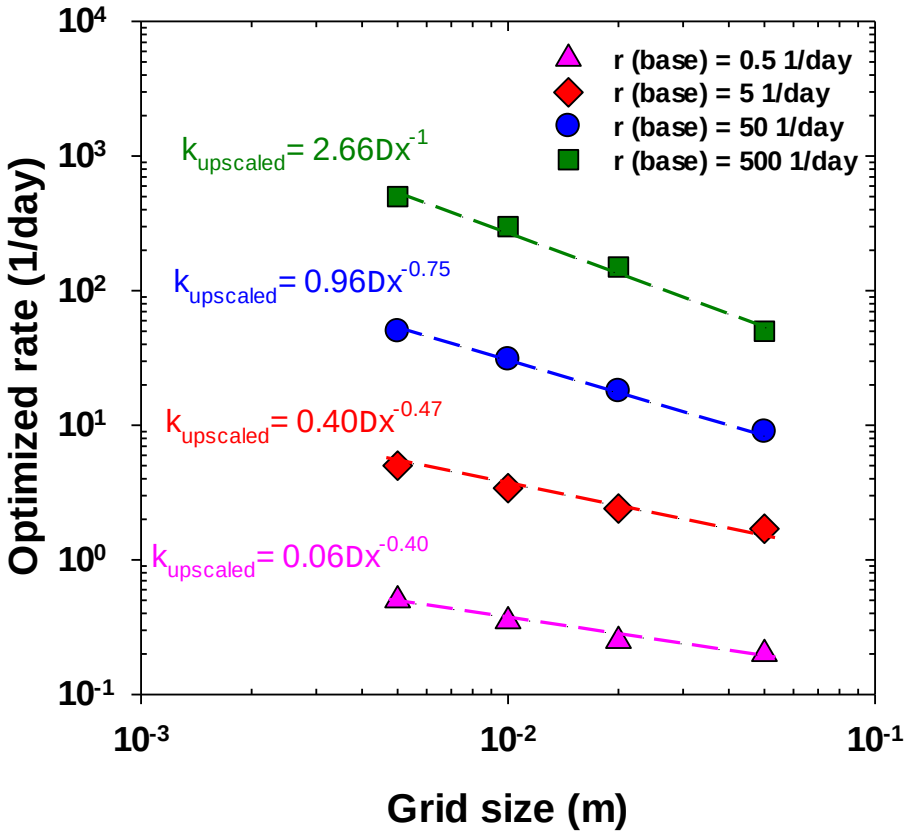

Figure 5.10: Upscaled deposition rates versus grid size; ▲, ♦, ●, ■ are data points, and ---- is a trendline.

As shown in Figure 5.10, regardless of the deposition rate of the base case, the upscaled or optimized values of the deposition rate is inversely proportional to Δx^b such that $k_{upscaled}=a\Delta x^{-b}$, where a and b are constant. Theoretically, when the size of the grid-block is considerably small the difference between the gird block composition and the equilibrium composition becomes indistinguishable, and therefore according to Equation 7, larger values of deposition rate are required to produce the same amount of deposited asphaltenes. However, choosing a small grid size with a requirement of a larger deposition rate can result in higher material balance errors as

was observed in our case with grid sizes less than 0.5 cm. Overall, the choice of the grid size should be tailored for each specific problem where the experimental deposition data can be successfully predicted.

5.8 Summary and Conclusions

Applications of solvents in heavy oil and bitumen recovery are inevitably increasing as an effort for the reduction of environmental footprints. However, introducing a new component to the reservoir fluids can complicate all the interactions and mechanisms involved in the oil recovery. One such complication is the destabilization of asphaltene components dissolved in the bitumen due to compositional changes. Although the phenomenon of asphaltene precipitation and deposition has been broadly studied, no study has addressed the proper utilization of experimental liquid-liquid phase equilibrium data in numerical simulation of asphaltene deposition in porous media induced by solvent injection.

In this work, we studied the asphaltene deposition in the miscible displacement of bitumen with hot pressurized liquid dimethyl ether. Athabasca bitumen was characterized by two pseudo-components of asphaltene and maltene. Then, the experimental viscosity and density data of DME/bitumen system were modeled and the liquid-liquid K-values of asphaltenes were generated based on the asphaltene yield curve of DME/bitumen system. A 2D numerical model was created by including a general reaction term to convert asphaltenes in the liquid phase to the solid phase through a non-equilibrium model. The non-equilibrium model utilizes the liquid-liquid K-values to transfer asphaltene components from the liquid phase to the solid phase in form of a first order reaction.

Our numerical simulation of miscible displacement of bitumen by DME demonstrates that viscous fingering plays a crucial role in the deposition of asphaltene due to excessive mixing of bitumen and the injected solvent. The results also revealed that one dimensional modeling of asphaltene deposition fails to capture the dynamics of the system and significantly underestimates the amount of deposition. Deposition of asphaltene at in-situ reservoir conditions is a multifaceted phenomenon since it can lead to upgrading of the produced oil and at the same time results in permeability reduction. Our results revealed that for DME/bitumen system the degree of upgrading can reach as high as 32% with a significant permeability reduction.

It was also found that the amount of deposition is a strong function of grid size that highlights the need for proper upscaling of the deposition rate. To address this challenge, fine grid and coarse grid numerical simulations were conducted and the rate of deposition in the coarse grid simulation was optimized to match the amount of asphaltene deposition. The results demonstrated that the upscaled rate of deposition is able to recover the amount of deposited asphaltene in fine grid simulations.

5.9 References

Akbarzadeh, K., Alboudwarej, H., Svrcek, W.Y., Yarranton, H.W., 2005. A generalized regular solution model for asphaltene precipitation from n-alkane diluted heavy oils and bitumens. Fluid Phase Equilib. 232, 159–170.

Al-Gawfi, A., Nourozieh, H., Ranjbar, E., Hassanzadeh, H., Abedi, J., 2019a. Mechanistic modelling of non-equilibrium interphase mass transfer during solvent-aided thermal recovery processes of bitumen and heavy oil. Fuel 241, 813–825.

Al-Gawfi, A., Zirrahi, M., Hassanzadeh, H., Abedi, J., 2019b. Development of Generalized Correlations for Thermophysical Properties of Light Hydrocarbon Solvents (C1-C 5)/Bitumen Systems Using Genetic Programming. ACS Omega 4, 6955–6967.

Canadian Association of Petroleum Producers (CAPP), Accessed September 10, 2020. URL https://www.capp.ca/energy/canadas-energy-mix/

Cartlidge, C.R., Dukhedin-Lalla, L., Rahimi, P., Shaw, J.M., 1996. Preliminary phase diagrams for bitumen/heavy oils and related mixtures. Fuel Sci. Technol. Int. 14, 163–178.

Civan, F., 2015. Reservoir formation damage, 2nd ed. Gulf Professional Publishing.

CMG-STARS user guide, 2018. . Computer Modeling Group Ltd., Calgary.

Bin Dahbag, M., Zirrahi, M., Hassanzadeh, H., 2019. Solubility and Liquid Density of Ammonia / Athabasca Bitumen Mixtures at Temperatures up to 463 K : Measurements and Modeling. J. Chem. Eng. Data 64, 3592–3597.

De La Cruz, J.L.M., Argüelles-Vivas, F.J., Matías-Pérez, V., Durán-Valencia, C.D.L.A., López-Ramírez, S., 2009. Asphaltene-induced precipitation and deposition during pressure depletion

on a porous Medium: An experimental investigation and modeling approach. Energy and Fuels 23, 5611–5625.

Dini, Y., Becerra, M., Shaw, J.M., 2016. Phase behavior and thermophysical properties of Peace River bitumen + propane mixtures from 303 K to 393 K. J. Chem. Eng. Data 61, 2659–2668.

Gao, J., Li, H.A., 2017. A Phase-Behavior Study for n-Hexane/ Bitumen and n-Octane/Bitumen Mixtures, in: SPE Canada Heavy Oil Technical Conference. Calgary, Alberta, Canada.

Gotawala, D.R., Gates, I.D., 2011. Stability of the edge of a SAGD steam chamber in a bitumen reservoir. Chem. Eng. Sci. 66, 1802–1809.

Haddadnia, A., Azinfar, B., Zirrahi, M., Hassanzadeh, H., Abedi, J., 2018a. Thermophysical properties of dimethyl ether/Athabasca bitumen system. Can. J. Chem. Eng. 96, 597–604.

Haddadnia, A., Sadeghi Yamchi, H., Zirrahi, M., Hassanzadeh, H., Abedi, J., 2018b. New Solubility and Viscosity Measurements for Methane-, Ethane-, Propane-, and Butane-Athabasca Bitumen Systems at High Temperatures up to 260 °c. J. Chem. Eng. Data 63, 3566–3571.

Johnston, K.A., Schoeggl, F.F., Satyro, M.A., Taylor, S.D., Yarranton, H.W., 2017. Phase behavior of bitumen and n-pentane. Fluid Phase Equilib. 442, 1–19.

Kariznovi, M., 2013. Phase Behaviour Study and Physical Properties Measurement for Athabasca Bitumen / Solvent Systems Applicable for Thermal and Hybrid Solvent Recovery Processes, PhD thesis. Calgary.

Keshmiri, K., Huang, H., Nazemifard, N., 2019. Microfluidic platform to evaluate asphaltene deposition during solvent-based extraction of bitumen. Fuel 239, 841–851.

Leontaritis, K.J., Mansoori, A.G., 1988. Asphaltene deposition: a survey of field experiences and research approaches. J. Pet. Sci. Eng. 1, 229–239.

Mansoori, G.A., 1997. Modeling of Asphaltene and other Heavy Organic Depositions. J. Pet. Sci. Eng. 17, 101–111.

Mokrys, I.J., Butler, R.M., 1999. In-situ upgrading of heavy oils and bitumen by propane deasphalting: The Vapex process, in: Production Operations Symposium. Oklahoma City, Oklahoma.

Monteagudo, J.E.P., Rajagopal, K., Lage, P.L.C., 2002. Simulating oil flow in porous media under asphaltene deposition. Chem. Eng. Sci. 57, 323–337.

Monteagudo, J.E.P., Silva, L.F.L.R., Lage, P.L.C., 2003. Scaling laws for network model permeability: Application to wellbore oil flow simulation with solid deposition. Chem. Eng. Sci. 58, 1815–1829.

Mousavi, S.M.R., Jafari, S., Schaffie, M., Norouzi-Apourvari, S., 2020. Experimental study and modeling permeability damage in porous media due to asphaltene deposition. J. Pet. Sci. Eng. 193, 107396.

Nghiem, L.X., Sammon, P.H., 1997. Non-equilibrium equation-of-state compositional simulator., in: SPE Symp. Reserv. Simul. Dallas, Texas.

Niessner, J., Hassanizadeh, S.M., 2009. Non-equilibrium interphase heat and mass transfer during two-phase flow in porous media-Theoretical considerations and modeling. Adv. Water Resour. 32, 1756–1766.

Nourozieh, H., 2013. Phase Partitioning and Thermo-physical Properties of Athabasca Bitumen /

Solvent Mixtures, PhD thesis. University of Calgary.

Panda, S., Pal, K., Merzara, S., Gray, M.R., Liu, Q., Choi, P., 2017. Transport and removal of a solvent in porous media in the presence of bitumen, a highly viscous solute. Chem. Eng. Sci. 165, 229–239.

Porter, K.E., 1989. An overview of formation damage. J. Pet. Technol. 41, 780–786.

Qi, Z., Abedini, A., Sharbatian, A., Pang, Y., Guerrero, A., Sinton, D., 2018. Asphaltene Deposition during Bitumen Extraction with Natural Gas Condensate and Naphtha. Energy and Fuels 32, 1433–1439.

Sabet, N., Hassanzadeh, H., Abedi, J., 2017. Selection of efficient solvent in solvent-aided thermal recovery of bitumen. Chem. Eng. Sci. 161, 198–205.

Sabet, N., Hassanzadeh, H., Abedi, J., 2020a. Dynamics of Viscous Fingering in Porous Media in the Presence of In Situ Formed Precipitates and Their Subsequent Deposition. Water Resour. Res. 56, 1–20.

Sabet, N., Mohammadi, M., Zirahi, A., Zirrahi, M., Hassanzadeh, H., Abedi, J., 2020b. Numerical modeling of viscous fingering during miscible displacement of oil by a paraffinic solvent in the presence of asphaltene precipitation and deposition. Int. J. Heat Mass Transf. 154.

Sadeghi Yamchi, H., 2014. Effect of Refining on Asphaltene Property Distributions, Master's thesis. University of Calgary.

Sadeghi Yamchi, H., Zirrahi, M., Hassanzadeh, H., Abedi, J., 2020. Measurements and NRTL modeling of liquid-liquid equilibrium of dimethyl ether/bitumen. Fluid Phase Equilib. 512, 112549.

Sadeghi Yamchi, H., Zirrahi, M., Hassanzadeh, H., Abedi, J., Fadaei, H., 2018. Effect of additives on liquid–liquid equilibrium properties of butane/bitumen systems with applications to solvent aided bitumen recovery processes. Chem. Eng. Res. Des. 137, 452–460.

Srivasfava, R.K., Huang, S.S., Dong, M., 1999. Asphaltene deposition during CO2 flooding. SPE Prod. Facil. 14, 235–245.

Wang, J., Anthony, E.J., 2003. A study of thermal-cracking behavior of asphaltenes. Chem. Eng. Sci. 58, 157–162.

Wang, S., Civan, F., Strycker, A.R., 1999. Simulation of paraffin and asphaltene deposition in porous media, in: SPE International Symposium on Oilfield Chemistry. Houston, Texas.

Yazdani, A., Maini, B.B., 2010. Measurements and modelling of phase behaviour and viscosity of a heavy oil/butane system. J. Can. Pet. Technol. 49, 9–14.

Zanganeh, P., Dashti, H., Ayatollahi, S., 2018. Comparing the effects of CH4, CO2, and N2 injection on asphaltene precipitation and deposition at reservoir condition: A visual and modeling study. Fuel 217, 633–641.

Zhang, K., Zhou, X., Peng, X., Zeng, F., 2019. A comparison study between N-Solv method and cyclic hot solvent injection (CHSI) method. J. Pet. Sci. Eng. 173, 258–268.

Zirahi, A., Sadeghi Yamchi, H., Haddadnia, A., Zirrahi, M., Hassanzadeh, H., 2019. Ethyl Acetate as a Bio-Based Solvent to Reduce Energy Intensity and CO2 Emissions of In-Situ Bitumen Recovery. AIChE J. 66.

Zirrahi, M., Hassanzadeh, H., Abedi, J., 2017. Experimental and modelling studies of MacKay River bitumen and light n-alkane binaries. Can. J. Chem. Eng. 95, 1417–1427.

Chapter Six: **Conclusions and Recommendations**

6.1 Conclusions

Liquid-liquid equilibrium measurements of different solvents (butane, dimethyl ether, and a mixture of butane and propane) and Athabasca bitumen were conducted in this thesis. To describe each equilibrium, the composition of the components along with the density and viscosity of the light phase were measured, and then the heavy yield was obtained based on mass balance calculations. Detailed characterization of the bitumen and the light and heavy cuts from LLE experiments was obtained combining the results from SD and GPC methods. NRTL thermodynamic model was tuned to predict the experimental K-value data. In addition, a modified approach was introduced to simulate asphaltene deposition in porous media using CMG-STARS by converting heavy yield data into K-values and implementing a non-equilibrium mass transfer term.

6.1.1 Effect of Additives on Liquid-Liquid Equilibrium of Butane/Bitumen

First, as a reference case, phase equilibrium properties of butane/bitumen system with a solvent concentration of 60 wt.% in the feed were measured. It was found that mixing 60 wt.% butane with bitumen would cause separation of two liquids at temperatures of 40 and 60 °C and pressure of 1 MPa. While the density and viscosity of the light phase in equilibrium condition were considerably low compared to the bitumen, the heavy phase was hardly mobile in the same conditions. It was demonstrated that adding fractions of propane as an additive to butane/bitumen mixture can increase the precipitation of heavy components from bitumen. On the contrary, the addition of both DME and toluene to the base mixture reduced asphaltene precipitation. The experiments revealed that DME can generate the same drive force as propane in the form of

saturation pressure meaning the saturation pressure of the mixture increased by adding both propane and DME to the butane/bitumen system. Compositional analysis of the light and heavy cuts with simulated distillation showed that the methodology may be adequate for characterization of the light cuts but it is unable to characterize the asphaltene components existing in the heavy cuts.

6.1.2 Liquid-Liquid Equilibrium of DME/Bitumen Mixtures

Experimental PVT measurements of DME/bitumen mixtures were conducted in this study. Measurements included the density and viscosity of the light phase, the composition of components in each phase (LLE K-values), saturation pressure of the mixtures, and heavy yield estimations. Molecular weight distribution of the light and heavy cuts was determined by coupled simulated distillation (SD) and gel permeation chromatography (GPC) method. Measurements were performed at four different temperatures of 40, 60, 80, and 100 °C and three different solvent concentrations of 60, 70, and 80 wt.%. Results showed that at a given temperature adding more DME to the mixture would extract more of the molecules with MW $\lesssim$ 1000 g/mol from the heavy phase and transfer them into the lighter phase. On the other hand, components with MW $\gtrsim$ 2000 g/mol were extracted from the light phase and accumulated in the heavy phase. The amount of precipitation with DME was shown to be comparable with that of pentane. Since DME has a dipole molecular structure, the compatibility of heavier and polar components in the bitumen such as asphaltene is more pronounced with DME than other non-polar hydrocarbons such as propane and butane. NRTL model was able to predict the composition of the solvent and pseudocomponents in the system and generate the LL region in the ternary diagrams with an accuracy of AARD 7.5%.

6.1.3 Liquid-Liquid Equilibrium of Propane + Butane + Bitumen Mixtures

Liquid-liquid equilibrium measurements of LPG (propane+butane)/bitumen system were conducted at temperatures from 21 to 80 °C and solvent concentrations of 45, 55, 65 wt.%. In addition to the PVT measurements, a detailed characterization of the light and heavy cuts was determined using SD and GPC methods. The results revealed that propane and butane tended to partition equally into the light phase. Detailed characterization of the cuts indicated that increasing the solvent concentrations, extracted more components with MW less than ~1000 g/mol from heavy phase and instead separated components with MW larger than ~2000 from the light phase. It was shown that mixing LPG with bitumen could result in precipitation as high as 45% leading to high quality oil. These results are in correspondence with asphaltene precipitations using n-pentane and n-heptane indicating that lower carbon number in the n-alkane leads to more asphaltene precipitation. Ternary diagrams created with tuning NRTL model with experimental data suggested a larger LLE region for LPG/bitumen mixtures compared to DME/bitumen mixtures which is another indication of heavy yield data.

6.1.4 Numerical Simulation of Asphaltene Deposition in Porous Media

In this work, we studied the asphaltene deposition in the miscible displacement of bitumen with hot pressurized liquid dimethyl ether. Athabasca bitumen was divided into two pseudo-components of asphaltene and maltene. Then, the liquid-liquid K-values of asphaltenes were generated based on the asphaltene yield curve of DME/bitumen system. A 2D numerical model was created by including a general reaction term to convert asphaltenes in the liquid phase to the solid phase through a non-equilibrium model. The numerical simulation of miscible displacement of bitumen by DME demonstrated that viscous fingering played an essential role in the deposition

of asphaltene due to excessive mixing of bitumen and the injected solvent. It was also shown that one-dimensional modeling of asphaltene deposition failed to capture the dynamics of the system and significantly underestimated the amount of deposition. The requirement for proper upscaling of the deposition rate was highlighted since it was demonstrated that the amount of deposition is a strong function of grid size. To address this challenge, fine grid and coarse grid numerical simulations were conducted and the rate of deposition in the coarse grid simulation was optimized to match the amount of asphaltene deposition.

6.2 Recommendations

In this study, we presented experimental measurement, modeling, and simulation results of LLE of solvent (dimethyl ether, butane, and butane + additives) and bitumen mixtures. Extension of this work with other solvents such as CO_2, n-pentane, and n-heptane is recommended. It is also recommended to conduct experiments with the presence of methane to evaluate LLE of live bitumen and solvent system which is a more realistic case considering the reservoir conditions.

In the modeling and simulation work, we did not consider the effect of asphaltene precipitation on the reduction of bitumen density and viscosity. It is recommended to measure the density and viscosity of both light and heavy cuts and incorporate them into the modeling and simulation work.

Appendix A: **Validation of the Experimental Apparatus**

A.1 Validation of the PVT Setup

The reliability of the PVT apparatus for liquid-liquid equilibrium measurements was confirmed with the available data in the literature. In this regard, we chose butane and Athabasca bitumen system to have it validated. It should be noted that the viscometer and densitometer were factory calibrated, however, before conducting new sets of experiments we checked the calibration of devices to ensure the validity of data. Table A.1 shows the results of this work and compares them with the findings from Kariznovi et al. (2013). A good agreement was found between the solubility and density data confirming the reliability of the setup.

Table A.1: Liquid-liquid equilibrium data for butane and Athabasca bitumen at 50 °C and 2MPa.

Experimental data	Solvent wt.% in the feed	This work	Kariznovi (2013)
Solvent wt.% in the light phase	50	51.8	49.8
	70	75.9	73.1
Density of the light phase	50	701.5	708.6
	70	615.3	618.2

A.2 References

Kariznovi, M., 2013. Phase Behaviour Study and Physical Properties Measurement for Athabasca Bitumen / Solvent Systems Applicable for Thermal and Hybrid Solvent Recovery Processes, PhD thesis, University of Calgary.

Appendix B: **Copyright Permissions**

Effect of additives on liquid–liquid equilibrium properties of butane/bitumen systems with applications to solvent aided bitumen recovery processes

Author: Hassan Sadeghi Yamchi,Mohsen Zirrahi,Hassan Hassanzadeh,Jalal Abedi,Hossein Fadaei

Publication: Chemical Engineering Research and Design

Publisher: Elsevier

Date: September 2018

Please note that, as the author of this Elsevier article, you retain the right to include it in a thesis or dissertation, provided it is not published commercially. Permission is not required, but please ensure that you reference the journal as the original source. For more information on this and on your other retained rights, please visit: https://www.elsevier.com/about/our-business/policies/copyright#Author-rights

BACK CLOSE WINDOW

Measurements and NRTL modeling of liquid-liquid equilibrium of dimethyl ether/bitumen

Author: Hassan Sadeghi Yamchi,Mohsen Zirrahi,Hassan Hassanzadeh,Jalal Abedi

Publication: Fluid Phase Equilibria

Publisher: Elsevier

Date: 15 May 2020